Ion Selective Gates

Active Device Component for 3D Microfluidic Architecture

Graduation committee:

Chairman:	Prof. dr. ir. A. Bliek	University of Twente
Promoters:	Prof. dr. ing. D.H.A. Blank	University of Twente
	Prof. dr. ir. A. van den Berg	University of Twente
Assistant promoter:	Dr. ir. J.E. ten Elshof	University of Twente
Committee members:	Prof. dr. U. Karst	University of Twente
	Dr. ir. K. Keizer	University of Twente
	Prof. dr. A. Manz	ISAS
	Prof. dr. ir. J.T.F. Keurentjes	TU Eindhoven

The research described in this thesis was carried out in the Inorganic Material Science group at the University of Twente and has been financially supported by the Micro Chemical Systems (*MiCS*) program of the MESA$^+$ Institute for Nanotechnology.

Ion Selective Gates
Active Device Component for 3D Microfluidic Architecture
R. Schmuhl
ISBN 90-365-2146-7

Printed by Febodruk BV, Enschede, The Netherlands.

ION SELECTIVE GATES

ACTIVE DEVICE COMPONENT FOR 3D MICROFLUIDIC ARCHITECTURE

DISSERTATION

to obtain
the doctor's degree at the University Twente,
on the authority of the rector magnificus,
prof. dr. W.H.M. Zijm,
on account of the decision of the graduation committee,
to be publicly defended
on Friday 25th February 2005 at 16.45

by

Riaan Schmuhl

born on 28th October 1973

in Rustenburg, South Africa

This dissertation is approved by the promoters:
Prof. dr. ing. D.H.A. Blank and Prof. dr. ir. A. van den Berg,

and the assistant promoter:
Dr. ir. J.E. ten Elshof.

Table of Contents

Summary

This thesis describes the development of porous ion-transport oxide interconnects that allow molecular communication between microchannels in complex microfluidic architectures. New methods to control the permeability of interconnects to certain species by externally tuneable parameters was investigated. DC electric fields were used to impose a driving force for the transport of selected cationic and anionic species. Electric fields are preferred over pressure gradients in nanochannels, because very large pressure drops are required to drive flow in small channels, while typical operating voltages are below the potential difference required for decomposition of water. Applying an external electric field across the interconnects, a potential difference is created across the membrane, which makes it is possible to selectively drive charged species from one liquid into the other through interconnects, by means of ion migration, Fick diffusion and/or electroosmotic flow.

An important potential application field of switchable gates is in microfluidic devices. However, there are potential difficulties associated with the implementation and incorporation of the state of the art mesoporous oxide membranes into these mostly Si-based devices. It was therefore essential to develop a new class of Si-compatible thin oxide films, which combines mesoporous and microporous oxide film technology with existing silicon technology. The general fabrication method of such Si-compatible thin oxide films on micromachined silicon microsieve support structures is described. This procedure to manufacture different types of microporous and mesoporous oxide films enables the incorporation of sol-gel type fabrication techniques into existing silicon technology; opening the way for constructing Si-supported oxide films.

Si-compatible oxide interconnects with external platinum electrodes were used as interconnects for selective gating of anionic and cationic species. The electric field-driven transport of species through three different types of oxide interconnects was measured. The influence of the applied potential difference on the transport rates of ionic probe species was also investigated along with other factors that play an important part in the transport such as ionic strength and pH, which regulate the tuneability and selectivity of the system. In these cases where external electrodes were used, the main transport mechanism of ionic species was ion migration and not Fick diffusion. This transport mechanism draws ionic species through the membrane to the oppositely charged electrode at the permeate side of the membrane.

Integrating the Si-supported oxide films into smaller device type set-ups is a potential way to establish communication between two microfluidic channels and may be an important component in future microfluidic devices since it allows extension of microfluidic architectures into the third dimension. Two designs are presented in this thesis.

In order to explore new methods to control the transport rate of ionic species through a mesoporous oxide layer, as well as the ion-selectivity of the layer, transport studies were performed on conventional mesoporous oxide membrane, as a model system. In one study a bias potential was imposed at the feed side surface of the membrane, and a potential

difference was generated over the membrane. State of the art α-alumina supported γ-alumina membranes were modified by depositing thin porous gold films on either side of the membrane. These gold layers were utilized as electrodes to apply a dc potential difference over the membrane. It was found that the membrane is completely cation-selective and that the potential difference can be used to promote or inhibit the transport of cations through the membrane. The transport rate is influenced by a number of external parameters, which include ionic strength, pH, concentration and ion valence. By controlling the sign of the applied potential over the membrane it is possible to either promote or stop the permselective transport of cations through the membrane.

From these investigations it became clear that there are a number of ways to open and close switchable mesoporous gates for certain ionic species. These include pH, ionic strength (double layer overlap) and applied electrical potential difference. An alternative way to control the permeability of a gate is by the co-addition of molecules to the system that alter the properties of the membrane. The use of different surfactants to influence the transport of ionic species through a membrane by steric blocking is investigated. Surfactants are known to adsorb strongly on oxide surfaces, and adsorption in membrane mesopores reduces the porosity and permeability of the membrane. Near-complete blocking of ion transport was achieved by formation of surfactant bilayers on or near the membrane surface at relatively high surfactant concentrations, while increased ion fluxes were obtained at lower concentrations. The latter phenomenon is thought to be due to the adsorption of a sub-monolayer of surfactant molecules that neutralizes the membrane surface charges, thus decreasing the electrostatic interaction between the ionic probe species and the membrane pore wall.

Samenvatting

Dit proefschrift beschrijft de ontwikkeling van dunne films van poreuze oxides die gebruikt kunnen worden voor ionentransport tussen verschillende typen microkanalen, hetgeen kan leiden tot nieuwe communicatiemethoden tussen deze kanalen. Er is onderzoek gedaan naar nieuwe manieren om de permeabiliteit van deze dunne oxide membranen voor bepaalde stoffen te controleren door middel van extern instelbare parameters. Elektrische velden, opgewekt met gelijkspanning, zijn gebruikt om een drijvende kracht aan te leggen voor het transport van specifieke positieve en negatieve geladen ionen. Door een extern elektrisch veld aan te leggen over het oxide-membraan wordt een potentiaalverschil gecreëerd. Dit maakt het mogelijk maakt om selectief bepaalde geladen ionen door het oxide te transporteren vanuit een vloeistof aan de ene kant van het membraan, naar een vloeistof aan de andere kant van het systeem. Een belangrijke mogelijke toepassing van dergelijke wisselbare poorten ligt op het gebied van de *microfluidic device technology*.

Een nieuwe klasse van silicium-compatibele oxide membranen met externe platina elektroden is in dit proefschrift gebruikt als *device component* met selectieve doorlaatbaarheid voor negatief en positief geladen ionen. Het door elektrische velden gedreven transport van ionen is voor drie verschillende typen oxides vergeleken. De invloed van het aangelegde potentiaalverschil op de transportsnelheden van ionen, en de selectiviteit en regelbaarheid van deze systemen, zijn onderzocht.

De mogelijkheid om de silicium-gedragen oxidische lagen te integreren in kleinere device-achtige opstellingen is een mogelijke manier om contact tussen twee vloeistof-microkanalen te bewerkstelligen. Het zou ook een belangrijk onderdeel kunnen zijn van toekomstige microfluidic devices aangezien het de mogelijkheid biedt om de architectuur van deze systemen uit te breiden naar de derde dimensie.

Om mogelijke nieuwe toepassingsmanieren te onderzoeken om het transport van ionen door een mesoporeus oxidisch membraan, maar ook door een ionselectieve laag te controleren, zijn er transportstudies uitgevoerd aan een model systeem: een conventioneel mesoporeus oxidisch membraan. In dit onderzoek is een bias potentiaal opgelegd aan het oppervlak aan de voedingskant van het membraan, en werd er een potentiaalverschil over het membraan aangelegd. Het huidige aluminiumoxide membraan is hiertoe gemodificeerd door een dunne poreuze goudlaag op beide kanten van het membraan aan te brengen. De goudlagen werden vervolgens gebruikt als elektroden om een gelijkspanningsverschil over het membraan aan te leggen. Door controle van het teken van de aangelegde potentiaal over het membraan bleek het mogelijk om het transport van positieve ionen door het membraan te versnellen of te stoppen.

Naar aanleiding van dit onderzoek werd duidelijk dat er een aantal manieren is om wisselbare mesoporeuze poortmembranen te openen en te sluiten voor bepaalde typen ionen. Een alternatieve manier om de permeabiliteit van een poortmateriaal te controleren is door adsorberende moleculen aan het systeem toe te voegen die de eigenschappen van het

membraan veranderen. Om deze reden is het gebruik van oppervlakte-actieve stoffen, die het transport van ionen door een membraan door middel van sterische hindering blokkeren, onderzocht.

Chapter 1

General Introduction

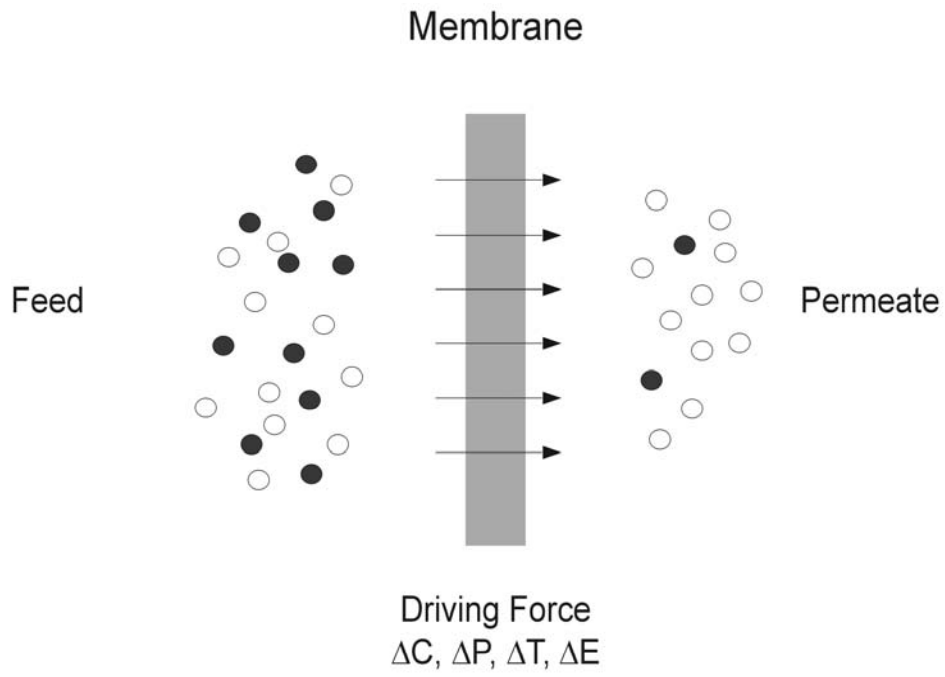

Schematic representation of a two phase system separated by a membrane.

Abstract: *This thesis describes the feasibility of utilizing an electric field for separation of charged species through a membrane. This forms the central theme in all chapters. The membranes can be regarded as an interconnect between two separate liquids. By applying an external electric field over the interconnect it is possible to transport charged species from one liquid to the other. In this chapter a general overview will be given on membranes in general and their use, as well as a short overview of the main physical and chemical factors influencing fluid flow in nanosized channels (pores). The aim is to shortly point out those factors that become especially relevant when the spatial dimensions drop below length scales of ~100 nm. The overview is followed by a review of recent studies on fluid flow and separation effects in ensembles of one-dimensional nanosized channels. The outline of the rest of this thesis is described in the final section of this chapter.*

1.1 Introduction

Membranes are used as a selective barrier between two phases, which allow the movement of different species under the presence of a driving force over the membrane. Depending on the actual membrane process the driving force for movement of species through the membrane may differ. Typical driving forces include concentration-, pressure-, temperature- and electrical potential gradients over the membrane. The selectivity of a membrane is often based on the principle of size differences between different species, which means that smaller species are separated from larger species, but this is not the only mechanism. Others include charged, chemical nature and affinity based separations and combinations of these.

Recently it was shown that a membrane, after mounting, could be externally manipulated so that the selectivity of the membrane was changed at will, without changing the process parameters. This means that the transport of species through the membrane could be tuneable or switchable.[1] The application of these types of tuneable/switchable membranes is largely envisioned in micro-chip fluidic devices, such as μTAS (micro-total analytical systems). Since the milestone work by Manz and co-workers in the field of liquid phase separation for μTAS,[2] an explosive growth of research occurred in the fabrication of silicon and polymer based components for microfluidic systems. These included mixers, valves, interconnect, filters and other elements required for a complete system.[3,4] As the architecture of microfluidic systems becomes more complex the need to integrate valves and interconnects into a design of such systems also increases. Further integration should enable designers to extend the systems in three dimensions, making it possible to connect channels with each other and leading to more complex microfluidic systems.

In this chapter a short overview of the main physical and chemical factors influencing fluid flow in nanosized channels and pores will be presented, without pretending to be exhaustive or complete. Its main aim is to shortly point out those factors that become especially relevant when the spatial dimensions drop below length scales of ~100 nm. The overview is followed by a brief overview of recent studies on fluid flow and separation effects in ensembles of one-dimensional nanosized channels.

1.2 Physical background of fluid flow in nanochannels

A natural extension of microfluidics would extend capabilities to structures of nanometer dimensions. Although microfluidics is nowadays mainly focusing on making more complex channel systems rather than on reduction of channel size, the specific phenomena associated with fluid transport in nanosize channels is of considerable interest to achieve active control over the transport of specific molecular or ionic species. This may lead to enabling technologies by permitting (i) new approaches to molecular separations, (ii) reactions in which one or more reagents are available in limited quantities, and (iii) coupling of powerful methods of molecular identification to spatially and temporally resolved molecular sampling methods.[5]

Fluid flow through nanochannels cannot be understood by extrapolating the behaviour of fluid transport in microchannels to smaller channel diameters. Firstly, there is the occurrence of double layer overlap in nanochannel geometries, which gives rise to physical phenomena that largely influence the transport properties of fluids. Secondly, because of the large surface area to volume ratio the physiochemical interactions between specific components in the fluid medium and the channel wall have to be taken into account explicitly. Thirdly, the finite dimensions of ions and molecules start playing a dominant role when the channel size is approaching molecular dimensions.[6] Furthermore, macroscopic fluid properties such as surface tension, permittivity and viscosity may take completely different values when the fluid is confined to nanometer-scale geometries, where most or the entire fluid medium is influenced by the presence of a nearby charged wall. These latter aspects fall outside the scope of the present chapter, and the reader is referred to treatments of these topics elsewhere.[7-10]

The Navier-Stokes and Nernst-Planck equations are generally applicable to model flows of fluids and ions in systems of arbitrary geometry, including nanochannels.[11] However, the predominant feature associated with the latter type of geometry is the occurrence of double layers and double layer overlap. The double layer in a fluid medium is caused by the surface charge that is naturally present on any surface.[12] The surface charge density, σ_s, is of critical importance in nanochannels, because the enhanced surface area to volume ratio implies that a significant fraction of the total charge is bound to the walls and is immobile. The surface charge density determines the magnitude of the surface potential and the applicability of the Debye-Hückel approximation for the description of the double layer length. It also provides an experimental handle to manipulate the molecular processes that influence fluid transport in nanochannels.[5]

Sophisticated models like the charge regulation model[13] incorporate the dynamic interactions between ions from the double layer and bound surface charges on the surface. Since the surface concentration of solute ions is a function of surface potential, the surface charge is related to the surface potential via surface association and dissociation reactions. For example, for an aqueous NaCl solution inside a channel with charged surface sites S^-, the following four association-dissociation reactions between mobile ions and surface sites have to be taken into account as shown in Scheme 1.1.

The equilibrium constant of each possible reaction must be known and be incorporated in the description. For the example described above, the surface charge density can be expressed as: $\sigma_s = e([SH_2^+] - [S^-])$, where e is the elementary electron charge and [Q] denotes the concentration of species Q. Most ions are known to exhibit some kind of interaction with bound surface charges. Specific interactions between surfaces and solutes are also known.[12] For instance, fluoride chemisorbs specifically on α- and γ-alumina surfaces through replacement of surface aqua groups following the net reaction $Al–OH_2^+ + F– = Al–F + H_2O$.[14,15] Maximum uptake of fluoride occurs at pH 5-6. Divalent cations are known to adsorb

on many oxide surfaces, giving rise to surface complexes S–MX, where M represents the divalent cation and X is a monovalent anion.[16,17]

$$SH \rightleftharpoons S^- + H^+$$

$$S^- + Na^+ \rightleftharpoons S\text{-}Na$$

$$SH_2^+ \rightleftharpoons SH + H^+$$

$$SH_2^+ + Cl^- \rightleftharpoons SH_2Cl$$

Scheme 1.1: The association-dissociation reactions between mobile ions and surface sites (S).

Most existing surface complexation models have been developed for unconfined solid-water interfaces, where overlap of the electrical double layer does not occur. In recent years a charge regulation model has been developed to describe the surface of porous materials.[18] The double layer overlap in a cylindrical cavity was taken into account by diminishing the effective radius of the cylinder. The model predicts a decrease in surface charge density with decreasing pore size. In contrast to this model, a recent experimental study of ion adsorption on mesoporous alumina indicates that nanoscale confinement has a considerable effect on ion adsorption onto mesoporous surfaces.[19] The effect is most likely explained by the overlap of the electrical double layer. It was found that the surface charge per mass on mesoporous alumina was as much as 45 times higher than on dense alumina particles. This effect could not be explained on the basis of specific surface area differences between the two materials. Density functional theory calculations in the same study indicated that a mesoporous material with a pore size of 2 nm could have an adsorption coefficient for a divalent ion that is 2 orders of magnitude higher or lower than the corresponding nonporous material. The typical length scale for the confinement effect to become significant is less than 10 nm. These findings show that the development of surface charge in nanochannel geometries may not be predictable a priori by the currently existing models for surface-liquid interactions.

With respect to the occurrence of double layer overlap the relevant parameter to consider is the product of channel radius a, and inverse Debye length κ. The Debye length can be roughly approximated by Eq. (1.1).

$$\kappa^{-1} = \sqrt{\frac{\varepsilon_0 \varepsilon_r k_B T}{e^2 \sum_i z_i^2 n_i^0}} \tag{1.1}$$

where e_0 is the permittivity of vacuum, ε_r the relative permittivity of the liquid medium, k_B the Boltzmann constant, T the temperature, n_i^0 the number density of the i^{th} ionic species in the bulk of the electrolyte solution and z_i the charge of the i^{th} ionic species.[12] Two extreme situations are illustrated in Figure 1.1.

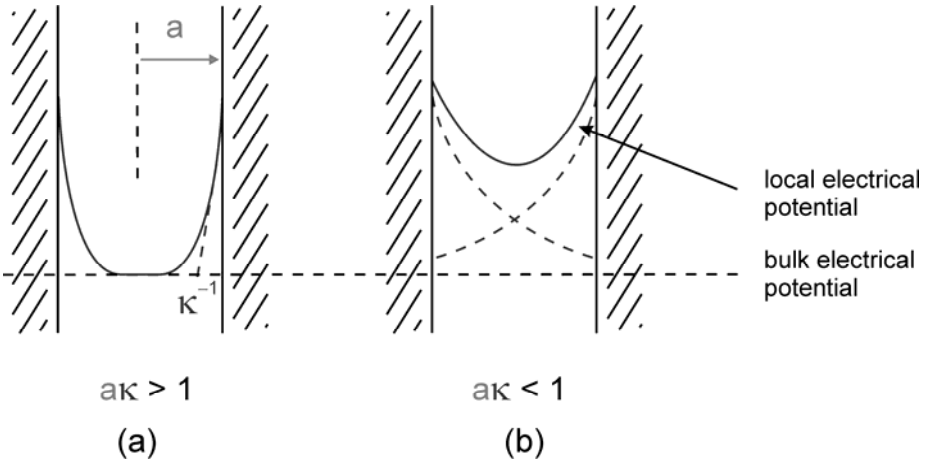

Figure 1.1: Schematic diagram showing (a) absence and (b) presence of double layer overlap in a nanochannel.

When $\kappa a < 1$, the electrical double layer extends across the entire channel. In aqueous systems κ^{-1} is very large, being limited by the autoprotolysis of water, which means that achieving channels with complete double layer overlap requires diameters of several hundreds nanometers or less. Under conditions of complete double layer overlap the channel becomes virtually impermeable to ions with the same charge as the surface charge, making it a selective barrier for transport of either cationic or anionic species. Alternatively, under conditions at which $\kappa a > 1$, the double layer is confined to a small region near the channel wall, and the center of the channel is electrically uncharged. Under these conditions both anionic and cationic species can be transported through the nanochannel, although the channel may still retain some permselectivity when the double layer length is of the same order of magnitude as the pore radius.

While the double layer can be described using the well-known Poisson-Boltzmann equation,[12] the simplest descriptions of double layers consider ions as simple point charges. Since the number of ions at the channel wall is higher than in the bulk, an unlimited number of ions could be accommodated in the interfacial region. This is physically impossible, and therefore it becomes necessary to assign a volume to the ions at high electrolyte concentration and/or small channel size. The spatial requirement for an ion is characterized by its hydrated radius, and both undissociated and dissociated hydrated electrolytes can be distinguished.[20] The expression for the distribution of dissociated ions from a binary electrolyte can be written in a modified form of the Boltzmann equation, Eq. (1.2):

$$\frac{n_i}{n_i^b}\left(\frac{v^{-1}-\sum_i n_i^b}{v^{-1}-\sum_i n_i}\right)=\exp\left(-\frac{z_i e\varphi(r)}{k_B T}-\frac{\Delta F_i}{k_B T}\right), \qquad (1.2)$$

where n_i is the number density of the i^{th} ionic species near the charged interface, v^{-1} the inverse volume of the hydrated ion, and $\varphi(r)$ the local electrical potential relative to the potential in the uncharged bulk of the electrolyte solution. ΔF_i indicates the hydration free

energy of the i[th] ion, a term that is associated with the change of dielectric permittivity of the solvent medium surrounding the ion.[20]

All molecular and ionic fluxes resulting from electrical potential and/or concentration gradients are due to one or more of three possible mechanisms of transport: Fick diffusion, ion migration and electro-osmotic flow.[21] This can be expressed as Eq. (1.3).

$$j_{\mathrm{i}} = j_{\mathrm{F,i}}(\nabla c_{\mathrm{i}}) + j_{\mathrm{IM,i}}(\nabla V) + j_{\mathrm{EOF,i}}(\nabla V). \tag{1.3}$$

The total flux, j_{i} of a species type i is expressed as the sum of the three flux contributions, i.e., Fick diffusion $j_{\mathrm{F,i}}$, ion migration $j_{\mathrm{IM,i}}$ and electro-osmotic flow $j_{\mathrm{EOF,i}}$, respectively. Eq. (1.4) expresses the Fickian flux $j_{\mathrm{F,i}}$ due to a concentration gradient ∇c_{i} over the membrane.

$$j_{\mathrm{F,i}}(\nabla c_{\mathrm{i}}) = -D_{\mathrm{i}} \nabla c_{\mathrm{i}}, \tag{1.4}$$

where D_{i} is the chemical diffusion coefficient of species i inside the membrane pores, and ∇c_{i} the concentration gradient.

Electro-osmotic flow (EOF), expressed by Eq. (1.5), is driven by the mobile double-layer inside the pores, and moves the entire liquid under the influence of an electrical potential gradient ΔV.

$$j_{\mathrm{EOF,i}} = \frac{\varepsilon \zeta}{\eta} c_{\mathrm{i}} \nabla V, \tag{1.5}$$

where ε is the dielectric constant of the solution inside the pores, ζ the zeta[22] of the oxide material, and η the fluid viscosity.

The third contribution, ion migration, is due to an electrical potential gradient over the interconnect, which moves charged species toward the oppositely charged electrode, as expressed by Eq. (1.6).

$$j_{\mathrm{IM,i}}(\nabla V) = -\frac{D_{\mathrm{i}} c_{\mathrm{i}} z_{\mathrm{i}} \mathrm{e}}{k_{\mathrm{B}} T} \nabla V, \tag{1.6}$$

here z_{i} is the ionic charge of species i, e is the elementary electron charge, k_{B} the Boltzmann constant, and T the temperature.

1.3 A brief literature overview

While a lot of effort has been made to understand the effect of surface potential and double layer overlap on the transport properties in nanochannels, relatively little attention has been given to the control of these properties. One of the most interesting applications of nano-channels or ensembles thereof concerns their use as interconnects between microfluidic channels with external control over the permeability and molecular selectivity. Such systems could be useful for controlling protein separation,[24] fabricating selective barriers for sensor applications,[25] and controlled delivery systems.[26] The concepts described in this section clearly demonstrate that by simultaneously manipulating buffer conditions, pore properties

and surface chemistry, it is possible to effect molecular transport with widely varying character.

Nanotubular membranes are generally made by template-directed syntheses, with either polycarbonate nuclear track-etched (PCTE) membranes or anodic aluminum oxide films as templates.[27,28] Commercial 6 μm thick PCTE membranes with channel densities of 5-10·10^8 cm^{-2} and channel diameters down to 10 nm are available. Due to the random nature of the pore production process, the pore direction can deviate from the surface normal up to 30°, while some channels may even intersect somewhere inside the PCTE film. Anodic alumina membranes are also commercially available. They are ~50 μm thick and contain cylindrical pores of uniform diameter that are arranged in a hexagonal array. They are prepared by anodization of aluminum metal foils in acidic solutions and have porosities of 25-40%, which is much higher than in PCTE. The channel diameter can be controlled by the applied voltage during anodization and is typically between 20 and 200 nm.

In recent years a significant number of works appeared that deal with the development of switchable interconnects with which certain species from fluids can be transported at will across a semi-permeable barrier.[29,30] One of the pioneering works on fluid transport through nanochannels was performed by C.R. Martin and co-workers.[31,32] The internal pore walls of PCTE membranes were coated with a gold layer using the electroless deposition technique, which yielded straight metallic nano-tubules with channel diameters of 0.8-10 nm. They placed a membrane between two KF electrolyte solutions of different concentration and varied the electrical potential of the membrane relative to the reference potential in the solution with the higher electrolyte concentration. Depending on the sign of the membrane potential relative to the reference electrode, the membrane exhibited complete anion- or cation-permselective behaviour. This effect was attributed to double layer overlap inside the nanotubules, by which means ions of the same sign as the membrane are rejected. The extent of membrane permselectivity can be ex-pressed quantitatively by the transference numbers for cations (t_+) and anions (t_-). For a 1:1 salt such as KF the potential E_m over the membrane is given by

$$E_m = \frac{k_B T}{e}(t_+ - t_-)\ln\left(\frac{a_h}{a_l}\right) \tag{1.6}$$

where a_h and a_l are the activities of the salt at high and low concentration, respectively.[33] The equation indicates that E_m is positive when the tubules are predominantly cation-permselective ($t_+ > t_-$), and negative when they are anion-permselective ($t_+ < t_-$).

The region over which ideal cation- or anion-permselective behaviour was displayed could be extended to higher salt concentrations upon decreasing the radius of the nanotubes. Studies on the permeabilities of complex cationic and anionic species of ~1 nm diameter showed high tuneability of the fluxes with variation of potential.[34] It was shown that the permeability in 1.5 nm channels was mainly due to electrostatic rather than to steric effects. The tuneability was shown to decrease with pore radius and electrolyte concentration. The latter effect is due to

the decrease of double layer thickness, which causes the permselectivity of the channel to decrease.

Another external handle to affect molecular transport in nanosized channels is pH. Bluhm et al. studied the diffusion of mono-, di- and trivalent cations across anodic alumina membranes with pore diameters of 20 and 100 nm as a function of ionic strength and pH.[35,36] It was concluded that the cation diffusion coefficients decreased with cation valency, which was attributed to larger electrostatic interactions between the cations and the positively charged alumina surface at pH below 9. The diffusion rates could be enhanced by increasing the pH of the electrolyte solution from 5 to 8, as this leads to a decrease of the positive surface charge density on the alumina pore walls and thus, to a decreased electrostatic repulsion between cations and channel wall.[35] Larger diffusion coefficients were observed when membranes with larger pore diameter were used, or when the electrolyte strength was increased from 10^{-4} to 0.1 M. Both effects can be explained by a reduction of the fraction of cross-sectional area occupied by the anionic double layer (higher a and κ, respectively).

Sweedler, Bohn and co-workers[5] developed a gateable interconnect for analyte injection in microfluidic devices based on an NTEP membrane, where transport was driven by electro-osmotic flow of the buffer solution through the interconnect, and the selectivity was determined by the double layer overlap in the pore. In contrast to the concept of Martin et al., these interconnects are not ion-selective, but they are capable of transporting small volumes of feed solution into an adjacent channel. Bohn and co-workers also studied the influence of electrolyte strength and pH on the permeability of cationic, anionic and neutral species in aqueous buffer solution.[5,30] They applied PCTE membranes with pore sizes of 15-200 nm. A driving force was established by dc potential differences up to 14 V imposed by two external electrodes. The nanotubes developed a negative surface charge in electrolyte solution, which suggests that the double layer formed at the surface is composed of an immobile adsorbed layer of anions, and a mobile double layer that consists mainly of cations. They found that electro-osmosis and electro-migration were the main modes of species transport under conditions of partial double layer overlap (46-78%) at low (~10 mM) ionic strength, while ion migration became predominant after collapse of the double layer thickness to 4-11% of the pore cross-sectional area at high (1 M) electrolyte concentration.[30] By increasing the pH from 7 to 11 the surface charge density was decreased, which led to a decrease of the electroosmotic flow velocity, and a relative increase of flux contributions from Fick diffusion and ion migration.[5]

1.4 Thesis outline

This thesis describes the feasibility of utilizing an electric field to transport selected charged species through a membrane. This forms the central theme in all chapters. The membranes used can be seen as model systems acting as interconnects between two separate liquids. Electric fields are preferred over pressure gradients as driving force in nanochannels, because very large pressure drops would be required to drive flow in small channels. By applying an external electric field over the interconnects, a potential difference is created

across the membrane, which makes it is possible to selectively drive charged species from one liquid into the other through interconnects, by means of ion migration, Fick diffusion and/or electroosmotic flow.

The investigation is started in Chapter 2 by utilizing state of the art inorganic mesoporous γ-alumina thin films supported on a macroporous α-alumina support structure. The membranes are modified by depositing thin porous gold layers on both sides of the membranes, so that the gold electrodes are incorporated onto the membrane-interconnect. By attaching the electrodes directly on the membrane surface, it transformed into an active membrane-interconnect of which the selectivity could be externally tuned by variation of pH, ionic strength and potential difference over the membrane. As will be shown in Chapter 2, this resulted in a membrane-gate with a tuneable transport rate for cationic species.

An important application field of these switchable gates will be in small fluidic and microfluidic devices. However, there are potential difficulties associated with the implementation and incorporation of the membrane-interconnects used in Chapter 2 into these mostly Si-based devices. It was therefore essential to develop a new class of Si-compatible thin oxide films, which would allow the combination of mesoporous and microporous oxide film technology with existing silicon technology. The general fabrication method of such Si-compatible thin oxide films on micromachined silicon microsieve support structures is presented in Chapter 3. By demonstrating the general fabrication procedure the possibility to incorporate sol-gel type fabrication techniques into existing silicon technology is opened.

The Si-compatible oxide interconnects described in Chapter 3 are used as interconnects to for selective transport of anionic and cationic species in Chapter 4. The electric field-driven transport of species through three different types of oxide interconnects is compared. In this study an electrical potential difference over the interconnect was generated using external platinum electrodes. The influence of the applied potential difference on the transport properties of species through the interconnects are also investigated, along with other factors that play an important part in the transport. These include ionic strength and pH, which regulate the tuneability and selectivity of the system, respectively.

From the investigations presented in Chapters 2 and 4 it became clear that there are a number of ways to open and close switchable gates. These include pH, ionic strength (double layer overlap) and applied electrical potential difference. An alternative way to control the permeability of a gate is investigated is Chapter 5. This chapter describes the use of different surfactants to influence the transport of ionic species through a membrane-interconnect by steric blocking. Surfactants are known to adsorb strongly on oxide surfaces, and adsorption in membrane mesopores will reduce the porosity and permeability of the membrane. Near-complete blocking of ion transport is achieved by formation of surfactant gel layers on or near the membrane-interconnect surface at relatively high surfactant concentrations, while slightly modified ion fluxes are obtained at lower concentrations. Different surfactant species with different tail lengths are compared.

In Chapter 6 the integration of the Si-compatible oxide interconnects that were described in Chapters 3 and 4 into a smaller device type set-up is described. The motivation for incorporating the Si-based interconnects into a smaller device is to simulate the potential behaviour of interconnects in microfluidic devices. Two designs are presented for the fabrication of these types of devices. With these it may be possible to investigate the transport behaviour of species under microfluidic conditions. The principal advantages of working under these conditions are also considered, as well as its importance in various fields of research.

Chapter 7 integrates the main results of the thesis and proposes some additional studies.

1.5 Reference

1. K. B. Jirage, J.C. Hulteen, C.R. Martin, *Science,* **1997**, 278, 655.
2. A. Manz, N. Graber, H.M. Widmer, *Sens. Actuators, B* **1990**, 1, 244.
3. M. Koch, C.G.J. Schabmueller, A.G.R. Evans, A. Brunnschweiler, *Sens. Actuators A* **1999**, 74 207.
4. X. Yang, J.M. Yang, Y.-C. Tai, C.-M. Ho, *Sens. Actuators A* **1990**, 73 184.
5. T.-C. Kuo, L.A. Sloan, J.V. Sweedler and P.W. Bohn, *Langmuir* **2001**, 17, 6298.
6. A, Berezhkovskii and G. Hummer, *Phys. Rev. Let.* **2002**, 89, 064503.
7. R.H. Nilson and S.K. Griffiths, *J. Chem. Phys.* **1999**, 111, 4281.
8. M.P. Moody and P. Attard, *J. Chem. Phys.* **2001**, 115, 8967.
9. D.C. Grahame, *J. Chem. Phys.* **1950**, 18, 903.
10. F. Booth, *J. Chem. Phys.* **1951**, 19, 391.
11. S. Basu and M.M. Sharma, *J. Membr. Sci.* **1997**, 124, 77.
12. R.J. Hunter, *Introduction to Modern Colloid Science*, Oxford University Press: Oxford, **1993**, 194-261.
13. D.E. Yates, S. Levine and T.W. Healy, *J. Chem. Soc. Faraday Trans. I* **1974**, 70, 1807.
14. J.L. Reyes Bahena, A. Roblero Cabrera, A. Lopez Valdivieso and R. Herrera Urbina, *Sep. Sci. Tech.* **2002**, 37, 1973.
15. Y.-H. Li, S. Wang, A. Cao, D. Zhao, X. Zhang, C. Xu, Z. Luan, D. Ruan, J. Liang, D. Wu and B. Wei, *Chem. Phys. Let.* **2001**, 350, 412.
16. L.J. Crisenti and D.A. Sverjensky, *Am. J. Sci.* **1999**, 299, 828.
17. P. Trivedi and L. Axe, *Environ. Sci. Technol.* **2001**, 35, 1779.
18. B.V. Schmud, *J. Colloid Interface Sci.* **1996**, 183, 111.
19. Y. Wang, C. Bryna, H. Xu, P. Pohl, Y. Yang, and C.J. Brinker, *J. Colloid Interface Sci.* **2002**, 254, 23.
20. M. Eigen and E. Wicke, *J. Phys. Chem.* **1954**, 58, 702.
21. H. Strathmann, In *Membrane Science and Technology Series, 9*, Elsevier: Amsterdam, **2004**.
22. R.J. Hunter, *Zeta Potential in Colloid Science: Principles and Applications*, 3rd ed., Academic Press, London, **1981**.
23. C. Wei, A.J. Bard and S.W. Feldberg, *Anal. Chem.* **1997**, 69, 4627.
24. K.-Y. Chun and P. Stroeve, *Langmuir* **2002**, 18, 4653.
25. Y. Kobayashi and C.R. Martin, *Anal. Chem.* **1999**, 17, 3665.
26. E.D. Steinle, D.T. Mitchell, M. Wirtz, S.B. Lee, V.Y. Young and C.R. Martin, *Anal. Chem.* **2002**, 74, 2416.
27. J.C. Hulteen and C.R. Martin, *J. Mater. Chem.* **1997**, 7, 1075.
28. A. Huczko, *Appl. Phys. A* **2000**, 70, 365.
29. A. van den Berg, W. Olthuis, P. Bergveld, (Eds.), *Micro Total Analysis Systems 2000*, Kluwer, Dordrecht, **2000**.
30. P.J. Kemery, J.K. Steehler and P.W. Bohn, *Langmuir* **1998**, 14, 2884.
31. M. Nishizawa, V.P. Menon and C.R. Martin, *Science* **1995**, 268, 700.
32. C.R. Martin, M. Nishizawa, K. Jirage and M. Kang, *J. Phys. Chem. B* **2001**, 105, 1925.
33. N. Lakshminarayanaiah, *Membrane electrodes*, Academic Press: New York, **1976**, 50-94.
34. M.-S. Kang and C.R. Martin, *Langmuir* **2001**, 17, 2753.
35. E.A. Bluhm, E. Bauer, R.M. Chamberlin, K.D. Abney, J.S. Young and G.D. Jarvinen, *Langmuir* **1999**, 15, 8668.
36. E.A. Bluhm, N.C. Schroeder, E. Bauer, J.N. Fife, R.M. Chamberlin, K.D. Abney, J.S. Young and G.D. Jarvinen, *Langmuir* **2000**, 16, 7056.
37. J. Sekulić, J.E. ten Elshof, D.H.A.Blank, *Adv. Mater.* **2004**, 16, 1546-1550.

Chapter 2

Controlling the Transport of Cations through a Permselective Mesoporous Alumina Layers

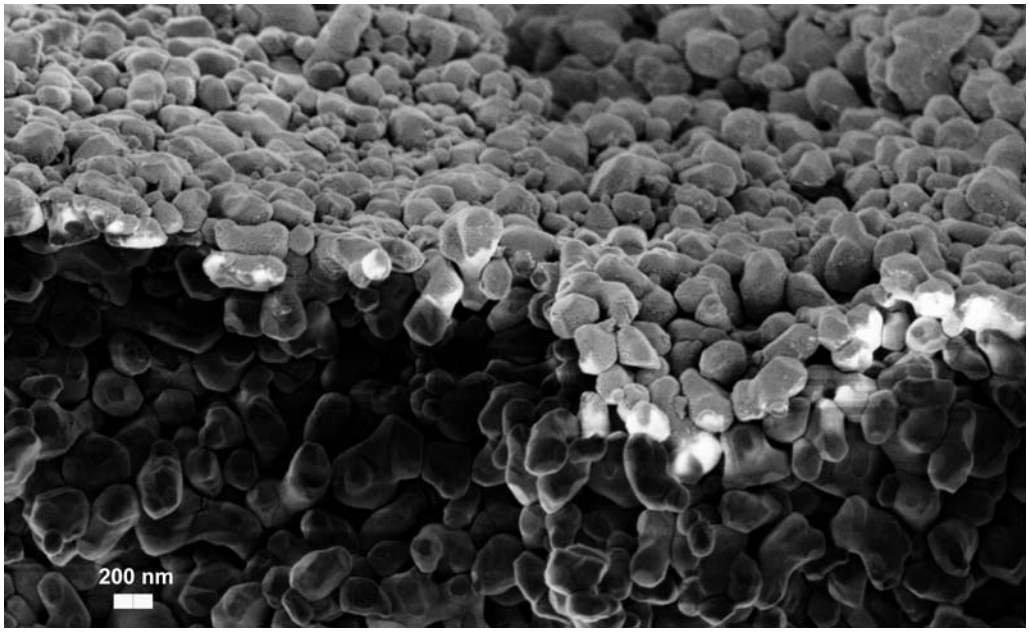

SEM photo of a cross-section of the γ-alumina layers sputtered with gold

Abstract: *The electric field-driven transport of ions through supported mesoporous γ-alumina membranes was investigated. The influence of ion concentration, ion valency, pH, ionic strength and electrolyte composition on transport behaviour was determined. The permselectivity of the membrane was found to be highly dependent on the ionic strength. When the ionic strength was sufficiently low for electrical double layer overlap to occur inside the pores, the membrane was found to be cation permselective and the transport rate of cations could be tuned by variation of the potential difference over the membrane. The cation permselectivity is thought to be due to the adsorption of anions onto the pore walls, causing a net negative immobile surface charge density, and consequently, a positively charged mobile double layer. The transport mechanism of cations was interpreted in terms of a combination of Fick diffusion and ion migration. By variation of the potential difference over the membrane the transport of double charged cations, Cu^{2+} could be controlled accurately, effectively resulting in on/off tuneable transport. In the absence of double layer overlap at high ionic strength, the membrane was found to be non-selective.*

2.1 Introduction

In recent years a significant number of works appeared that deal with the development of switchable interconnects with which certain species from fluids can be transported at will across a semipermeable barrier.[1,2] The development of selective barriers that allow active control over the transport of specific molecular or ionic species may ultimately lead to new intelligent interconnects between fluid channels in micro-chemical systems (MiCS) and micro-total analysis systems (μTAS).[3,4] The ability to move molecules with high precision, selectivity and temporal control may result in smaller devices, lower power consumption and improved accuracy. Materials with switchable molecular functions may lead to completely new approaches to valves, chemical separation and detection.

This chapter demonstrates this principle and shows that high tuneability of flux can be achieved, using a γ-alumina membrane and Cu^{2+} ions as model membrane and species, respectively. The transport of ionic and neutral species through charged γ-alumina membranes mediated by a variable external electric field can be regarded as a model system for some of the types of applications mentioned above earlier.[2,5] Due to the small pore sizes of typically ~5 nm in the γ-alumina layer and the amphoteric surface charge that is present on the internal pore walls, partial or complete overlap of a negatively or positively charged diffuse double-layer may occur inside the pores, depending on the total ionic strength[2] and pH.[6] This may make γ-alumina a predominantly anion-, cation- or non-selective barrier depending on externally tuneable parameters. Further control over the transport of species is obtained by application of an external electric field over a membrane via gold electrodes that are attached to both sides of the membrane.[2,5,7] In the present study the influence of electrolyte type, ionic strength and dc potential difference on the transport rates of ions and neutral solutes through a stacked Au/α-Al_2O_3/γ-Al_2O_3/Au membrane is investigated.

2.2 Experimental

2.2.1 Membrane preparation

The membranes consist of two components: a macroporous support and a thin mesoporous layer with a separative ability. α-Alumina is used as macroporous support and coated with mesoporous γ-alumina layers. The method of preparation of the α-alumina support is by so-called colloidal filtration. A colloidal suspension was made by dispersing 50 wt% α-alumina powder (AKP 30) in 0.02 M nitric acid solution using ultrasonic treatment for 15 minutes. The suspension was filtered over polyester filters (pore size 0.8 μm). The resulting filter cake was dried overnight and fired at 1100 °C for 1h. After firing the supports were machined to the required size and polished.[8] The γ-alumina membranes were prepared by dip coating the sintered α-alumina supports in a homemade boehmite sol. The boehmite sol was prepared by a colloidal sol-gel route, where aluminium-tri-sec-butoxide (ATSB) was hydrolysed and subsequently peptised with HNO_3.[8] The boehmite sol was mixed with a PVA solution, in a

PVA: boehmite mass ratio of 2:3. Dip coating was preformed under class 1000 clean room conditions in order to minimise particle contamination of the membrane layer. After dipping, the membranes were dried in a climate chamber at 40 °C and 60 % R.H. to avoid crack formation in the boehmite layer. γ-Alumina membranes were formed by firing the dried layers at 600 °C for 3 h in air. Laterally conductive macroporous gold layers were sputtered on both sides of the α/γ-alumina composite membrane at room temperature.

2.2.2 Permporometry

The permporometry technique[9] was used to determine the average pore size and pore size distribution of the membranes. Permporometry is based on the controlled blocking of the pores by capillary condensation and the simultaneous measurement of the gas diffusion flux through the remaining open pores. When a condensable vapour (cyclohexane) is introduced at low vapour pressure, first a molecular adsorption layer (the so-called "t-layer") is formed on the inner surface of the pores. When the relative vapour pressure P/P_0 of the condensable gas is increased further from zero to unity, pores with increasingly large radius become blocked due to capillary condensation. The simultaneous gas flux through the remaining open pores provides a measure for the fraction of pores with pore size larger than the pores that are already blocked. Upon desorption the same processes occur in reverse order. The relationship between relative vapour pressure and the capillary condensation of pores with Kelvin radius r_K upon desorption is given by Eq. (2.3):

$$\ln\left(P/P_0\right) = -\frac{2\gamma_s V_m}{r_K RT}, \tag{2.3}$$

where γ_s and V_m are the surface tension and molar volume of the condensable gas, respectively, R is the gas constant and T the temperature.

The relationship between the real pore width (d_p) and the Kelvin radius (r_K) is given by Eq. (2.4):

$$d_p = 2\left(r_K + t\right), \tag{2.4}$$

where t is the thickness of the "t-layer" formed on the inner surface of the pores, which is usually 0.3-0.5 nm. A more detailed description of the permporometry set-up can be found in the article of Cao *et al.*[9]

2.2.3 Transport experiments

The experimental set-up is schematically depicted in Figure 2.1. The membrane was placed between the two halves of a U-shaped tube with the γ-alumina layer exposed to the so-called A side of the membrane (surface area 3.3 cm^2). Aqueous electrolyte solutions (500 ml volume) were added to the A and B side cells and stirred vigorously. The pH was regulated with NaOH or HNO_3 solutions. A dc potential difference ΔV was imposed[5] using a potentiostat. Here ΔV is defined as $\Delta V = V_B - V_A$, with V_A and V_B the electrode potentials at

the A and the B side, respectively. ΔV was typically kept between –0.5 and +0.5 V to prevent Cu reduction. The bias potential $\Delta V_{bias} = V_A - V_{ref}$ between the electrode and the A side solution was monitored with an Ag/AgCl reference electrode. All experiments were performed at room temperature. The ion concentrations were analysed by atomic absorption spectroscopy (Thermo-Optec BV SOLAAR system 939) for Cu^{2+} and ion chromatography (Dionex 120) for K^+, Na^+, Cl^-, F^- and NO_3^-. The ion fluxes were calculated from the concentration changes with time after reaching steady state conditions. Prior to the experiment the membranes were left for 12 h in the B side electrolyte solution to ensure complete wetting. Electro-osmotic flow (EOF) measurements were carried out by adding 8 mM d-tryptophan to the A side and monitoring the concentration change at the B side by a BMG Floustar$^+$ (model 403) microplate reader at the excitation (emission) maximum of 289 (366) nm. The detection limit of d-tryptophan was determined to be 0.5 μM. The pH was regulated with a phosphate buffer at pH 6.9 after imposing a dc potential difference ΔV between –0.5 and +0.5 V. X-ray Photoelectron Spectroscopy (XPS) analysis on membrane fragments was done with a PHI Quantum 2000 scanning X-ray microprobe.

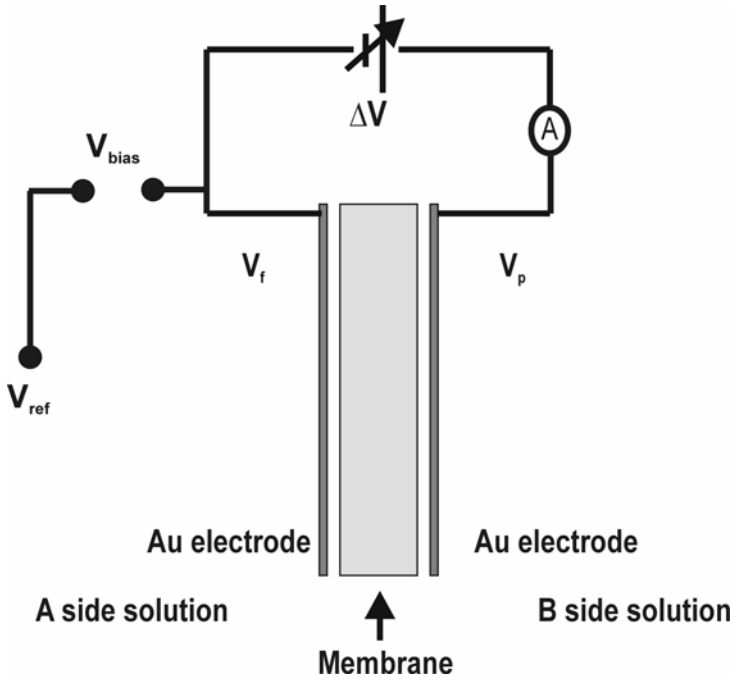

Figure 2.1: Schematic diagram of the experimental set-up for transport experiments.

2.3 Results and discussion

2.3.1 Characterization

The support has a thickness of 2 mm, a pore size of 80-100 nm and a porosity of ~30 %.[10] The γ-alumina layer is ~1 μm thick and has a porosity of 40-50 % as described elsewhere[10] The pore size distribution of the γ-alumina layer supported on α-alumina as determined by

permporometry are shown in Figure 2.2. There is a sharp increase in the number of pores around a Kelvin radius of 2.5 nm using Eq. (2.3), which corresponds to pore sizes in the range of 4.5-7.5 nm. The technique was also used to check for the absence of defects >8 nm in the γ-Al_2O_3 layer.

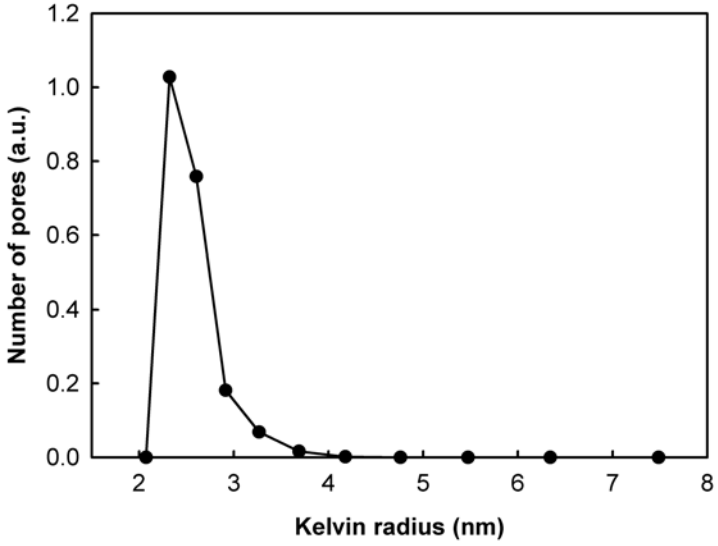

Figure 2.2: Pore size distribution of γ-Al_2O_3 layer, as measured by permporometry.

2.3.2 Transport phenomena

The transport of water-soluble neutral, anionic and cationic species under the influence of a variable electric field over the mesoporous alumina membrane was investigated. The flux of these species was investigated as a function of different parameters such as concentration, pH and electrolyte type. The absolute values of fluxes were found to differ slightly from one membrane to another, however the general trends were reproducible. The electrolyte bulk concentrations in all experiments correspond with Debye lengths κ^{-1} in the range of 3-11 nm, unless stated otherwise. Since r_K is 2.0-3.5 nm, it is expected that complete double-layer overlap occurs inside the γ-Al_2O_3 layer. Figure 2.3 shows the concentration of Cu^{2+} at the B side versus time after the start of the experiment and at various potential differences ΔV over the membrane.

When ΔV was positive, Cu^{2+} ions were transported across the membrane, but under field off conditions and at negative ΔV no transport of Cu^{2+} occurred. The electrolyte compositions were different on the A and B sides of the membrane, so that the transport of all species could be monitored easily. Although the electrolyte strengths on both sides were similar, they were not exactly the same. This leads to a small osmotic pressure difference $\pi = RT\Delta c$ between the two membrane sides (Δc is the ion concentration difference), but since π is typically <0.1 bar, the effect is considered negligible in comparison with the driving force exerted by the electrical field.[11] By varying the potential difference over the membrane no significant

changes in the concentration of anions (NO_3^- and F^-) at the A or B sides were observed, while transport of K^+ and Cu^{2+} did occur.

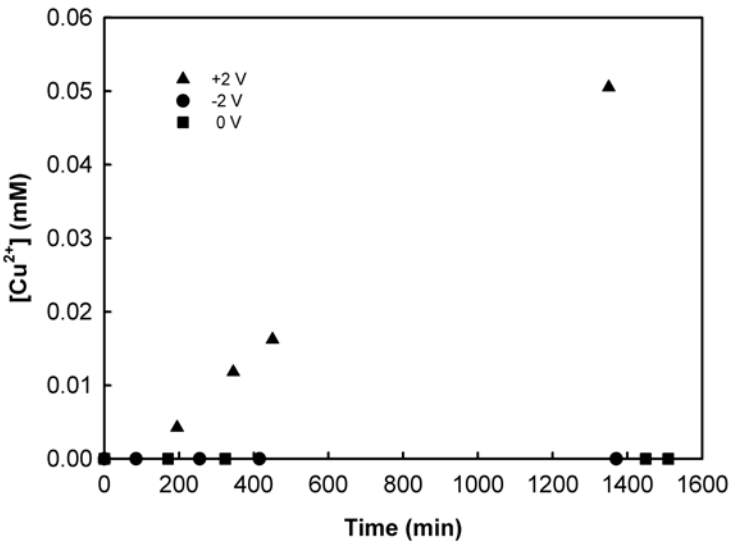

Figure 2.3: Plots of Cu^{2+} ions transported to B side with time at indicated potential differences ΔV. pH = 5.5; Initial concentrations: $[Cu(NO_3)_2]$ = 1.33 mM (A), [KF] = 0.86 mM (B).

Figure 2.4 shows the effect of a positive potential difference over the membrane on the transport of ions. Immediately after the start of the experiment a linear increase of the K^+ concentration on the A side of the membrane with time could be observed. The K^+ accumulation corresponded to a steady K^+ flux of $(1.44\pm0.05)\cdot10^{-5}$ mol/m^2.s. After about 140 min a Cu^{2+} flux of $(3.7\pm0.1)\cdot10^{-7}$ mol/m^2.s in the opposite direction developed. No significant changes in the concentrations of NO_3^- and F^- could be observed during the course of the experiment. To check for the absence of anion transport, a number of other anions including Cl^- and MnO_4^- were also investigated, but irrespective of pH and applied potential difference, no anion transport was observed in any experiment. These results suggest that the γ-alumina membrane has a high permselectivity towards cations.

In all experiments the current was also measured. The Au electrodes were found to be stable as Atomic Absorption Spectroscopy (AAS) analysis did not show any Au present in the A or B side solutions after the experiments. No gas evolution was detected at the electrodes. Therefore, the main electrode reactions occurring are thought to be the oxidation and reduction of H_2O at underpotential.

In general, the imposed potential difference will induce an electrokinetic flow, so that all ion fluxes are due to one or more of three contributions: (1) electro-osmotic flow, which is driven by the mobile double-layer inside the pores and moves the entire liquid under the influence of an electric field gradient, (2) ion migration, which moves charged species toward the oppositely charged electrode, and (3) diffusion, which moves both charged and uncharged species under the influence of a concentration gradient.[2] EOF experiments were carried out

using typical electrolyte solutions containing d-tryptophan as a neutral probe molecule, but it was established that this mode of transport does not contribute significantly to the observed fluxes up to field strengths of at least $\pm 10^3$ V/m ($|i|<1.2$ mA/cm^2).

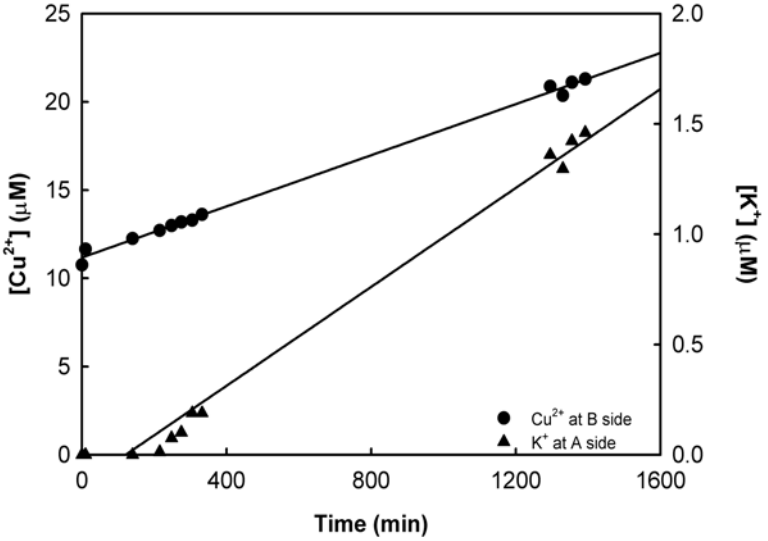

Figure 2.4: Concentration changes of K^+ at the A side and Cu^{2+} at the B side with time. ΔV = 2 V; ΔV_{bias} = – 24 mV, i = 1.0 mA/cm^2; pH = 5.6; Initial concentrations: [$Cu(NO_3)_2$] = 2.67 mM (A), [KF] = 0.86 mM (A), [KF] = 0.86 mM (B). Drawn lines serve as a guide to the eye.

In the experiment shown in Figure 2.4 the net K^+ flux was directed from the positive to the negative electrode while no concentration gradient was initially present. Hence, in this case the K^+ flux must be attributed to ion migration. In contrast, the Cu^{2+} fluxes cannot be explained by the same mechanism, since they were always directed towards the positively charged electrode at low ionic strength. One possible explanation for the observed Cu^{2+} flux could be surface diffusion, since divalent metal cations are known to diffuse over the interior membrane surface.[12] However, the typical surface diffusion coefficients (~10^{-12} m^2 s^{-1}) for this process are too small to explain the magnitude of the observed Cu^{2+} flux entirely.[12] Normal Fick diffusion of solvated Cu^{2+} species will probably contribute much more to the observed flux, but this does not explain the ΔV dependence of the Cu^{2+} flux that is shown in Figure 2.4. The latter effect will be explained later.

2.3.3 Influence of feed concentration and pH

The influence of the Cu^{2+} concentration on flux is shown in Figure 2.5. The flux of Cu^{2+} increased with increasing feed concentration at constant ΔV and pH, although not linearly. It was found that the flux of Cu^{2+} also varied with pH at constant potential difference, as is shown in Figure 2.6.

The flux of Cu^{2+} increased with pH in the range 4.3 to 6.3. On the other hand the flux of K^+ appeared to remain unaffected upon changing pH. This is a further indication that Cu^{2+} and K^+ migrate via different transport mechanisms. There are several possible ways to explain the

effect of pH on Cu^{2+} flux, and either one or a combination of reasons may hold here. The first explanation is that in addition to the observed Cu^{2+} and K^+ fluxes, there is an H^+ flux that is charge-coupled to the Cu^{2+} flux. Since the concentration of H^+ ions, which are ~10 times more mobile than other anions or cations[13], increases with a decrease of pH, an increased H^+ flux may somehow suppress the flux of Cu^{2+}.

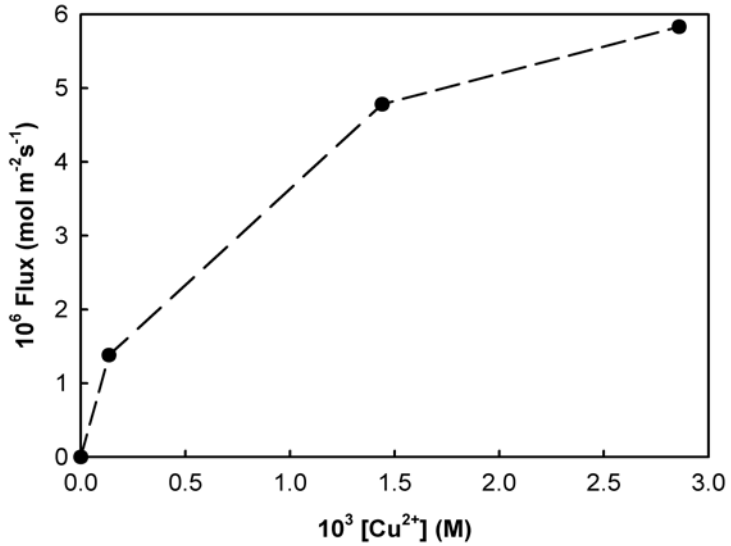

Figure 2.5: Cu^{2+} flux versus initial copper concentration. ΔV = 1 V; pH 6.5; [$CuCl_2$] = 0.14, 1.4 and 2.9 mM (A); [KCl] = 1.34 mM (B).

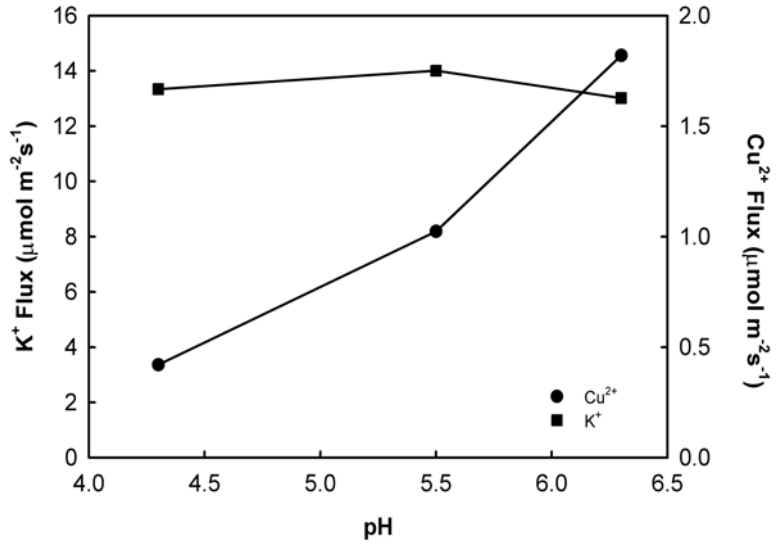

Figure 2.6: K^+ and Cu^{2+} flux as function of pH. ΔV = 0.5 V; ΔV_{bias} = – 0.25 V, i = 0.04 – 0.1 mA/cm^2; Initial concentrations: [$Cu(NO_3)_2$] = 2.7 mM (A), [KF] = 0.86 mM (B).

An alternative explanation is that upon increasing pH the positive surface charge density of α- and γ-alumina decreases via replacement of charged OH_2^+ surface groups by chemisorption of F^- according to the net reaction $Al–OH_2^+ + F^- = Al–F + H_2O$, which occurs maximally at

pH around 6.[14] The decreased concentration of positive surface charge will lead to an increased local concentration of positive charge in the double layer of the pore, thereby promoting the transport of positively charged species (Cu^{2+}) through the pores. Thirdly, the pH may also affect the surface charge density in the pores of the membrane directly via Al–OH_2^+ = Al–OH + H^+, although the alumina surface is saturated with positive charge at pH < 7.[6] However, the effect on the permeability of positively charged species will be similar as the chemisorption of F.

2.3.4 Influence of electrolyte type

It was found that the composition of the electrolyte solution at constant pH and ΔV also influenced the flux of copper ions through the membrane The influence of four electrolyte compositions on Cu^{2+} flux was determined, as shown in Figure 2.7. These included KNO_3, KF, KCl solutions and a mixture of KF and KCl. The presence of chloride in the electrolyte solution strongly promoted the flux of copper ions, while F^- and NO_3^- did not seem to have the same effect. This phenomenon can possibly be explained by chemisorption of chloride on to the gold electrodes, resulting in a negatively charged outer surface of the membrane, and the subsequent local accumulation of Cu^{2+} following Eq. (2.2). A similar phenomenon was reported by Martin *et al.* [15]

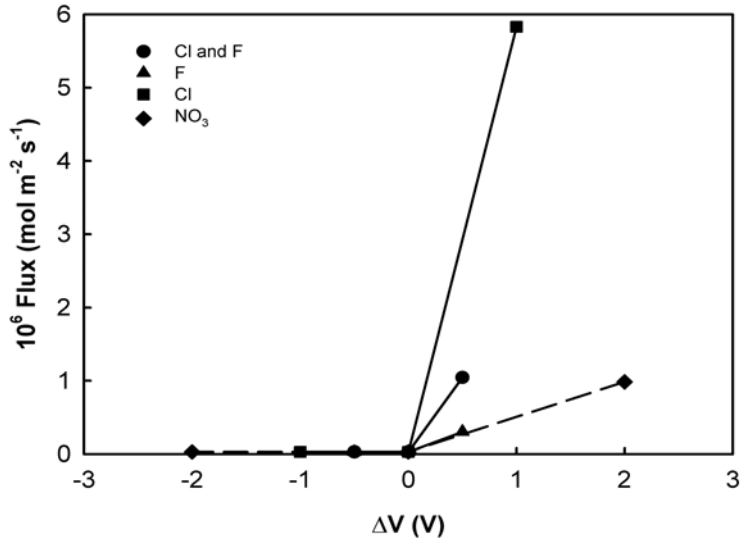

Figure 2.7: Cu^{2+} flux versus ΔV as a function of electrolyte composition. ●: [$CuCl_2$] = 2.3 mM (A); [KF] = 1.8 mM (B); [KCl] = 0.2 mM (B); pH 5.5. ♦: [$Cu(NO_3)_2$] = 2.0 mM (A); [KNO_3] = 2.0 mM (B); pH 5.5. ■: [$CuCl_2$] = 2.8 mM (A); [KCl] = 1.3 mM (B); pH 5.5. ▲: [$CuCl_2$] = 2.3 mM (A); [KF] = 0.8 mM (B); pH 5.6.

The general observation of total permselectivity towards cations under double layer overlap conditions at pH values between 4.3 and 6.5 indicates that the mobile part of the double-layer consists of positively charged ions, which in turn suggests that the interior zeta potential should be negative. This feature cannot be explained by the amphoteric behaviour of the native oxide, which predicts a positive surface charge for alumina below pH 9.1.[14] It

therefore seems more likely that preferential anion adsorption occurred inside the mesopores, producing a largely immobile negative charge density. XPS analysis of several locations on a cross section of the α-Al_2O_3 support after exposure to $Cu(NO_3)_2$ and KF containing solutions showed the presence of F and Cu (<1 at.%), as well as trace amounts of Ca, as is illustrated in Figure 2.8. As was already mentioned, fluoride is known to adsorb specifically on α- and γ-alumina surfaces by chemisorption[14,16], and maximum uptake of fluoride occurs at pH 5-6.[14] Under the assumption that F^- is incorporated and/or physisorbed only at the interior pore surface, the F content measured by XPS appears sufficiently high to cause a net negative fixed surface charge and explain the observed cation permselectivity. Possibly some of the F enrichment can be attributed to precipitated products such as CaF_2, while the formation of surface complexes Al-O-$M^{2+}X^-$, with M^{2+} a divalent metal cation and X^- a negatively charged anion, has also been reported.[17] XPS analysis of alumina membrane fragments after exposure to Cl^- containing solutions also indicated the presence of small amounts of Cl. Hence, a similar explanation may hold here, namely the formation of a net negative membrane surface charge due to adsorption of Cl^- inside the mesopores.[7]

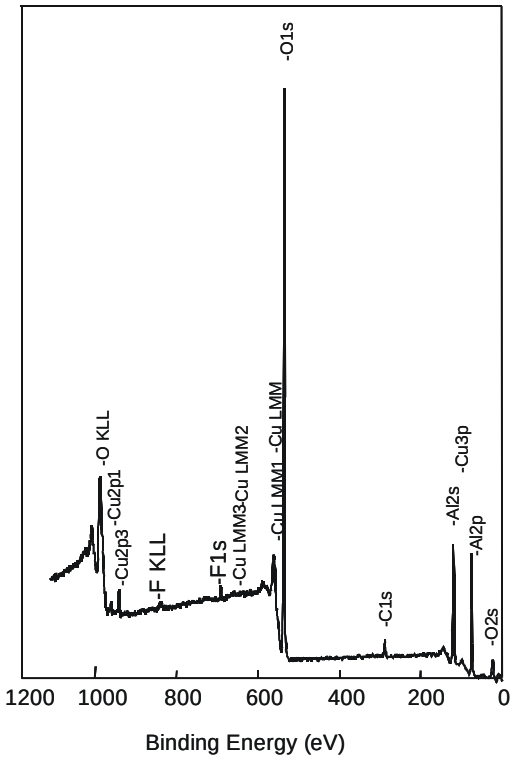

Figure 2.8: XPS analysis of a cross-section of the γ-alumina layer of the membrane after transport experiments with $Cu(NO_3)_2$ and KF containing solutions.

2.3.5 Influence of electrolyte strength

In Figure 2.9 the influence of electrolyte concentration over a wide range of ΔV is shown. At low electrolyte concentrations the flux of Cu^{2+} is especially sensitive to changes of ΔV, while the flux of K^+ is also affected by ΔV, albeit to a lesser extent. On the other hand, at high electrolyte concentrations both anion and cation fluxes were observed. This supports the

hypothesis of total permselectivity towards cations due to double layer overlap. At ionic strengths larger than 0.4 M, the Debye length κ^{-1} is <0.5 nm, so that the double-layer is confined to a small region near the pore walls, and double-layer overlap does not occur. Since chloride and fluoride transport occurs at ΔV=0, the main mode of transport of these species is Fick diffusion. However, the magnitude of these fluxes can be manipulated to some extent by variation of ΔV, and it is seen that anion transport through the membrane is promoted when the electrode with the higher potential is on the other side of the membrane, while the transport rate is suppressed when the electrode with the lower potential is on the other side of the membrane. These trends indicate that ion migration also plays a significant role in the transport of these species.

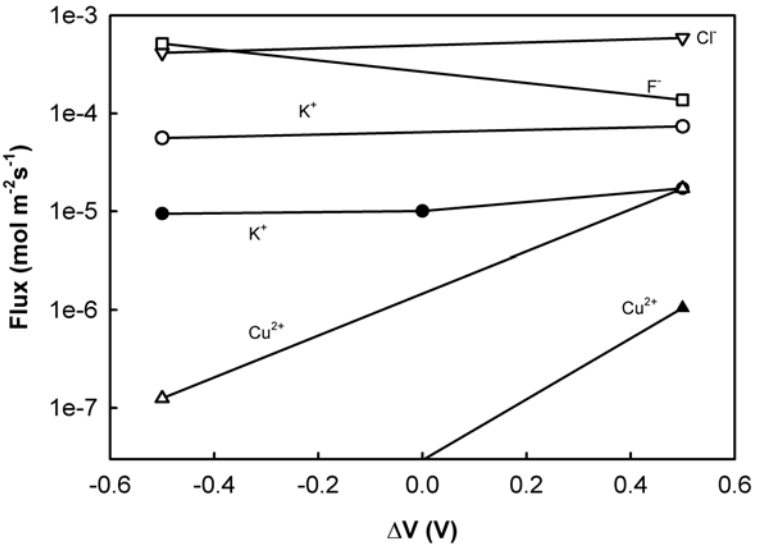

Figure 2.9: Ionic fluxes versus ΔV at high and low bulk ionic strength. Closed symbols: low ionic strength; [$CuCl_2$]=2.3 mM (A), [KF]=1.8 mM (B), [KCl]=0.2 mM (B); pH 5.5. Open symbols: high ionic strength; [$CuCl_2$]=0.23 M (A), [KF]=0.36 M (B), [KCl]=0.04 M (B); pH 6.5. Drawn lines serve as a guide to the eye.

The transport behaviour of K^+ can be explained as well by a combination of Fick diffusion and ion migration both at high and low electrolyte strength. But in contrast to singly charged species, higher Cu^{2+} fluxes were obtained with increasingly positive ΔV for a given feed concentration, i.e., Cu^{2+} is transported preferentially towards the electrode with the higher potential. This counter-intuitive behaviour may be explained by taking into account the changes of bias potential ΔV_{bias} that accompany changes of ΔV. Measured bias potentials for the experiments shown in Figure 2.9 are listed in Table 2.1.

It can be seen that ΔV_{bias} was negative when ΔV was positive, while ΔV_{bias} was positive when $\Delta V \leq 0$. In view of Eq. (2.2), a negative ΔV_{bias} will cause Cu^{2+} to accumulate near the A side interface, while a positive ΔV_{bias} will have the reverse effect. This will alter the driving force for Fick diffusion considerably, so that much higher or lower fluxes will be observed in practice than are expected on the basis of the driving force that is calculated from the bulk

concentration difference over the membrane. Monovalent species are much less sensitive to this effect. Apparently, the effect of a non-zero bias potential on the concentration difference of divalent species such as Cu^{2+} outweighs the effect of ΔV on the rate of ion migration, while it does not for monovalent species. This is illustrated in Figure 2.10.

Table 2.1: Variation of apparent ion permeability P and bias potential ΔV_{bias} with ΔV and ionic strength. Experimental conditions are described in the caption of Figure 2.9.

Ionic strength	ΔV	ΔV_{bias}	Permeability P_i ($cm^2\ s^{-1}$)			
(mM)	(V)	(mV)	Cu^{2+}	K^+	Cl^-	F^-
2-7	0.50	–11	$(1.6\pm0.8)\cdot10^{-5}$	$(1.9\pm0.2)\cdot10^{-4}$	$< 2\cdot10^{-7}$	$< 2\cdot10^{-7}$
	0	41	$< 2\cdot10^{-7}$	$(1.1\pm0.1)\cdot10^{-4}$	$< 2\cdot10^{-7}$	$< 2\cdot10^{-7}$
	–0.50	61	$< 2\cdot10^{-7}$	$(9.9\pm0.9)\cdot10^{-5}$	$< 2\cdot10^{-7}$	$< 2\cdot10^{-7}$
400-700	0.50	–70	$(1.6\pm0.4)\cdot10^{-6}$	$(3.6\pm0.9)\cdot10^{-5}$	$(3.0\pm0.9)\cdot10^{-5}$	$(2.3\pm0.6)\cdot10^{-5}$
	–0.50	137	$(1.1\pm0.8)\cdot10^{-8}$	$(2.7\pm0.7)\cdot10^{-6}$	$(5.2\pm0.1)\cdot10^{-5}$	$(9.9\pm0.9)\cdot10^{-5}$

Although the cation fluxes shown in Figure 2.9 increased strongly with feed concentration, the permeability of the membrane towards cations decreased with increasing ionic strength and decreasing ΔV, while the permeability of anions increased. Permeability coefficients for K^+, Cu^{2+}, Cl^- and F^- are listed in Table 2.1. Here the apparent permeability P_i of species i is defined as $P_i = j_i L/\Delta c_i$, where j_i is the ionic flux, L the total membrane thickness, and Δc_i the bulk concentration difference of i over the membrane.[2]

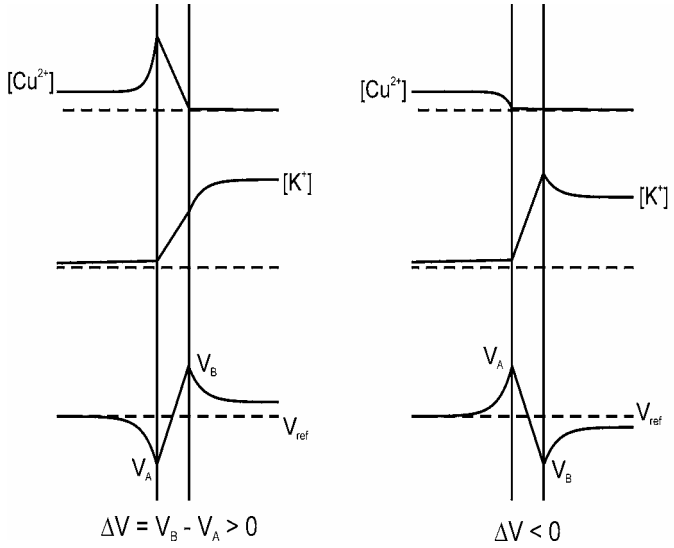

Figure 2.10: Schematic diagram representing the concentration and potential profile, of cations transported, under electrical field conditions.

Figure 2.11 shows the *i*-*V* dependence at high and low ionic strength. At low strength the *i*-*V* dependence was strongly asymmetrical around ΔV=0, while it appeared nearly symmetrical

at high ionic strength. Wei *et al.* observed similar current-rectifying behaviour at low ionic strength in quartz nanopipet electrodes in KCl solutions.[18] The phenomenon was explained by a combination of double-layer overlap near the nanopipet electrode orifice and the geometric asymmetry of the orifice itself. Since double-layer overlap also occurs in γ-alumina at low ionic strength, and the γ-alumina layer has dissimilar interfaces on both sides, the *i*-*V* asymmetry observed here may be explained in a similar way. The asymmetry is most likely due to the dissimilar concentrations and electrolyte types on opposite sides of the membrane. As was shown in Figure 2.9, the transport of all cations was promoted by a positive Δ*V*, and this is reflected by a higher current than found at negative Δ*V*. The symmetrical *i*-*V* behaviour at high ionic strength is consistent with this explanation. Since double-layer overlap does not occur under these conditions, current rectification will not occur either.

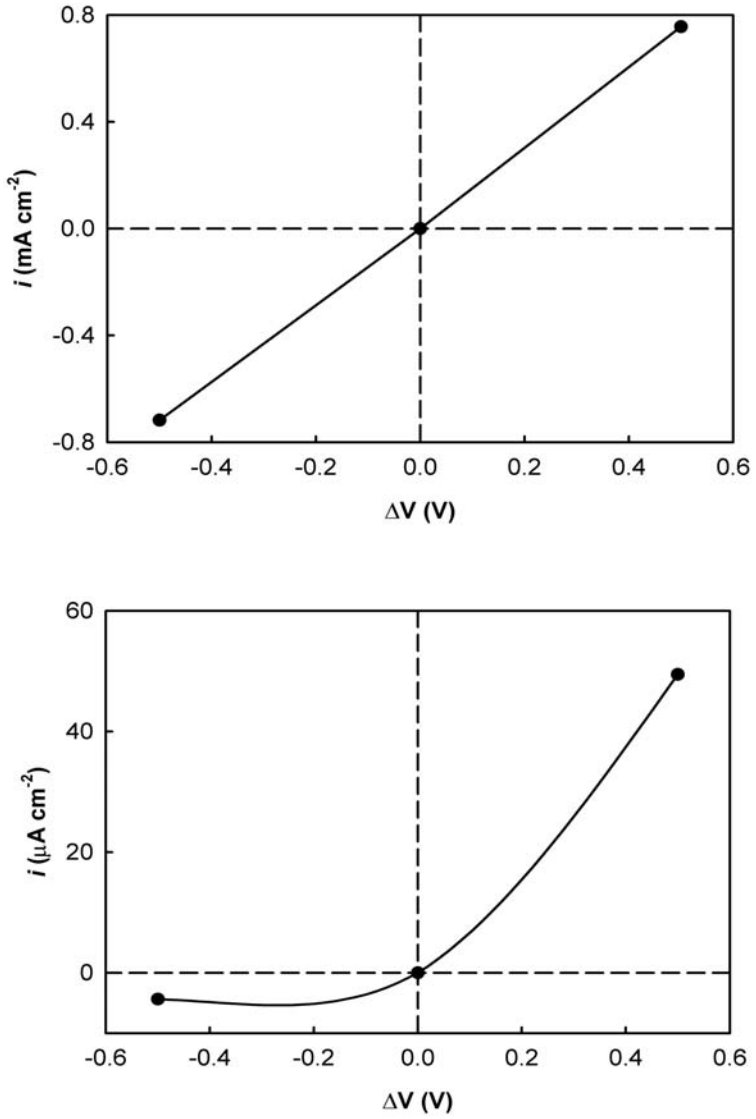

Figure 2.11: Current density *i* versus Δ*V*. (a) High electrolyte strength and (b) at low electrolyte strength. Experimental conditions are described in the caption of Figure 2.5.

2.4 Conclusions

It was shown that it is possible to control the transport rate of cations through γ-alumina membranes by variation of the potential difference over the membrane. The permeability of ions was found to be strongly dependent on the dimensions of the electrical double layer relative to the pore diameter and the sign of the applied potential. Cation permselective behaviour was observed at low ionic strengths, which suggests a net negative charge density on the inner pore walls due to anion adsorption. In the absence of double layer overlap both anion and cation transport was observed. The transport mechanism of single charged ions was a combination of Fick diffusion and ion migration and the rate of transport could be controlled to some extent by variation of ΔV. The transport of doubly charged Cu^{2+} ions was found to occur mainly by Fick diffusion and could be controlled completely by variation of ΔV.

2.5 References

1. A. van den Berg, W. Olthuis, P. Bergveld, (Eds.), *Micro Total Analysis Systems 2000*, Kluwer, Dordrecht, **2000**.
2. P.J. Kemery, J.K. Steehler, P.W. Bohn, *Langmuir* **1998,** 14, 2884.
3. A. van den Berg and T.S.J. Lammerink, *Topics Curr. Chem.* **1997,** 194, 21.
4. Y. Fintschenko, A. van den Berg, *J. Chrom A.* **1998,** 819, 3.
5. T.-C. Kuo, L.A. Sloan, J.V. Sweedler, P.W. Bohn, *Langmuir* **2001**, 17, 6298.
6. E.A. Bluhm, E. Bauer, R.M. Chamberlin, K.D. Abney, J.S. Young, G.D. Jarvinen, *Langmuir* **1999,** 15, 8668.
7. M. Nishizawa, V.P. Menon, C.R. Martin, *Science* **1995**, 268, 700.
8. N. Benes, A. Nijmeijer, H. Verweij, in: N.K. Kanellopoulos, (Eds.), *Recent advances in gas separation by microporous ceramic membranes*, Elsevier: Amsterdam, **2000**, 335-372.
9. G.Z. Cao, J. Meijerink, H.W. Brinkman, A.J. Burggraaf, *J. Membrane Sci.* **1993**, 83, 221.
10. P.M. Biesheuvel, H. Verweij, *J. Membrane Sci.* **1999**, 156, 141.
11. For dilute solutions the driving forces exerted by the pressure and electric field gradients can be expressed as $-(v_i / k_B T)(d\Pi / dx)$ and $-(z_i e / k_B T)(dV / dx)$, respectively, with v_i the species velocity and x the direction of transport (L. Pupunat, G.M. Rios, R. Joulié, *Sep. Sci. Technol.* **1999**, 34, 1947). Evaluation of the magnitude of these driving forces indicate that the force exerted by the electrical field is a factor of ~1000 higher than the force exerted by the osmotic pressure.
12. P. Trivedi, L. Axe, *Environ. Sci. Technol.* **2001**, 35, 1779.
13. P. Atkins, J. de Paula, *Atkins' Physical Chemistry*, Oxford University Press: Oxford, **2002**.
14. J.L. Reyes Bahena, A. Roblero Cabrera, A. Lopez Valdivieso, R. Herrera Urbina, *Sep. Sci. Technol.* **2002**, 37, 1973.
15. C.R. Martin, M. Nishizawa, K. Jirage, M. Kang, S-K. Lee, *Adv. Mater.* **2001**, 13, 1351.
16. Y.-H. Li, S. Wang, A. Cao, D. Zhao, X. Zhang, C. Xu, Z. Luan, D. Ruan, J. Liang, D. Wu, B. Wei, *Chem. Phys. Let.* **2001**, 350, 412.
17. L.J. Crisenti, D.A. Sverjensky, *Am. J. Sci.* **1999**, 299, 828.
18. C. Wei, A.J. Bard, S.W. Feldberg, *Anal. Chem.* **1997**, 69, 4627.

Chapter 3

Preparation of Silicon-Supported Oxide Interconnects

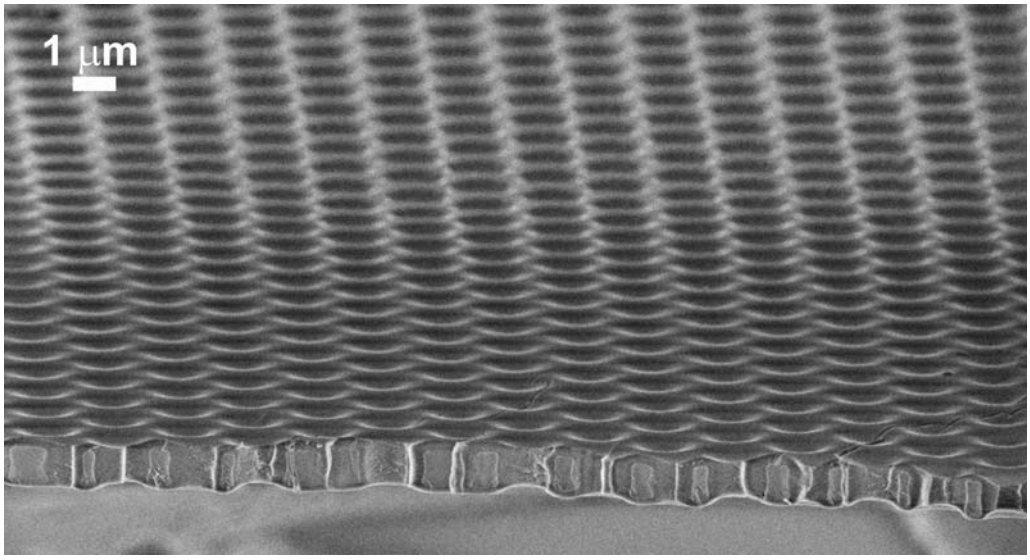

SEM photo of a cross section of MCM-48 interconnect

Abstract: *A new class of Si-compatible porous oxide interconnects for gateable transport of ions is presented in this chapter. The integration of such thin oxide films in microfluidics devices has been hampered by the compatibility of oxides with silicon technology. A general fabrication method is given for the manufacture of silicon-microsieve support structures by micromachining, on which a thin oxide layer is deposited by the spin coating method. The deposition method was used for constructing γ-alumina, MCM-48 silica and amorphous titania films on the support structures. Both water-based and solvent-based oxide sols were used. The final structures can be applied as ion-selective electrophoretic microporous and mesoporous interconnecting walls between two microchannels.*

3.1 Introduction

Switchable interconnects for controlled transport of molecular or ionic species, charged nanoparticles or biomolecules may lead to enabling microchip-based technologies for molecular separation, detection and dosing. One of the issues in microfluidic device technology concerns the development of such selective gates. Although permselective mesoporous and microporous oxide membranes with well-defined pore sizes and pore architectures on ceramic supports have been developed in the past years, their application in microfluidic devices remains a challenge due to the need for these films to be compatible with silicon technology. The current interest in microfluidics is largely motivated by their envisaged applications. Microfluidic analyses are quickly becoming an established technology in analytical chemistry and biotechnology,[1] while the large potential that microfluidic approaches may offer in the field of synthetic chemistry has only started to be explored.[2] Micro-chip based fluidic devices for chemical analyses or syntheses have several unique advantages over macroscopic approaches, such as a very high degree of temporal control over temperature and chemical environment, high accuracy, and relatively easy automation and integration of functional components like heaters, temperature controllers and feeding channels.[3,4]

Till date, selective interconnects for microfluidic devices[4,5] are based on track-etched polymeric (NTEP) membranes and anodic aluminum oxide (AAO) thin films.[6] For instance, Sweedler, Bohn and co-workers[7] developed a gateable interconnect for analyte injection in microfluidic devices based on an NTEP membrane. NTEP membranes are made by bombarding 6-20 μm thick nonporous sheets of polycarbonate or polyester with nuclear fission fragments which create straight damage tracks in the sheet, which are subsequently turned into pores by chemical etching. Commercially available NTEP membranes have pores densities of $3\text{-}10 \cdot 10^8$ cm^{-2} and pore diameters down to 10-15 nm.[7] AAO films are thicker, typically ~50 μm, and contain straight cylindrical pores of 10 nm diameter or larger.[8] They are prepared by anodization of aluminum metal foils in acidic solutions and have porosities of 25-40 %, much higher than in NTEP membranes.

Integration of AAO and NTEP with existing silicon technology is not straight-forward. This motivated the development of a new class of interconnects. It has a silicon-based support structure for mechanical stability, with a selective oxide top layer. The composition, microstructure and permeability can be varied at will depending on the targeted function of the interconnect. The oxide films that were used here cover a wide range of pore sizes with narrow pore size distributions. The principle is demonstrated for mesoporous γ-alumina and template-directed MCM-48 silica films,[9] as well as for microporous titania coatings. These thin films can be made cheaply and easily. The pore architectures of the oxide films are all different: γ-alumina has a disordered mesopore structure, while MCM-48 has a mesostructured template-directed pore architecture, and titania is microporous. Because of its

silicon-based support structure these gates can be easily integrated with existing silicon technology.

3.2 Experimental

3.2.1 Preparation of microsieves

The microsieve[10] was made using silicon micromachining. This is schematically represented in Figure 3.1. A single crystalline silicon wafer (type <110>) was coated with a thin layer of lpcvd (low pressure chemical vapor deposition) silicon nitride. At a temperature of 850°C, a gas mixture of dichlorosilane (SiH_2Cl_2) and ammonia (NH_3) will react and will form silicon nitride. Using an excess of dichlorosilane (70:18), silicon rich nitride was formed that has less internal stress than stoichiometric nitride and is as such a good membrane material.[11] In step 2, by exposure to ultra violet light, a pattern containing the small openings (1.2 μm or 500 nm) in a mask was exposed using a wafer stepper. After development, the pattern was etched in the silicon nitride using reactive ion etching (RIE), with a gas mixture of CHF_3 (25 sccm.) and O_2 (5 sccm.) at 10 mTorr, 75 Watt (step 3).

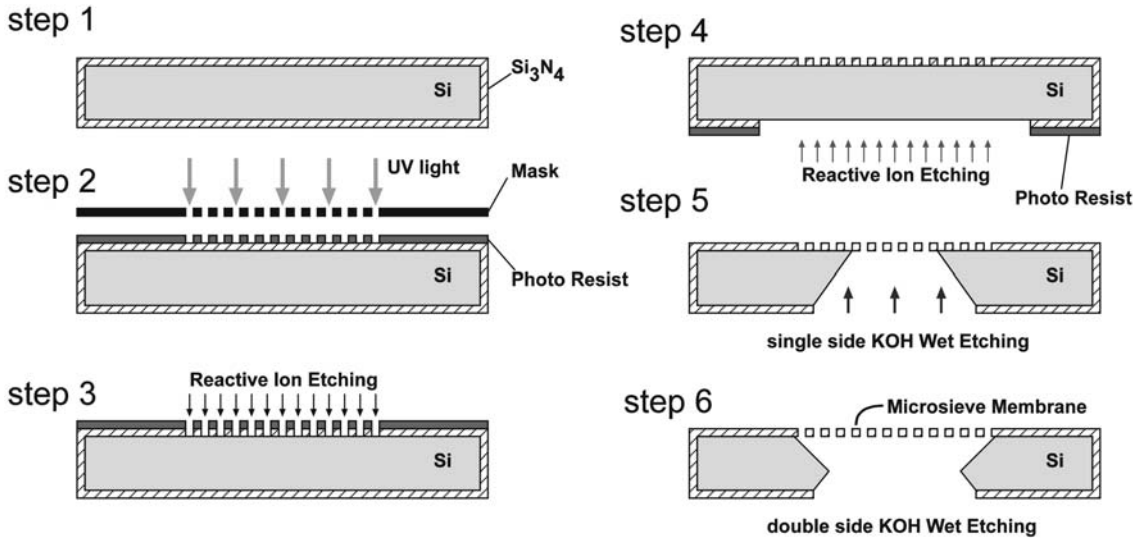

Figure 3.1: Schematic representation of the processing steps for the microsieve membrane.

To obtain a free hanging membrane, the silicon wafer was etched as a support structure by first etching openings from the back of the wafer by lithography and reactive ion etching (step 4). Then by wet etching of KOH the silicon was removed from the back until the front side of the wafer was reached (step 5). In the last step, the silicon under the membrane was removed completely. A SEM picture indicating the pattern of perforated areas is shown in Figure 3.2(a) and the hexagonal array of circular perforations in Figure 3.2(b). The effective thickness of the perforated area is 1 μm with an overall porosity of 30%.

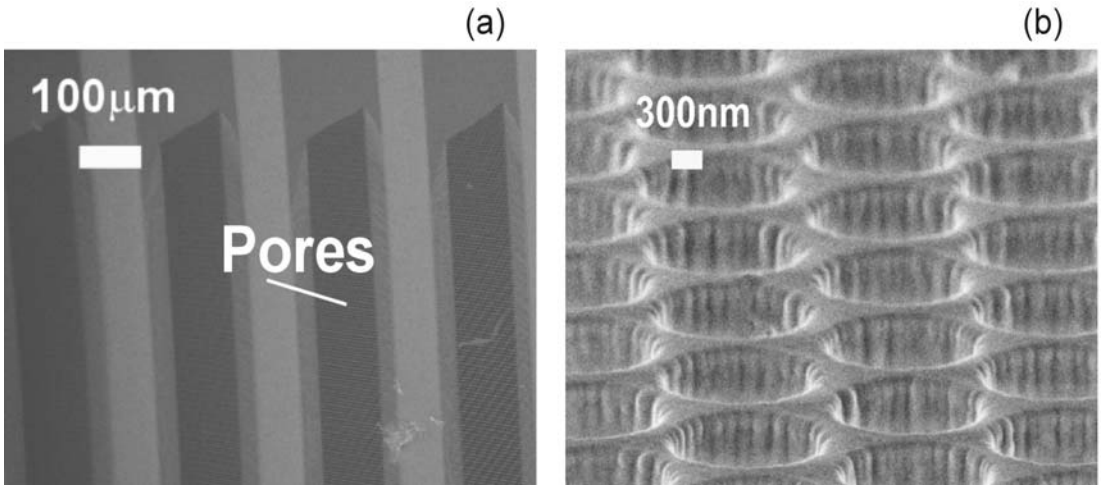

Figure 3.2: (a) SEM picture of the perforation pattern on silicon nitride microsieves. (b) Overview of uncoated 1.2 μm perforations.

3.2.2 Preparation of porous oxide interconnects

(i) Surfactant-templated silica sols were synthesized using the cationic surfactant cetyl-trimethyl-ammonium bromide (CTAB, Aldrich) and tetraethoxy-orthosilicate (TEOS, Aldrich) derived sols as described elsewhere.[12] The required amount of TEOS was mixed with 1-propanol and stirred. TEOS was then hydrolyzed by addition of an aqueous HCl solution. 2-Butanol was added to the sol and the mixture was stirred for another 30 min. The surfactant and water solution was prepared separately and added to the TEOS sol and stirred for 60 min.

(ii) Polymeric titania sols were prepared using titanium tetra-ethoxide (Aldrich) as precursor, and nitric acid (Merck, 65 % solution) as acid catalyst to promote the formation of polymeric sols. A given amount of water / nitric acid solution was dissolved in alcohol and added under vigorous stirring to a titanium alkoxide / alcohol solution. The synthesis was performed in a dry nitrogen atmosphere to avoid possible reactions of the alkoxides with water vapor from ambient air.[13]

(iii) Boehmite sols were prepared by a colloidal sol-gel route, in which aluminium-tri-sec-butoxide (Merck) was hydrolysed in water and subsequently peptised with HNO_3.[14] The boehmite sol was mixed with a PVA solution, in a PVA: boehmite mass ratio of 2:3.

Spin-coating was used to deposit the sols on silicon nitride Microsieves® with 500 or 1200 nm perforations. Spin coating was preformed under class 1000 clean room conditions in order to minimise contamination of the membrane layers. The water-based boehmite sols were applied in two successive coatings, while one coating was applied for the alcohol-based silica and titania sols. The silica layers were dried at room temperature and heated to 450°C in air for 2 h to calcine the film and remove residual organics. The titania layers were dried in a moisture-free alcohol vapour-saturated atmosphere and calcined at 300°C for 3 h. The

boehmite layers were dried in a climate chamber at 40°C and 60 % R.H. to avoid crack formation in the layer. The γ-alumina phase was formed after firing the dried layers at 600°C in air.

3.2.3 Oxide film characterization techniques

X-ray diffraction (XRD) patterns were recorded using a Philips SR5056 with Cu Kα radiation. The internal surface area, pore volume and average pore size distribution were obtained from nitrogen sorption isotherms using an adsorption porosimeter (Micromiretics, ASAP 2400). The Berret-Joyner-Halenda (BJH) method was used in data processing. Assuming cylindrical pores geometry, the pore sizes were calculated from the Kelvin equation.[15] The permporometry technique is described in detail in the article of Cao *et al.*[16] The thickness and quality of oxide layers was checked with HR-SEM (LEO Gemini 1550 FEG-SEM, UK).

The pore size of microporous titania was determined by the Stokes-Einstein radius model[17] from molecular weight cut-off tests with 0.5 wt % of various molecular weight polymers (ethylene glycol (EG), diethylene glycol (DEG), triethylene glycol (TEG), and polyethylene glycol (PEG), all obtained from Merck) at a pressure of 8 bar.

Reflectometry measurements were performed on high resolution 4-circle diffractometer (PHILIPS, The Netherlands). The instrumental resolution stays within a range of 0.035 - 0.15° for parafocusing geometry and within 0.0015 - 0.3° for parallel beam geometry. Data processing was carried out using Philips software X'Pert Reflectivity.

3.3 Results and discussion

The fabrication technique is demonstrated by fabricating three different oxide interconnects.[18-21] To give these layers sufficient mechanical stability they were deposited onto 0.5x0.5 cm Microsieves of 1 μm effective thickness, which contained areas with hexagonal arrays of circular perforations of 0.5 or 1.2 μm and have a total porosity of 30%.[10]

Interconnects with different types of oxide top layers were prepared, namely conventional mesoporous γ-alumina layers, mesoporous MCM-48 silica layers obtained by template-directed synthesis of self-assembled surfactants,[21] and microporous amorphous titania layers. Figure 3.3(a) shows an interconnect with a calcined MCM-48 layer that was deposited on the microsieve by spin coating. The MCM-48 layer penetrated the perforations of the sieve, yielding an average thickness of 970 nm and a thickness of 650 nm in the center of the perforations. Top and cross-section views of microsieves spin-coated with titania and γ-alumina are shown in Figures 3.3(b) and (c), respectively. Cross sections of the α-alumina and titania layers spin coated on microsieves reveal that plugs formed inside the perforations, with thicknesses of ~300 nm and ~500 nm for the γ-alumina and titania layers, respectively. To achieve a defect-free γ-alumina layer from the water-based boehmite sol, it was necessary to apply two coatings to overcome surface tension effects that resulted in non-closed pores

after a single coating. This was not necessary for the solvent-based sols where one coating sufficed to form a defect-free layer. The thicknesses of the oxide films are listed in Table 3.1. The thickness of the films could be varied by variation of the concentrations of the sols, and was also partly determined by variations in diameter of the 0.5-1.2 μm perforations.

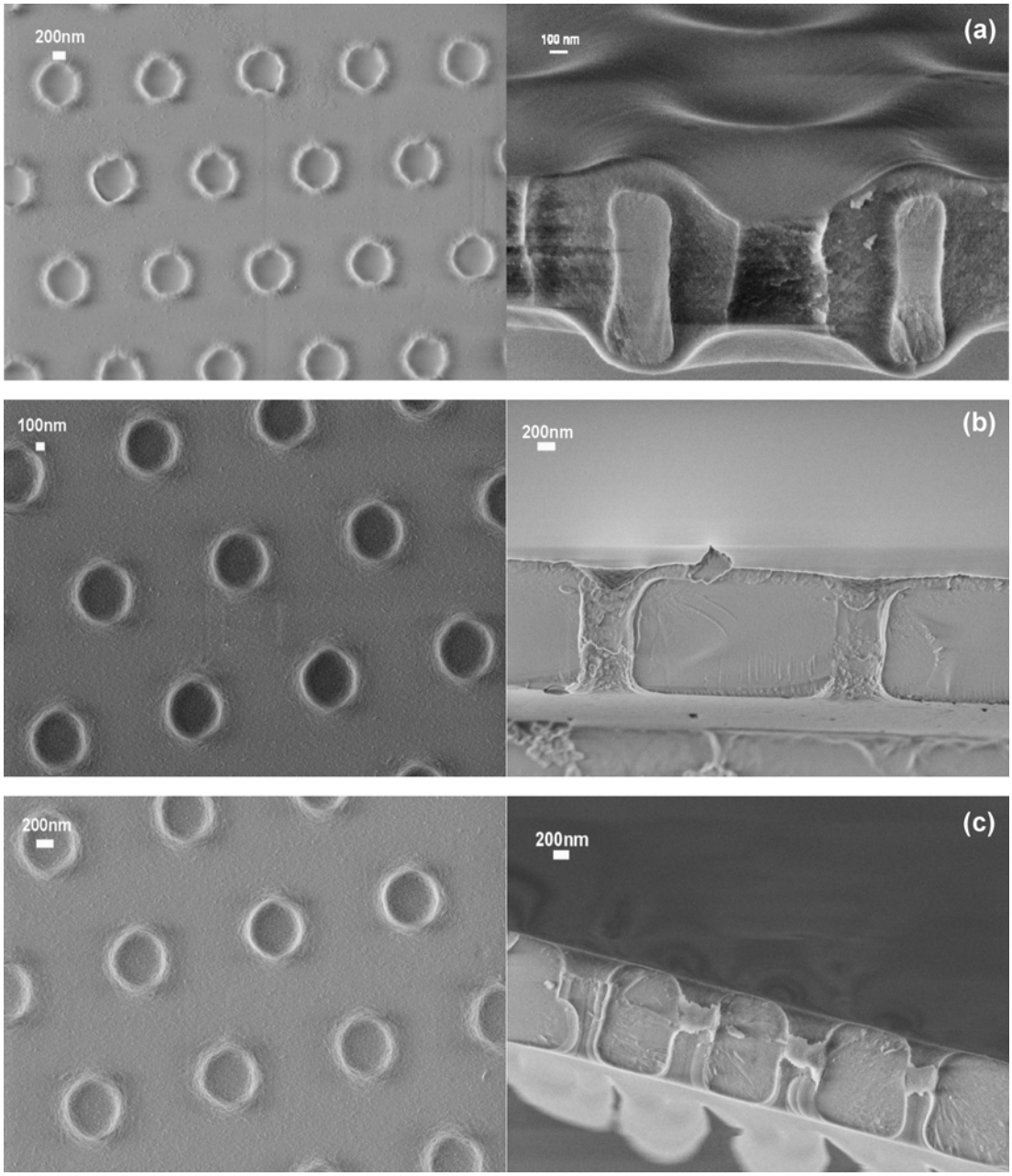

Figure 3.3: SEM pictures of three different oxide layers spin coated on microsieves with 500 nm and 1.2 μm perforations. Top and cross section views of (a) MCM-48, (b) Microporous TiO_2 and (c) γ-alumina layers deposited on microsieves.

The presence of ordered mesoporosity in the silica films is illustrated in Figure 3.4(a), where a small angle XRD pattern of a calcined silica film spin coated on a silicon substrate is

shown. The pattern matches that of an ordered mesoporous MCM-48 phase with unit cell a~9.4 nm.[22] The peak at 2θ 2.3 and the shoulder at 2.6° are the 211 and 220 reflections, respectively, while the broad shallow peak at 2θ 4.5-6° indicates a series of higher order reflections. While Figure 3.4(b) shows that MCM-48 powder has a typical type I adsorption/desorption curve, indicating that it has a microporous structure with ~42% of the total porosity being microporous. The BET surface area is 1030 m^2 g^{-1} and a typical value for MCM-type materials. The average pore diameter of MCM-48 was calculated from nitrogen sorption data of unsupported MCM-48 powder and was found to be 2.1 nm. The overall porosity of MCM-48 was 54%.

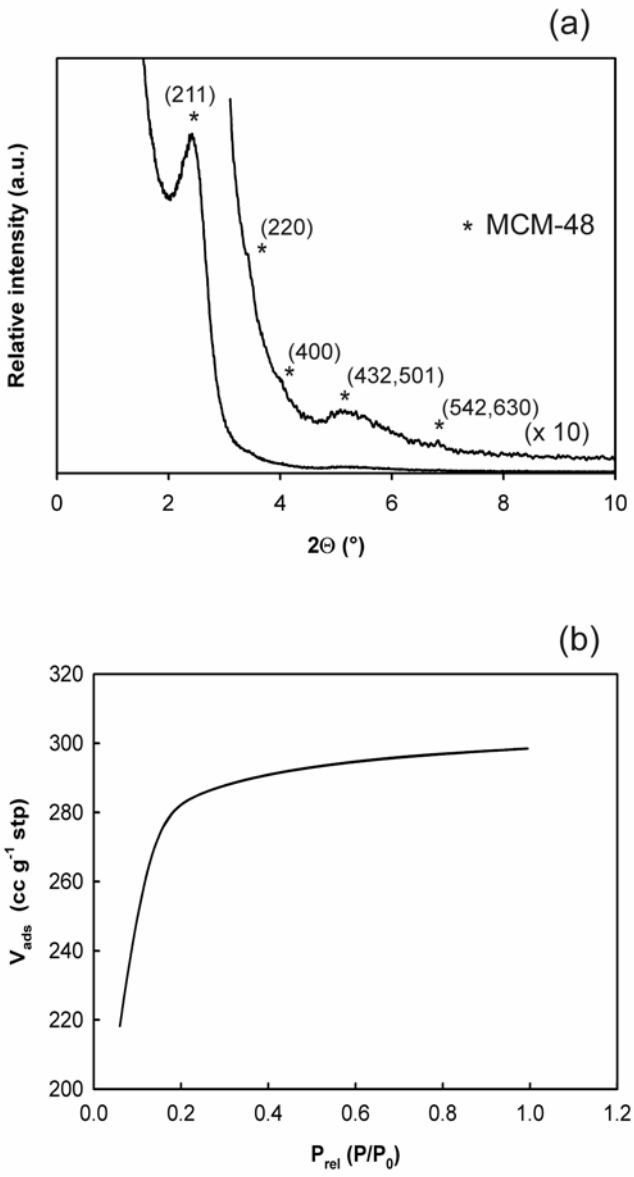

Figure 3.4: (a) XRD diagrams of uncalcined air-dried and calcined MCM-48 silica thin films on silicon (004), (b) Nitrogen adsorption/desorption isotherms of MCM-48 powder.

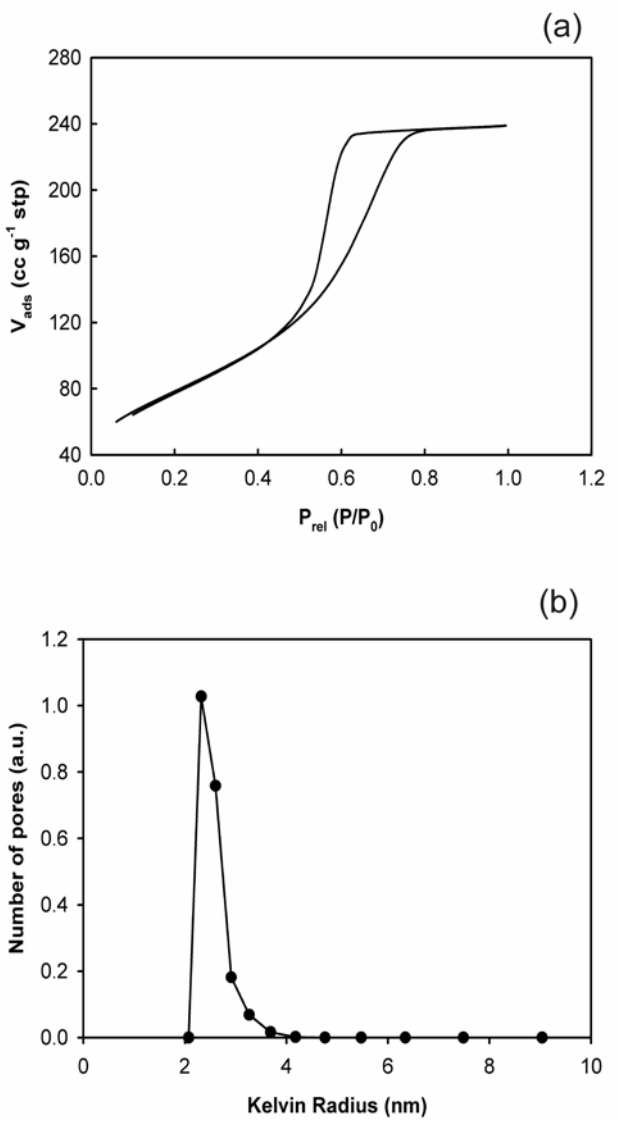

Figure 3.5: (a) Nitrogen adsorption/desorption isotherms of γ-alumina. (b) Pore size distribution of γ-alumina film calcined at 600°C as determined by permporometry.

Figure 3.5(a) shows the nitrogen adsorption/desorption isotherms of γ-alumina powder. The shape of the curve is type IV, which indicates that the γ-alumina powder has a mesoporous pore structure, a BET surface of 285 m^2 g^{-1}, an average pore size of 4.4 nm and a total porosity of 54%. The pore size distribution was directly determined from a supported γ-alumina thin film by the permporometry technique[20] and is shown in Figure 3.5(b). Since the pore diameter is equal to $2(r_K + t)$, where t is the t-layer thickness (t=0.3-0.4 nm),[15] the pore sizes of γ-alumina are in the range of ~5 to 7.5 nm. This is in agreement with the pore size of 4.4 nm calculated from the adsorption/desorption isotherms of powders, when it is taken into account that the pore sizes in unsupported powders are smaller than those in a supported film. Figure 3.6(a) shows the temperature programmed XRD spectra of dried polymeric TiO_2 sols. The material retained its amorphous structure until 300-350°C. At 400°C a (partial) phase transformation into the crystalline anatase phase occurred. Unlike anatase, which is mesoporous, the amorphous phase of titania is microporous.

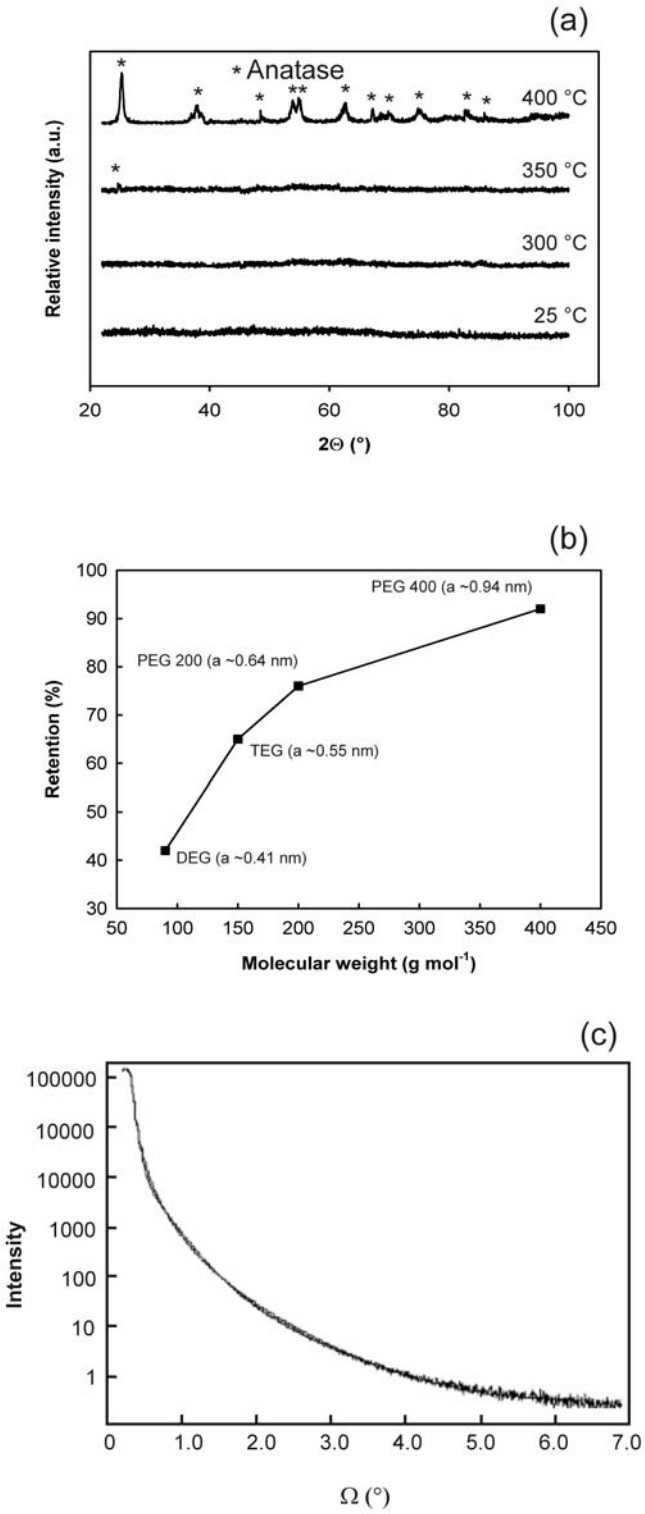

Figure 3.6: (a) High-temperature XRD diagrams of amorphous microporous titania. (b) Retention behaviour of microporous titania membrane, (c) Reflectivity curves (experimental and fitted values) of amorphous TiO_2 layer

The maximum pore size of the titania membrane was estimated by nanofiltration tests with solutions containing ethylene glycol based compounds with molecular weights in the range of

60-400 g mol^{-1}. The molecular weights of the glycol molecules were correlated with their molecular sizes via the Stokes radius model, according to the equation:

$$a \approx 0.1673 \cdot M^{0.557} \tag{3.1}$$

where a is the Stokes radius in Å, and M is the molecular weight in g mol^{-1}.[23] As can be seen in Figure 3.6(b), the retention of ethylene-glycol molecules increases with molecular size, and exceeds a value of 90 % for PEG, M_w = 400 g mol^{-1}. A relatively high retention is observed for all employed molecular sizes. Taking the calculated Stokes radii Eq. (3.1) of various molecules into account, the pore size of the titania membrane can be estimated to be ≤0.9 nm. Although the molecular weight cut-off measurements can only give a rough estimate of membrane pore size, the result is in good agreement with the observations from the other characterization techniques. This confirms the successful formation of a stable, defect-free titania membrane with pore size in the sub-nanometer range.

For further characterisation of the layers, reflectivity measurements were carried out. X-ray reflectivity is a non-destructive technique used for estimation of layer thickness, density and surface (or interface) roughness. It is based on total external reflection of x-rays and a measurement of the scattering from a set of layers (not atomic planes) that have a contrast of density and scattering power.[24] An advantage of the method is that it is insensitive to the crystallinity of the layer and it may therefore be applied to amorphous, polycrystalline or epitaxial layers. A wide angle XRD scan was made prior to the reflectivity measurement to ensure the absence of additional crystalline phases that could disturb the reflectivity measurements. No trace of a crystalline titania phase was found. The reflectivity data are shown in Figure 3.6(c). After data processing the porosity was calculated to be 18 %.

Table 3.1: Physical, structural and transport properties oxide interconnects**.**

	TiO_2	MCM-48	γ-Al_2O_3
Iso-electric point	4.2-4.8	2-3	8.5-9
Pore size (nm)	~0.9[a]	~2.1[b]	5-7.5[c]
Porosity of oxide	18	54	55
Total porosity of interconnect (%)[e]	5.4	16	16
Film thickness[f] (nm)	~500	~970	~300

[a] Based on molecular weight cut-off nanofiltration experiments with polyethylene glycol (PEG) solutions. [b] Based on nitrogen sorption data of unsupported calcined powder. [c] Determined by permporometry. [d] Estimated by reflectometry. [e] Porosity is calculated for oxide layers supported on microsieve. [f] Thickness of the MCM-48 layer was determined on a microsieve with perforation of 1.2 μm, while for the others a microsieve with 500 nm perforations were used.

The main physical and structural properties of the oxide top layers of which interconnects were made are summarized in Table 3.1. From the summary it is clear that oxide layers with different intrinsic materials properties can be fabricated.

3.4 Conclusions

In summary, this chapter describes a new class of porous oxide interconnects with a silicon nitride support structure for application in Si-based microfluidic devices. The general applicability of the fabrication method was demonstrated by constructing γ-alumina, MCM-48 silica and amorphous titania interconnects from water- and solvent-based sols. Both conventional and template-directed sol-gel methods were employed. In the latter case regular mesostructured mesoporous oxide films (MCM-48 type) with a very high porosity of ~16%, and a narrow pore size distribution with mean diameter of ~2 nm can be formed. The microsieve-supported γ-alumina interconnects have a porosity of 16% and a pore size of 5-7 nm. Interconnects with smaller pores, i.e., < 0.9 nm, were made via a recently developed polymeric titania synthesis route. The advantage of constructing thin films of different oxides is that the properties of the interconnects can be varied depending on the application.

Acknowledgements

We want to thank Aquamarijn Micro Filtration B.V., Berkelkade 11, 7201 JE Zutphen, The Netherlands for supplying the Microsieves used in this chapter and Chapter 4.

3.5 References

1. a) D.R. Reyes, D. Iossifidis, P.-A. Ayroux, A. Manz, *Anal. Chem.* **2002**, *74*, 2623. b) P.-A. Ayroux, D. Iossifidis, D.R. Reyes, A. Manz, *Anal. Chem.* **2002**, *74*, 2637. c) F.E. Regnier, B. He, S. Lin, J. Busse, *Trends Biotechnol.* **1999**, *17*, 101. d) H. Andersson, A. van den Berg, *Sens. and Actuators B.* **2003**, *92*, 315.
2. a) J.B. Edel, R. Fortt, J.C. deMello, A.J. deMello, *Chem. Commun.* **2002**, 1136. b) H. Wang, H. Nakamura, M. Uehara, M. Miyazaki, H. Maeda, *Chem. Commun.* **2002**, 1462. c) E.M. Chan, R.A. Mathies, A.P. Alivisatos, *Nano Lett.* **2003**, *3*, 199. d) H. Nakamura *et al*., *Chem. Commun.* **2002**, 2844.
3. A. van den Berg, T.S.J. Lammerink, *Topics Curr. Chem.* **1997**, *194*, 21.
4. Y. Fintschenko, A. van den Berg, *J. Chrom. A.* **1998**, *819*, 3.
5. a) A.M. Hollman, D. Bhattacharyya, *Langmuir* **2002**, *18*, 5946. b) M. Nishizawa, V.P. Menon, C.R. Martin, *Science* **1995,** *268*, 700. c) T.-C. Kuo, *et al*., *Anal. Chem.* **2003,** *75*, 1861. d) S.B. Lee, C.R. Martin, *Anal. Chem.* **2001,** *73*, 768. e) R.B.M. Schasfoort, S. Schlautmann, J. Hendrikse, A. van den Berg, *Science* **1999**, *286*, 942.
6. J.C. Hulteen, C.R. Martin, *J. Mater. Chem*. **1997**, *7*, 1075.
7. T.-C. Kuo, D.M. Cannon JR, M.A. Shannon, P.W. Bohn, J.V. Sweedler, *Sensor Actuat. A* **2003**, *102*, 223.
8. a) R. Vacassy, C. Guizard, V. Thoraval, L. Cot, *J. Membrane Sci.* **1997**, 132, 109. b) C.-H. Chang, R. Gopalan, Y.S. Lin, *J. Membrane Sci.* **1994**, 91, 27. c) T. van Gestel, C. Vandecasteele, A. Buekenhoudt, C. Dotremont, J. Luyten, R. Leysen, B. van der Bruggen, G. Maes, *J. Membrane Sci.* **2002**, 207, 73.
9. S. Roy Chowdhury, R. Schmuhl, K. Keizer, J.E. ten Elshof, D.H.A. Blank, *J. Membrane Sci.* **2003**, 225, 177.
10. C.J.M. van Rijn, M.C. Elwenspoek, *IEEE proc. MEMS* **1995**, pp. 83-87.
11. C.J.M. van Rijn, *Nano and Micro Engineered Membrane Technology*, 1st ed.; Elsevier Press: Amsterdam; **2004**.
12. I. Honma, H.S. Zhou, D. Kundu, A. Endo, *Adv. Mater*. **2000**, 12, 1529.
13. J. Sekulić, J.E. ten Elshof, D.H.A.Blank, *Adv. Mater.* **2004**, in press.
14. N. Benes, A. Nijmeijer, H. Verweij, In *Membrane Science and Technology Series, 6* (Eds: N.K. Kanellopoulos), Elsevier: Amsterdam **2000**, 335-372.
15. F. Rouquerol, J. Rouquerol, K. Sing, *Adsorption by powders & porous solids - principles, methodology and application*, Elsevier Press: Amsterdam; **1999**.
16. G.Z. Cao, J. Meijerink, H.W. Brinkman, A.J. Burggraaf, *J. Membrane Sci*. **1993,** *83*, 221.
17. P. Puhlfürss, A. Voigt, R. Weber, M. Morbé, *J. Membrane Sci*. **2000,** *174*, 123.
18. C.R. Martin, M. Nishizawa, K. Jirage, M. Kang, S.B. Lee, *Adv. Mater*. **2001**, *13*, 1351.
19. a) D.-H. Park, N. Nishiyama, Y. Egashira, K. Ueyama, *Ind. Eng. Chem. Res.* **2001**, *40*, 6105. b) N. Nishiyama, D.H. Park, A. Koide, Y. Egashira, K. Ueyama, *J. Membrane Sci.* **2001,** *182*, 235. c) Y.-S. Kim, S.-M. Yang, *Adv. Mater.* **2002**, *14*, 1078.
20. M. Klotz, A. Ayral, C. Guizard, L. Cot, *Sep. Purif. Tech.* **2001**, *25*, 71.
21. S. Roy Chowdhury, R. Schmuhl, K. Keizer, J.E. ten Elshof, D.H.A Blank,. *J. Membrane Sci.* **2003,** *225*, 177.
22. J. Xu, Z. Luan, H. He, W. Zhou, L. Kevan, *Chem. Mater.* **1998**, *10*, 3690.
23. (a) I. Voigt, P. Puhlfuss, J. Topfer, *Key Engin. Mater.* **1997**, *1735* 132. (b) S. Singh, K.C. Khulbe, T. Matsuura, P. Ramamurthy, *J. Membrane Sci.* **1998**, *142*, 111.
24. V. Kogan, K. Bethke, R. de Vries, *Nuclear Instruments and Methods in Physics Research*, **2003**, *A 509* 290. (b) S. Kundu, *Nuclear Instruments and Methods in Physics Research, Section B: Beam Interactions with Materials and Atoms*, **2003**, *212*, 489.

Chapter 4

Si-Supported Mesoporous and Microporous Oxide Interconnects as Electrophoretic Gates for Application in Microfluidic Devices

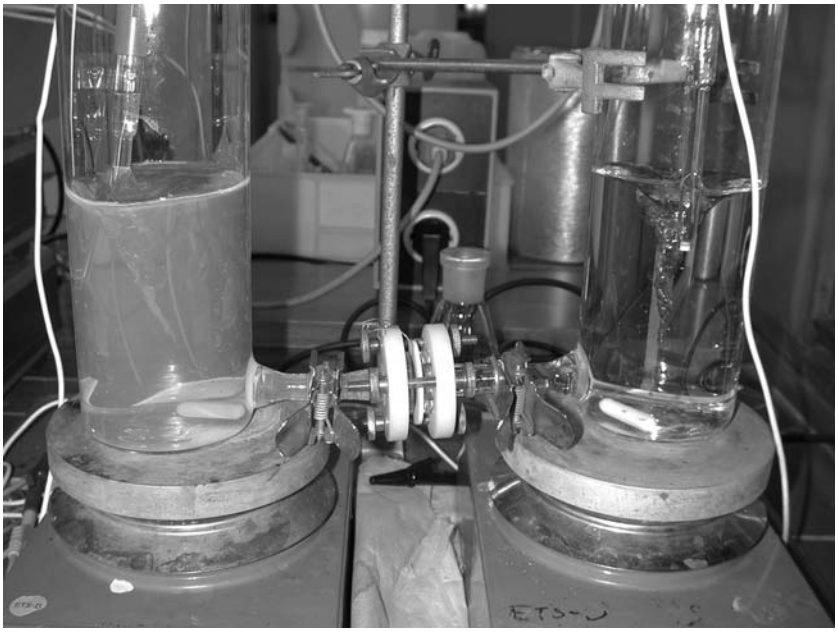

Experimental set-up

Abstract: *Microfluidic analysis systems are becoming an important technology in the field of analytical chemistry. An expanding area is concerned with the control of fluids and species in microchannels by means of an electric field. In this chapter the interconnects described in Chapter 3 are used to demonstrate that they can be operated as ion-selective electrophoretic gates. It was found that the interconnects suppress Fick diffusion of both charged and uncharged species, so that they can be utilized as ionic gates with complete external control over the transport rates of anionic and cationic species, thus realizing the possibility for implementation of these Si-compatible oxide interconnects in microchip analyses for use as dosing valves or sensors.*

4.1 Introduction

The current interest in microfluidics is largely motivated by their envisaged applications. Microfluidic analyses are quickly becoming an established technology in analytical chemistry and biotechnology,[1] and the large potential that microfluidic approaches may offer in the field of synthetic chemistry is only starting to be explored.[2] Micro-chip based fluidic devices for chemical analyses or synthesis have several unique advantages over macroscopic approaches, such as a very high degree of temporal control over temperature and chemical environment, high accuracy, relatively easy automation and integration of functional components like heaters, temperature controllers and feeding channels.[3] One of the issues in microfluidic technology concerns the development of selective barriers that allow active control over the transport of specific molecular or ionic species. Switchable interconnects[4] with which certain components can be transported at will from one microchannel into the other may lead to enabling technologies by permitting new ways of molecular separation, improved control over reactions in which one or more reagents have to be dosed in limited quantities, and coupling of methods for molecular identification, where it is necessary to inject small samples for a series of complex chemical manipulations or analysis.[5] Such molecular or ionic gates could be used in chromatography, for instance by collecting samples of bands separated by electrophoresis for further analysis or characterization.

In this chapter the developed microsieve-supported γ-alumina, MCM-48 and titania interconnects are used to illustrate their application as electrophoretic gates. It will be shown that under double layer overlap conditions selective ionic transport can be established by an externally variable potential difference across the interconnect, which allows either cationic, anionic or no transport depending on the magnitude and sign of the applied potential difference. Results of ion transport experiments are presented here for the three systems, and the influence of applied potential, electrolyte concentration, pH and pore size on the type and magnitude of transport is discussed.

4.2 Experimental

The experimental set-up is schematically depicted in Chapter 2 (Figure 2.1).[5,6] The interconnects were placed between the two halves of a U-shaped tube with the oxide layer exposed to the so-called feed side of the interconnect (porous surface area $3.8 \cdot 10^{-2}$ cm^2). Aqueous electrolyte solutions (500 ml volume) were added to the feed and receive side cells and stirred vigorously. The pH was regulated with phosphate buffer solutions prepared from mono- and dibasic potassium phosphate salts (pH = 6.9 for γ-alumina and pH = 7.8 for MCM-48 and titania interconnects) unless stated otherwise. A dc potential difference ΔV was imposed[1] over the interconnect using a potentiostat and external Pt electrodes separated by 4 mm. Here ΔV is defined as $\Delta V = V_{receive} - V_{feed}$, with V_{feed} and $V_{receive}$ the electrode potentials at the feed and receive side, respectively. ΔV was typically kept between –2 and +2 V to prevent substantial electrolysis of water. All experiments were performed at room

temperature. The fluxes were calculated from the concentration changes with time after reaching steady state conditions. Prior to the experiment the interconnects were left for 12 h in the receive side electrolyte solution to ensure complete wetting of the oxide layer. Transport experiments were carried out with fluorescein (Fl^{2-}) as divalent anion, d-tryptophan (d-Trp) as zwitterion and methylviologen (MV^{2+}) as divalent cation. Fluorescent probes were analyzed with a BMG Floustar^{+} (model 403) microplate reader at the excitation (emission) maximum of 488 (510) and 289 (366) nm, respectively, for Fl^{2-} and d-Trp. The detection limit of Fl^{2-} and d-Trp was determined to be 0.1 and 0.5 μM, respectively. Analysis of MV^{2+} was carried out by UV spectroscopy (Agilent Technologies) at 257 nm.

4.3 Results and discussion

Ion transport experiments were carried out with fluorescein (Fl^{2-}), methylviologen (MV^{2+}) and d-tryptophan (d-Trp) on all types of interconnects.

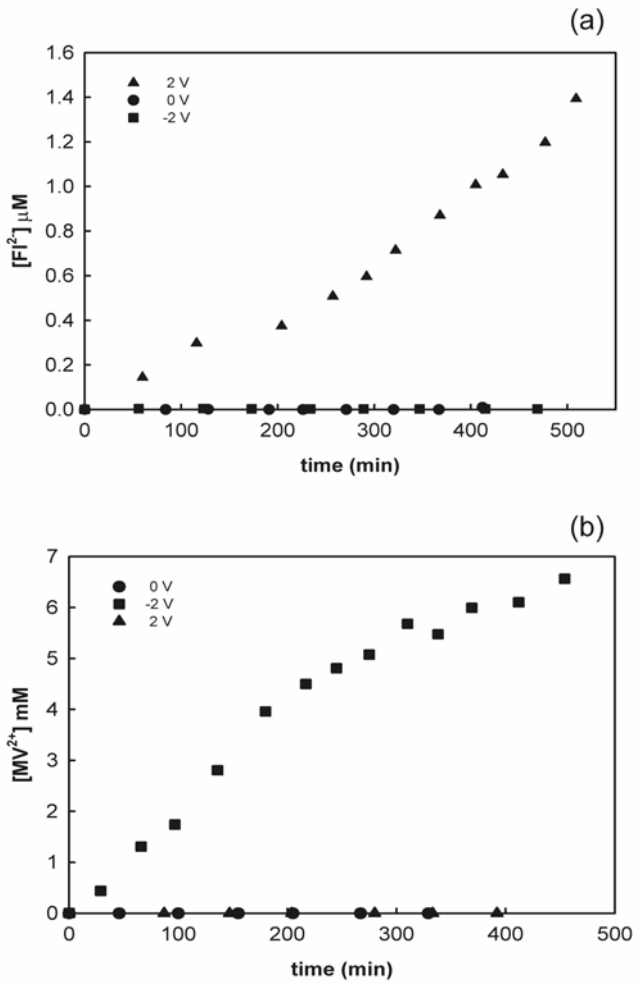

Figure 4.1: (a) Concentration increase of Fl^{2-} at the receive side versus time, through a MCM-48 interconnect and (b) the concentration increase of MV^{2+} at the receive side versus time through a TiO_2 interconnect. At ΔV= –2, 0 and +2 V. Feed side probe and electrolyte strength concentration is 0.8 mM and 10 mM, respectively.

Figure 4.1(a) shows the concentration increase of negatively charged Fl^{2-} with time at the receive side after a potential difference ΔV= +2 V had been imposed over the MCM-48 interconnect. However, when ΔV =. 0 V no noticeable concentration increase occurred in 8 h time. The opposite trend was observed for positively charged MV^{2+}, as illustrated with a TiO_2 interconnect in Figure 4.1(b).

All molecular and ionic fluxes resulting from electrical potential and/or concentration gradients are due to one or more of three possible mechanisms of transport: Fick diffusion, ion migration and electro-osmotic flow. This can be expressed as Eq. (4.1).

$$j_{\mathrm{i}} = j_{\mathrm{F,i}}(\nabla c_{\mathrm{i}}) + j_{\mathrm{IM,i}}(\nabla V) + j_{\mathrm{EOF,i}}(\nabla V)\,. \tag{4.1}$$

The total flux, j_{i} of a species type i is expressed as the sum of the three flux contributions, i.e., Fick diffusion $j_{\mathrm{F,i}}$, ion migration $j_{\mathrm{IM,i}}$ and electro-osmotic flow $j_{\mathrm{EOF,i}}$, respectively. Eq. (4.2) expresses the Fickian flux $j_{\mathrm{F,i}}$ due to a concentration gradient ∇c_{i} over the membrane.

$$j_{\mathrm{F,i}}(\nabla c_{\mathrm{i}}) = -D_{\mathrm{i}}\nabla c_{\mathrm{i}}\,, \tag{4.2}$$

where D_{i} is the chemical diffusion coefficient of species i inside the membrane pores, and ∇c_{i} the concentration gradient. In our experiments $\nabla c_{\mathrm{i}} \sim c_{\mathrm{f}}/L_{\mathrm{m}}$, with c_{f} the probe feed concentration and L_{m} the interconnect thickness (~0.3-1.0 μm). In view of the results shown in Figure 4.1, the absence of a noticeable flux for all species under field-off (ΔV = 0 V) conditions at electrolyte strength of 10 mM and a probe feed concentration of 0.8 mM indicates that transport by Fick diffusion was absent under these conditions.

Electro-osmotic flow (EOF), expressed by Eq. (4.3), is driven by the mobile double-layer inside the pores, and moves the entire liquid under the influence of an electrical potential gradient ΔV.

$$j_{\mathrm{EOF,i}} = \frac{\varepsilon\zeta}{\eta} c_{\mathrm{i}}\nabla V\,, \tag{4.3}$$

where ε is the dielectric constant of the solution inside the pores, ζ the zeta potential[7] of the oxide material, and η the fluid viscosity. In our experiments $\nabla V \sim \Delta V/L_{\mathrm{e}}$, where L_{e} is the distance between the electrodes. Since experiments with uncharged d-Trp did not show significant fluxes within experimental error under either field-on or field-off conditions, this suggests that solvent and ion transport by electro-osmotic flow is also negligible.

The third contribution, ion migration, is due to an electrical potential gradient over the interconnect, which moves charged species toward the oppositely charged electrode, as expressed by Eq. (4.4).

$$j_{\mathrm{IM,i}}(\nabla V) = -\frac{D_{\mathrm{i}} c_{\mathrm{i}} z_{\mathrm{i}} \mathrm{e}}{k_{\mathrm{B}} T}\nabla V\,. \tag{4.4}$$

Here z_{i} is the ionic charge of species i, e is the elementary electron charge, k_{B} the Boltzmann constant, and T the temperature. In Figure 4.2, the ionic fluxes of Fl^{2-} (ion charge

–2) and MV^{2+} (ion charge +2) through different oxide interconnect versus applied potential difference are presented.

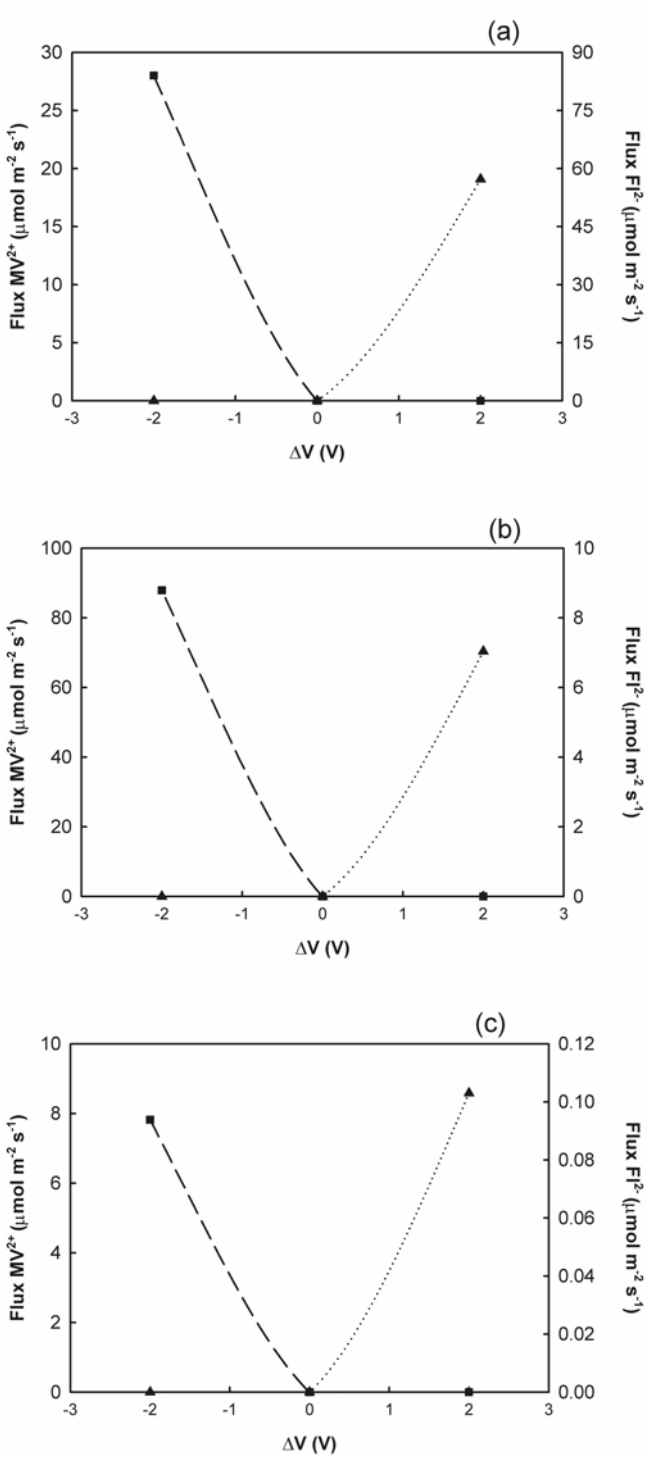

Figure 4.2: Fluxes of fluorescein (▲ Fl^{2-}) and viologen (■ MV^{2+}) versus electrode potential difference ΔV. Through (a) TiO_2, (b) MCM-48 and (c) γ-alumina interconnect. Drawn lines serve as a guide to the eye. Feed side probe and electrolyte strength concentration is 0.8 mM and 10 mM, respectively.

As can be seen in Figure 4.2 the ionic species permeate to electrodes of opposite charge. In all experiments measurable ionic fluxes were directed towards an oppositely charged electrode at the receive side of the membrane. This shows that the species are transported through the interconnect under the influence of an applied potential gradient and thus, that the mechanism of transport is ion migration.

The behavior of the interconnects described here differs substantially from the NTEP nanofluidic gates with 15-200 nm channels that were developed by Sweedler, Bohn and co-workers.[1] The transport through their interconnects was dominated by non-ion-selective EOF, which makes them applicable for injection of small amounts of analyte solutions from a feed solution into a microchannel. Our interconnects can be used as switchable cation- or anion-selective gates with three stable transfer levels, corresponding with a cation pumping mode, an anion pumping mode, and a closed gate mode. The concept also differs from the ion-permselective Au-NTEP membranes of Martin and coworkers,[8] which operate on the basis of a controlled variation of the concentration gradient over the membrane, thus manipulating the rate of Fick diffusion.

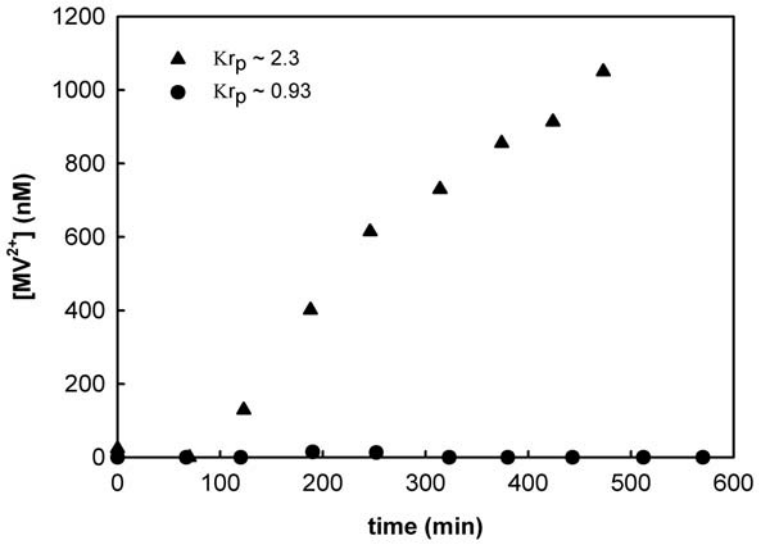

Figure 4.3: Concentration increase of MV^{2+} at the receive side versus time at ΔV= 0 V, through a MCM-48 interconnect as a function of electrolyte concentration. Feed side probe concentration is 0.8 mM. $\kappa r_p \sim 2.3$ indicates high electrolyte strength and $\kappa r_p \sim 0.93$ indicates low electrolyte strength.

In Figure 4.3 the effect of electrolyte strength on membrane permselectivity is shown. The electrical double layer theory predicts that as the electrolyte strength increases the double layer thickness decreases. The thickness of the diffuse double layer can be estimated from the Debye screening length κ^{-1} as seen in Eq. (4.5):[5,9,10]

$$\kappa^{-1} = \sqrt{\frac{\varepsilon k_B T}{e^2 \sum_i z_i^2 n_i^0}}, \qquad (4.5)$$

where n_i^0 the number density of ionic species i in the bulk of the electrolyte solution, and $\sum z_i^2 n_i^0$ is the electrolyte strength.[10] The double layer thickness is not constant but decreases with electrolyte strength and increases with surface charge density.[11]

When $\kappa r_p < 1$, where r_p is the pore radius, the dimensions of narrow-sized channels approach the length of the double layers and double layer overlap occurs from opposite sides of the pore. Under these conditions the channel becomes less permeable to ions with the same charge as the surface charge, thus making it a selective barrier for transport of either cationic or anionic species.[12] Alternatively, under conditions at which $\kappa r_p > 1$, the double layer is confined to a small region near the channel wall, and the center of the channel is electrically uncharged, i.e., the fluid contains both anions and cations, the total amounts of positive and negative charge being the same. Under these conditions both cationic and anionic species can be transported through the center of the channel,[11] as shown in Figure 4.3. This concept of a diffuse double layer holds for pore sizes >2 nm (mesopores); for pore sizes <2 nm (micropores) the fluid behavior inside the pores can no longer be described in terms of a continuum approximation, and the transport of species under such conditions will be dominated by the molecular size and shape of the permeating molecule,[13] as well as by dielectric exclusion effects.[14] Since r_p is 1.4 nm for MCM-48, κr_p is ~2.3 at an ionic strength of 0.5 M (κ^{-1} = 0.6 nm), so that the double-layer is confined to a region close to the pore walls, and double-layer overlap does not occur. At an ionic strength of 0.01 M, κr_p is ~0.93 (κ^{-1} = 1.5 nm), i.e., double-layer overlap occurs. The flux of methylviologen with a feed side concentration of 0.8 mM was measured at both low (0.01 M) and high (0.5 M) electrolyte strength, and the results are shown in Figure 4.3. Since $\Delta V = 0$ V, any transport should be due to Fick diffusion. No transport of species was observed at low electrolyte strength, while an increase of MV^{2+} occurred at high electrolyte concentration. This clearly shows that the permselectivity of the interconnect is a result of double layer overlap.

The effective diffusion coefficient D_i ,Eq (4.6), of the interconnect toward a species i can be defined by rewriting Eq. (4.4).

$$D_i = \frac{j_{\mathrm{IM},i} k_B T L_e}{c_i z_i e \Delta V}, \tag{4.6}$$

From the flux data presented in Figure 4.2, the chemical diffusion coefficients can be calculated. The diffusion of Fl^{2-}, MV^{2+} and d-Trp are shown in Figure 4.4.

It is noted that for MCM-48 the diffusion of MV^{2+} at $\Delta V = -2$ V was much higher than the diffusion of Fl^{2-} at $\Delta V = +2$ V. The same phenomenon occurred in the γ-alumina system, while the diffusion of Fl^{2-} and MV^{2+} in the titania system were similar. The very low Fl^{2-} diffusion in the γ-alumina layer is probably due to strong chemisorption of anions by γ-alumina, resulting in negatively charged pore walls, and thus, in an intrinsically cation-selective interconnect as shown elsewhere.[6] To explain the behavior of the MCM-48 and titania interconnects it is necessary to consider the transport of MV^{2+} through the interconnects at constant potential difference and varying pH, as shown in Figure 4.5.

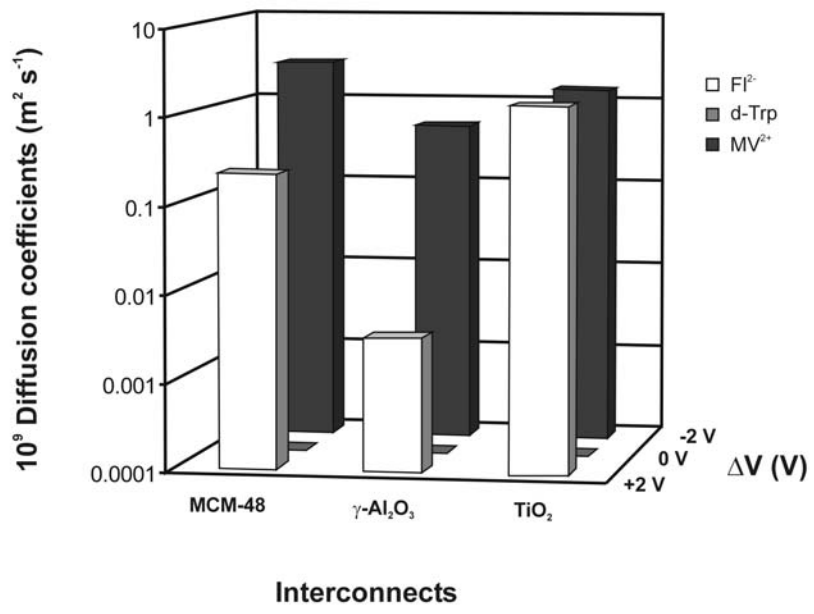

Figure 4.4: Diffusion coefficients of Fl^{2-}, d-Trp and MV^{2+}, at given potential differences for different membranes. Transport experiments were done at pH 6.9 for γ-alumina interconnects due to the lack of stability of the γ-alumina layer, at pH = 7.8.

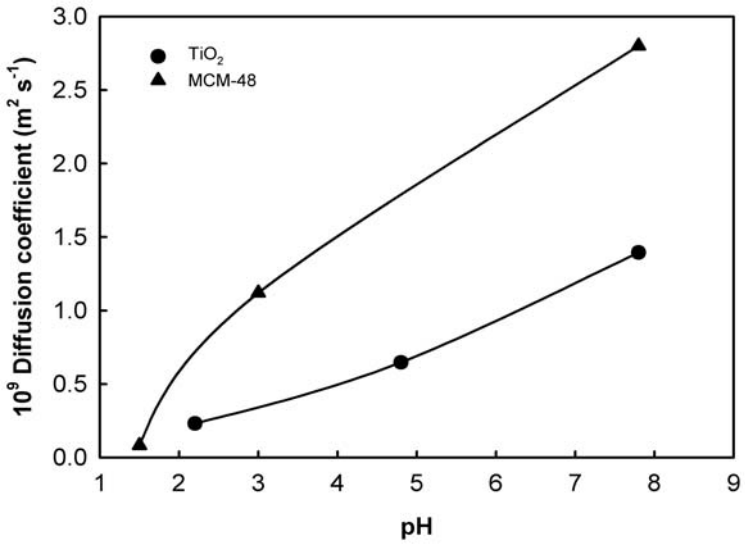

Figure 4.5: Concentration increase of MV^{2+} at the receive side versus time at ΔV= –2 V through a TiO_2 and MCM-48 interconnects as a function of pH. Feed side probe and electrolyte strength concentration is 0.8 mM and 10 mM, respectively. Drawn lines serve as a guide to the eye.

The transport rate of MV^{2+} in the titania interconnect decreased gradually with pH in the range from 7.8 to 1.5. The same effect, though much more pronounced, was observed for the MCM-48 interconnect, where the transport rate of MV^{2+} decreased rapidly at pH below 3. The effect of pH on MV^{2+} transport rate can be explained by the surface charging behavior of

the two oxides. The iso-electric points (IEP) of silica (IEP = 2-3) and titania (IEP = 4.2-4.8) are well below the pH of 8 at which the experiments shown in Figure 4.5 were carried out. Hence, the pore walls can be assumed to be effectively negatively charged,[15] so that the mobile counter charges present inside the pores will consist mainly of positively charged ions. On the other hand, at pH below the IEP the oxide will be positively charged, so that negative counter charges will be dominant in the double layer. This opens up the possibility to tune the surface charge on the pore walls by changing the pH of the system and thus regulate the nature of the double layer in the pore,[12,16] as illustrated in Figure 4.6(a) for the mesoporous MCM-48 and γ-alumina interconnects.

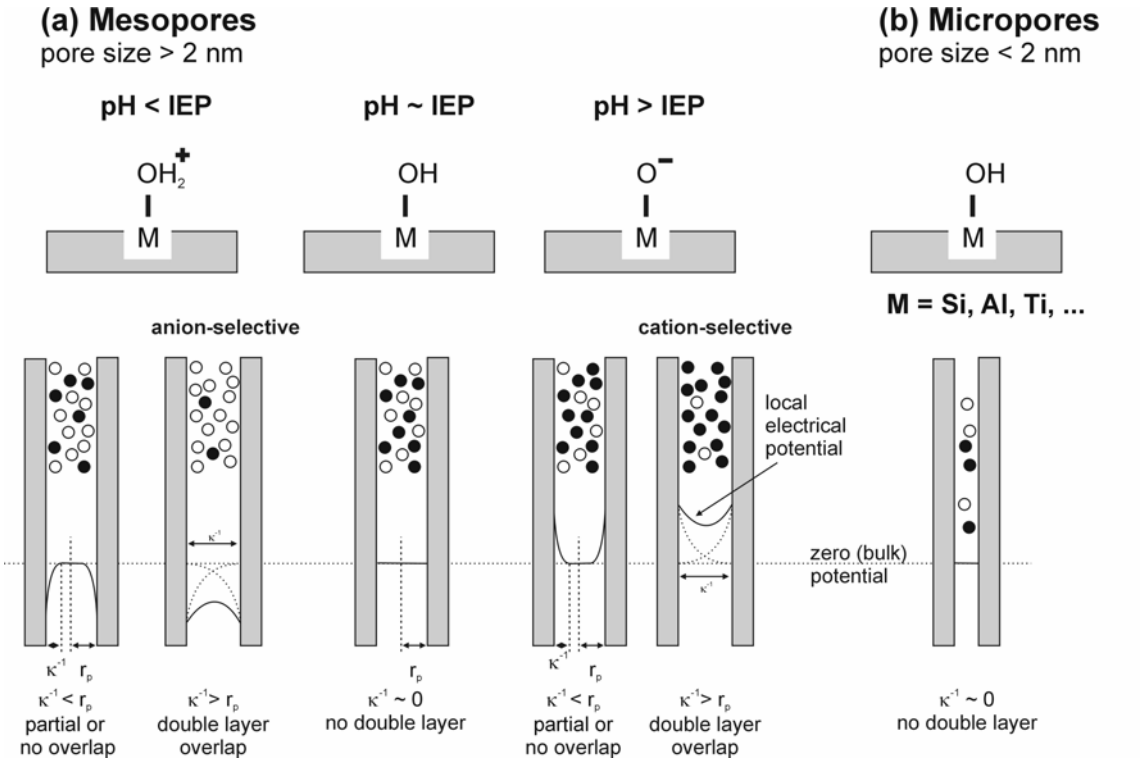

Figure 4.6: Schematic representation of the surface charge and electrical double layer behavior of micro- and mesoporous interconnects under the influence of pH and electrolyte strength.

As the pH of the solution is gradually lowered the net surface charge changes from negative to neutral and then to positive. This induces a change in the net charge of the double layer of MCM-48 from positive to negative, leading to a lower transport rate of positively charged species. This explanation is supported by the relatively sharp change of the transport rate of MV^{2+} in MCM-48 at pH below 3 in Figure 4.5. The transition is observed around pH 2-3 and this is in the same range as the IEP of MCM-48 (silica). Hence, a high cation permeability is expected at pH > 3, as was indeed found to be the case for MCM-48. These experiments suggest that the transport rate of anions will be higher at pH < 3.

The same phenomenon is less prominent in TiO_2, although the results in Figure 4.5 show that the trend is qualitatively the same. This and the seemingly non-ion-selective behaviour of

the titania interconnect for anions and cations as indicated in Figure 4.4 is most likely related to the microporous nature of this film, which makes that diffuse double layer formation cannot occur due to the confined dimensions of the pore, as illustrated in Figure 4.6(b). The transport rate through the titania interconnect is dominated by molecular size, shape, and polarity, and by dielectric exclusion effects.[14] Because the molecular sizes of Fl^{2-} and MV^{2+} are in the same range of ~ 0.9 nm as the pore size of titania, and the molecules are chemically relatively similar, the diffusion coefficients of the two molecules can also be expected to lie in the same order of magnitude. The effect of ionic charge on diffusivity will thus be more modest than for mesoporous systems, and this is reflected by the pH-dependency of the titania system in Figure 4.5.

4.4 Conclusions

The Si-compatible porous oxide interconnects with a silicon microsieve support structure were applied as electrophoretic gates in Si-based microfluidic devices. Ion transport experiments indicated that these interconnects can be utilized as ion-selective gates through control of electrolyte strength and potential difference over the interconnect. As the interconnects effectively suppress Fick diffusion of charged and uncharged species, they can be utilized as ionic gates with complete external control over the transport rates of anionic and cationic species. The selectivity of the interconnects is achieved by proper choice of electrolyte concentration and pH, while the diffusion is based on molecular size, chemical nature and ionic charge of the species. This technology can be envisioned in alternative injection techniques, nanocapillary gated injectors for application in microfluidics electrophoretic separations, but also as on-demand therapeutic agents.

4.5 References

1. T.-C. Kuo, L.A. Sloan, J.V. Sweedler, P.W. Bohn, *Langmuir* **2001**, 17, 6298.
2. a) J.B. Edel, R. Fortt, J.C. deMello, A.J. deMello, *Chem. Commun.* **2002**, 1136. b) H. Wang, H. Nakamura, M. Uehara, M. Miyazaki, H. Maeda, *Chem. Commun.* **2002**, 1462. c) E.M. Chan, R.A. Mathies, A.P. Alivisatos, *Nano Lett.* **2003**, *3*, 199. d) H. Nakamura *et al*., *Chem. Commun.* **2002**, 2844.
3. a) A. van den Berg, T.S.J. Lammerink, *Topics Curr. Chem.* **1997**, *194*, 21. b) Y. Fintschenko, A. van den Berg, *J. Chrom. A.* **1998**, *819*, 3.
4. a) A.M. Hollman, D. Bhattacharyya, *Langmuir* **2002**, *18*, 5946. b) M. Nishizawa, V.P. Menon, C.R. Martin, *Science* **1995,** *268*, 700. c) T.-C. Kuo, *et al*., *Anal. Chem.* **2003,** *75*, 1861. d) S.B. Lee, C.R. Martin, *Anal. Chem.* **2001,** *73*, 768. e) R.B.M. Schasfoort, S. Schlautmann, J. Hendrikse, A. van den Berg, *Science* **1999**, *286*, 942.
5. a) D.R. Reyes, D. Iossifidis, P.-A. Ayroux, A.Manz, *Anal. Chem.* **2002**, 74, 2623. b) P.-A. Ayroux, D. Iossifidis, D.R. Reyes, A. Manz, *Anal. Chem.* **2002**, 74, 2637. c) F.E. Regnier, B. He, S. Lin, J. Busse, *Trends Biotechnol.* **1999**, 17, 101. d) H. Andersson, A. van den Berg, *Sens. and Actuators B.* **2003**, 92, 315.
6. R. Schmuhl, K. Keizer, A. van den Berg, J.E. ten Elshof, D.H.A. Blank, *J. Colloid Interface Sci.* **2004**, 273, 331.
7. R.J. Hunter, *Zeta Potential in Colloid Science: Principles and Applications*, 3rd ed., Academic Press, London, **1981**.
8. M. Nishizawa, V.P. Menon, C.R. Martin, *Science* **1995**, 268, 700.
9. N. Benes, A. Nijmeijer, H. Verweij, In *Membrane Science and Technology Series*, 6; Kanellopoulos, N.K.,Ed.; Elsevier: Amsterdam, 2000; 335-372.
10. R.J. Hunter, *Foundations of Modern Colloid Science*, 2nd ed., Oxford University Press, Oxford, **2001**.
11. M. Mulder, *Basic Principles of Membrane Technology*, 2nd ed., Kluwer, Dordrecht, **1996**.
12. P.J. Kemery, J.K. Steehler, P.W. Bohn, *Langmuir* **1998**, 14, 2884.
13. P.M. Bungay, H. Brenner, *Int. J. Multiphase Flow* **1973**, *1*, 25.
14. J. Lyklema, In *Fundamentals of Interface and Colloid Science*, *Vol. 2. Solid-Liquid interfaces*, 1st ed., Academic Press: London, **1995**; Chapter 5.
15. A.C. Pierre, *Introduction to Sol-Gel Processing*, 1st ed., Kluwer: Dordrecht; **1998**.
16. M-S. Kang, C.R. Martin, *Langmuir* **2001**, 17, 2753-2759. b) Chun, K-Y.; Stroeve, P. *Langmuir* **2001**, 17, 5271.

Chapter 5

In situ Switchable Ion Selective Membranes by Addition and Removal of Surfactant Molecules

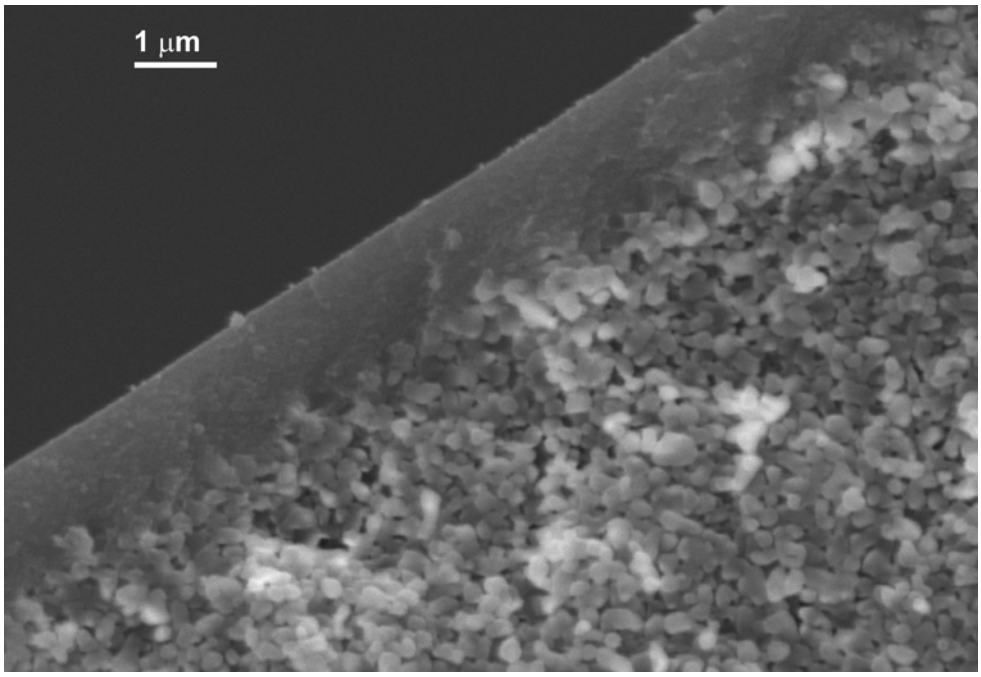

Cross-section SEM photo of an γ/α-alumina membrane

Abstract: *This chapter describes the in situ modification of effective pore size and porosity of γ-alumina membranes by reversible adsorption and desorption of surfactant molecules. The effect of the presence of three different types of surfactant molecules, namely C6TEA, CTAB and SDS, on the flux of ion-migration driven probe species is investigated. It is shown that addition of low concentrations of surfactant increases the flux of the ionic probe through the membrane, while at high concentrations the surfactant forms a bilayer structure on the internal membrane surface, which inhibits the flux of the probes. Low concentrations of surfactant are thought to neutralize the effective charge present on the membrane pore wall, thereby decreasing flux-retarding Coulombic interactions between the probe and the membrane pore walls. The formation of a bilayer at high surfactant concentrations leads to steric blocking of probe species transport, and increased Coulombic interactions between bilayer charges and probe. Steady state experiments indicate that the addition and removal of surfactants to/from the system can be utilized to switch the membrane reversibly between a closed and an open mode, creating selective gates, e.g., for use in biological sampling routines.*

5.1 Introduction

In Chapters 2 and 4 the transport properties of ionic species under the influence of a potential difference across a membrane was investigated. It was found that ionic species can be driven through a membrane by ion migration. By changing the sign of the applied potential it is possible to facilitate or block the transport of certain ionic species. It was shown that it is not only possible to control the transport rates of the species, but also the selectivity of the membrane by adjusting the ionic strength and pH of the system.[1-3] However, the use of ionic strength to manipulate the selectivity of a membrane has limitations, especially because double layer overlap can occur only at relatively low ionic strengths. In principle, the concept of steric blocking of species transport through a membrane remains a more general way to tune transport rates irrespective of ionic strength and pH. Upon physically blocking or de-blocking the pores in a membrane, an open or closed membrane-gate can be created. This could be especially useful when for instance certain biological species are present in the system, which structure and function depend on ionic strength and pH. In such cases the use of steric blocking could be a safe and alternative way to create a switchable gated interconnect.

The use of surfactants to induce steric blocking is interesting because of their ability to adsorb onto a membrane. This offers the possibility to modify the external and internal membrane surface chemically. From literature it is known that surfactant molecules adsorbed on alumina modify the properties of the alumina surface.[4] Surfactant molecules are characterized by having both hydrophobic and hydrophilic moieties, with the ability of self-organization in water, resulting in aggregates called micelles above a certain concentration called the critical micelle concentration. One of the characteristic features of surfactant molecules is their tendency to adsorb at interfaces, mostly in an orientated fashion. The orientation of surfactant molecules at the surface/interface determines how the surface/interface is affected by adsorption, making it a surface-active agent. That is, the details of the adsorption process determine whether the surface/interface becomes more hydrophilic or more hydrophobic. The behavior of the surfactant molecules at the interface is determined by a number of forces, including electrostatic attraction, covalent bonding, hydrogen bonding, hydrophobic bonding and solvation of various species.[5] A number of mechanisms are known by which surface-active molecules may adsorb onto the solid substrates from an aqueous solution. In general the absorption of surfactants involves single ions rather than micelles.[5]

A four region adsorption model[6] has been proposed to explain the adsorption of surfactants at charged interfaces. This has been shown successful in the modeling of surfactant adsorption onto alumina.[7] The model allows predicting the general morphology of the adsorbed surfactant layer from the adsorption isotherm. The general form of the isotherm and the morphology of the adsorbed structures associated with each region are depicted in Figure 5.1. In region I of the isotherm, surfactant monomers are electrostatically adsorbed to the membrane-interconnect, with head groups in contact with the surface. The hydrocarbon tail

groups may interact with any hydrophobic region of the surface. Region II sees strong lateral interaction between adsorbed monomers, leading to the formation of primary aggregates. Fan *et al*. showed that the surfactant is adsorbed with the head groups to the surface while the hydrocarbon tails protrude into the solution.[6] This way hydrophobic patches are created on the surface, which are known as hemimicelles. Increases in the surface excess, which means that the local concentration at the surface will exceed the concentration in the bulk solution, in region III are thought to result from the growth of the structures formed in region II, without any increase in the number of surface aggregates.

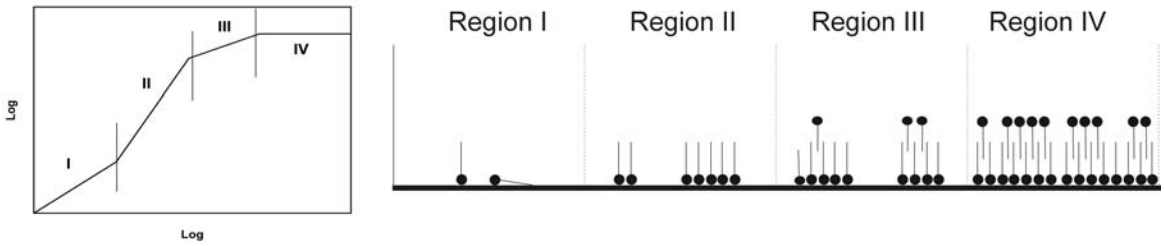

Figure 5.1: A schematic representation of the four-region adsorption model and the morphology of the surfactant aggregates on the surface of the membrane-interconnect.[6]

The presence of head groups facing into the solution renders the surface hydrophilic again. This transition from region II to III is believed to be due to the neutralization of the surface charge. Finally in region IV the surface morphology is assumed to be a fully formed bilayer.[8] It is known that bilayers formed on a membrane surface can act as a secondary membrane. This is due to surfactant concentration polarization at the membrane surface. Its occurrence is characterized by the gel concentration c_g, which is probably associated with the formation of stable viscous phases such as hexagonal, lamella or cubic phases depending on temperature, but independent on pore size and cross-flow velocity. The phase behavior of surfactants is strongly influenced by the presence of electrolytes. A high valency electrolyte makes the effect even more pronounced, enhancing inter-surfactant association and leading to early gel-polarization.[9] The flow through the membrane is slowed in the presence of this gel layer, and the flow mechanism is affected by the type of gel structure and the nature of the surfactant/membrane interaction. When the membrane/surfactant interaction is strong, i.e., for an oppositely charged membrane/surfactant pair or a hydrophobic membrane/surfactant system in a polar medium, gel formation occurs on the membrane wall and covers the entire cross section of the pore. Rapid gel polarization is expected under these conditions. It has been shown that gel polarization can also occur at low surfactant concentrations when the surfactant is more hydrophobic.[9] However, if gel growth is due to micelle interaction instead of gel polarization, diffusion can occur through the inter-micellar spaces or through defects in the liquid crystalline surfactant phase.[9] In this case the effect of the surfactant phase reduces the membrane pore size and porosity but does not eliminate the membrane porosity entirely.

In this chapter, the co-addition of surfactant molecules to a system of probe molecules, which are transported through a membrane under the influence of a potential difference, is

studied. Due to the adsorption behaviour of surfactant micelles onto the membrane surface, the co-species (surfactant) are able to facilitate or block the transport of probe molecules. Three different surfactants are used with varying carbon lengths as shown in Figure 5.2, namely cetyl-trimethyl-ammonium bromide (CTAB), sodium dodecyl sulfate (SDS) and triethylhexyl-ammonium bromide (C6TEA), which have carbon tail lengths of 16, 12 and 6, respectively. The influence of these surfactants and their concentrations on the transport of species through a γ/α-alumina membrane-interconnect is investigated.

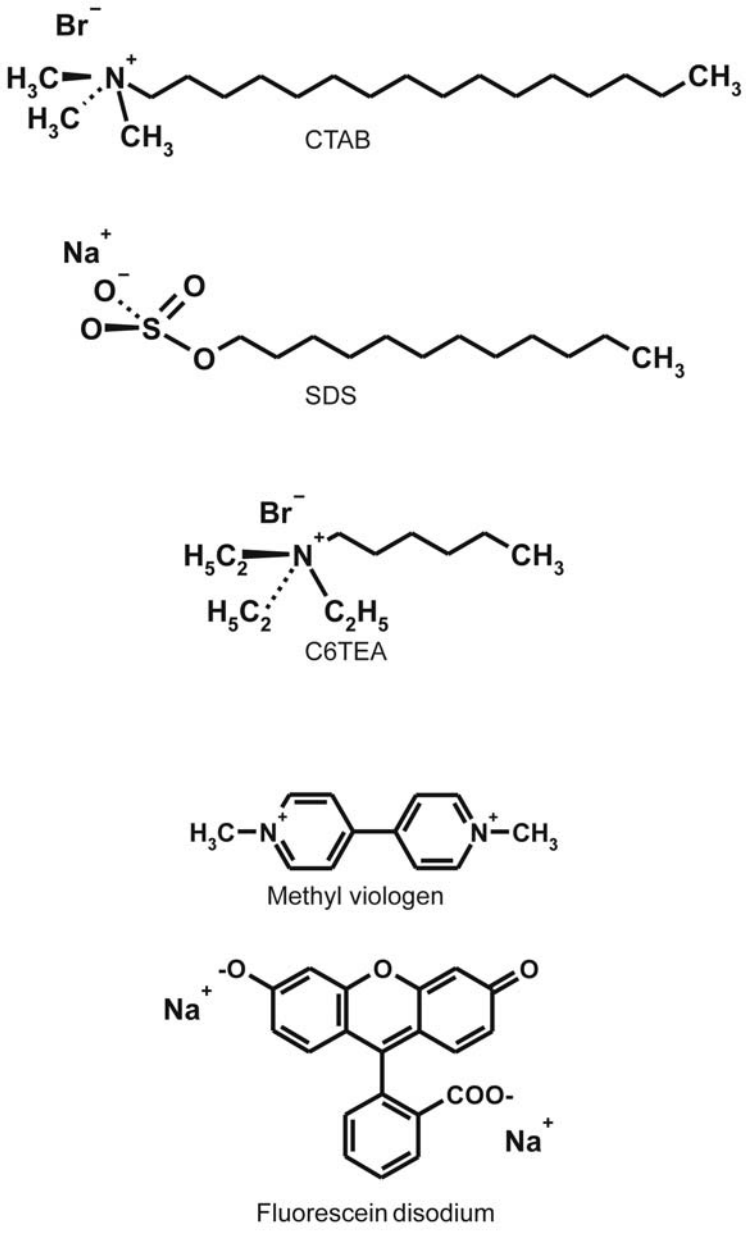

Figure 5.2: Schematic drawing of the three surfactants molecules, cetyl-trimethyl-ammonium bromide (CTAB), sodium dodecyl sulfate (SDS) and triethylhexyl-ammonium bromide (C6TEA) and the two probe molecules, methyl viologen (MV^{2+}) and fluorescein disodium salt (Fl^{2-}).

5.2 Experimental

5.2.1 Membrane characterization

The membranes consist of two components: a macroporous support and a thin mesoporous layer with a separative ability. α-Alumina is used as macroporous support and coated with mesoporous γ-alumina layers. The method of preparation of the α-alumina support is by so-called colloidal filtration. A colloidal suspension was made by dispersing 50 wt% α-alumina powder (AKP 30) in 0.02 M nitric acid solution using ultrasonic treatment for 15 minutes. The suspension was filtered over polyester filters (pore size 0.8 μm). The resulting filter cake was dried overnight and fired at 1100 °C for 1 h. After firing the supports were machined to the required size and polished.[10] The γ-alumina membranes were prepared by dip coating the sintered α-alumina supports in a homemade boehmite sol. The boehmite sol was prepared by a colloidal sol-gel route, where aluminium-tri-sec-butoxide (ATSB) was hydrolysed and subsequently peptised with HNO_3.[10] The boehmite sol was mixed with a PVA solution, in a PVA: boehmite mass ratio of 2:3. Dip coating was preformed under class 1000 clean room conditions in order to minimise particle contamination of the membrane layer. After dipping, the membranes were dried in a climate chamber at 40 °C and 60 % R.H. to avoid crack formation in the boehmite layer. γ-Alumina membranes were formed by firing the dried layers at 800 °C for 3 h in air. Calcining the membrane at 800°C results in larger pore sizes compared to firing at 600 °C. The pore size distribution of the γ-alumina layer was determined by permporometry as shown in Figure 5.3.[11]

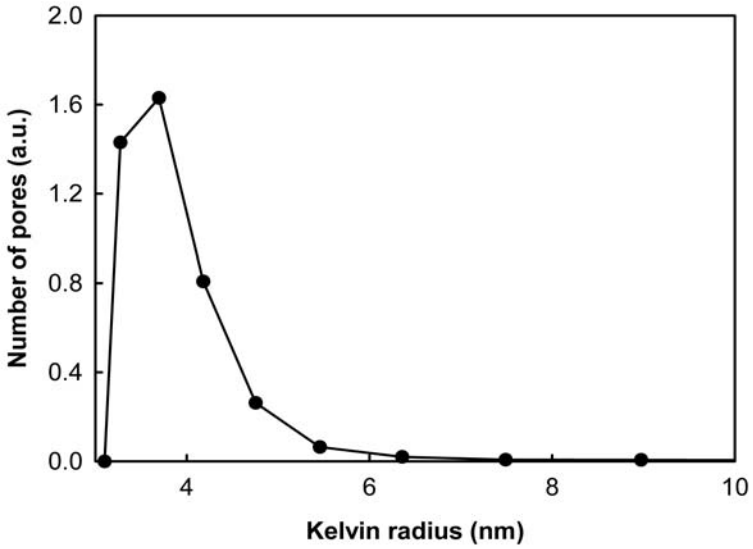

Figure 5.3: Pore size distribution of γ-Al_2O_3 layer calcined at 800°C, as measured by permporometry.

The electrophoretic mobility measurements were performed on γ-Al_2O_3 powder calcined at 800°C using a Malvern ZetaSizer 3000HSa. The temperature of the samples during the

measurements was maintained at 25 ± 0.2 °C using a Haake D8 water bath with water-cooling. Further experimental detail concerning the measurements can be found elsewhere.[12]

5.2.2 Permeability measurements

The experimental set-up is schematically depicted in Chapter 2 in Figure 2.1.[3] The membrane was placed between the two halves of a U-shaped tube with the oxide layer exposed to the so-called feed side of the membrane (porous surface area 3.32 cm^2). Aqueous electrolyte solutions (500 ml total volume) were added to the feed and receive side cells and stirred vigorously. The pH was regulated with aqueous phosphate buffer solutions prepared from mono- and dibasic potassium phosphate salts (pH = 6) at low ionic strength concentration (6.6 mM). A dc potential difference ΔV was imposed[13] over the interconnect using a potentiostat and external Pt electrodes separated by 4 mm. Here ΔV is defined as $\Delta V = V_{receive} - V_{feed}$, with V_{feed} and $V_{receive}$ the electrode potentials at the feed and receive side, respectively. ΔV was typically kept between –2 and +2 V to prevent substantial electrolysis of water. All experiments were performed at room temperature. The fluxes were calculated from the concentration changes with time after reaching steady state conditions. Prior to the experiment the membranes were left for 12 h in the receive side electrolyte solution to ensure complete wetting of the oxide layer. Transport experiments were carried out with methyl viologen dichloride (MV^{2+}) as divalent cation and fluorescein disodium salt (Fl^{2-}) as divalent anion, with an initial feed concentration of $2 \cdot 10^{-4}$ M. The surfactants cetyl-trimethyl-ammonium bromide (CTAB), sodium dodecyl sulfate (SDS) and triethylhexyl-ammonium bromide (C6TEA) were added at various concentrations into the feed side solution unless stated differently. For the removal of surfactant the feed and permeate side liquids were refreshed with new electrolyte solution with the required probe and buffer concentration. Analysis of MV^{2+} was carried out by an UV/Visual spectroscopy (Varian, Cary, 50 Scan) at 257 nm. Fl^{2-} was detected with a BMG Floustar$^+$ (model 403) microplate reader at the excitation (emission) maximum of 488 (510) nm, with a detection limit of Fl^{2-} of 0.1 μM.

5.3 Results and discussion

5.3.1 Influence of surfactant co-addition on transport rate of probe molecules

As shown in Figure 5.3 the Kelvin radii of the γ-alumina membrane were in the range of 3.5-7 nm, which corresponds with a true pore diameter of 8-15 nm. The influence of the surfactants SDS, CTAB and C6TEA, on the transport of MV^{2+} (methyl viologen ion) and Fl^{2-} (fluorescein ion) through the α/γ-alumina membrane-interconnect under an applied electrical potential difference over the membrane was investigated. In Figure 5.4 the influence of the surfactants on the flux of MV^{2+} through the alumina membrane-interconnect is presented. The flux of MV^{2+} species is shown as a function of surfactant concentration. The surfactant concentration was increased at 24 h intervals after steady state conditions had been reached. The gray band in the figure indicates the average steady state flux of MV^{2+} when no

surfactant was present in the system. When the MV^{2+} flux in the absence of surfactant is compared with the flux of MV^{2+} in the presence of surfactant it is clear that in all three cases at low surfactant concentration the flux of MV^{2+} was enhanced, while a high surfactant concentration led to a much lower flux than without any surfactant present. In the case of CTAB and SDS the flux decreased drastically when the surfactant concentration was increased from 10^{-4} to 10^{-3} M. A qualitatively similar though less pronounced trend was observed in the presence of C6TEA. These results clearly indicate that the flux of ionic species through the membrane can be manipulated by addition of surfactant to the system.

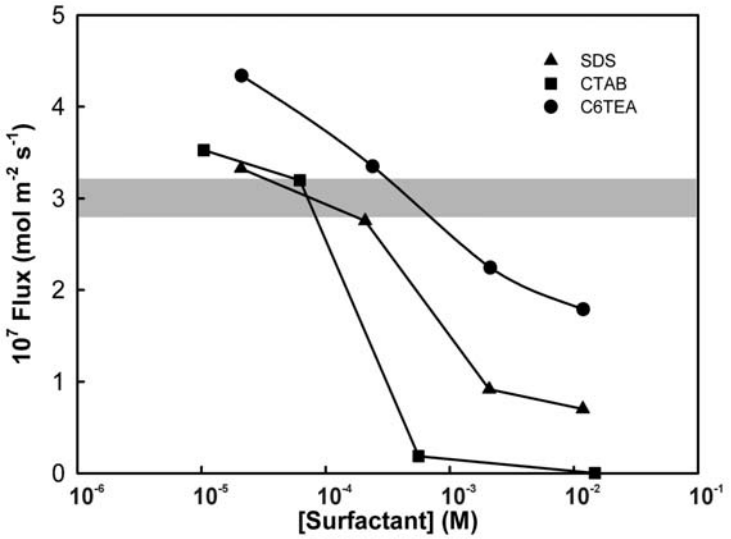

Figure 5.4: The influence of surfactant concentration on transport rate of MV^{2+} through a γ/α-alumina membrane. The potential difference over the membrane is ΔV = -2 V. The gray area represents the average flux of MV^{2+} when no surfactant was present in the system. [MV^{2+}] at feed side = $2 \cdot 10^{-4}$ M. Surfactant was added to both feed and permeate side solutions.

5.3.2 Switching ability of membrane in presence of surfactants

The open/close switching ability of the membrane by co-addition of C6TEA, CTAB and SDS at the feed side on the flux of MV^{2+} can be seen in Figure 5.5(a), (b) and (c), respectively. The fluxes presented here were measured under steady state conditions, as in Figure 5.4. But in contrast to Figure 5.4 both stepwise addition and removal of surfactants was investigated to explore the switching ability of the membrane resulting from the introduction and removal of surfactants to the system. It can be seen in the figure that partial or almost complete pore blocking was achieved at high surfactant concentrations and that this is a reversible effect. After removal of surfactant the pore is effectively open again for transport and the transport rate comes back to values that are close to its original value.

The co-addition of C6TEA to the probe molecule MV^{2+} in the feed side of the membrane is shown in Figure 5.5(a). The system was left for 24 h after which the concentration of MV^{2+} at the permeate side of the membrane was analysed.

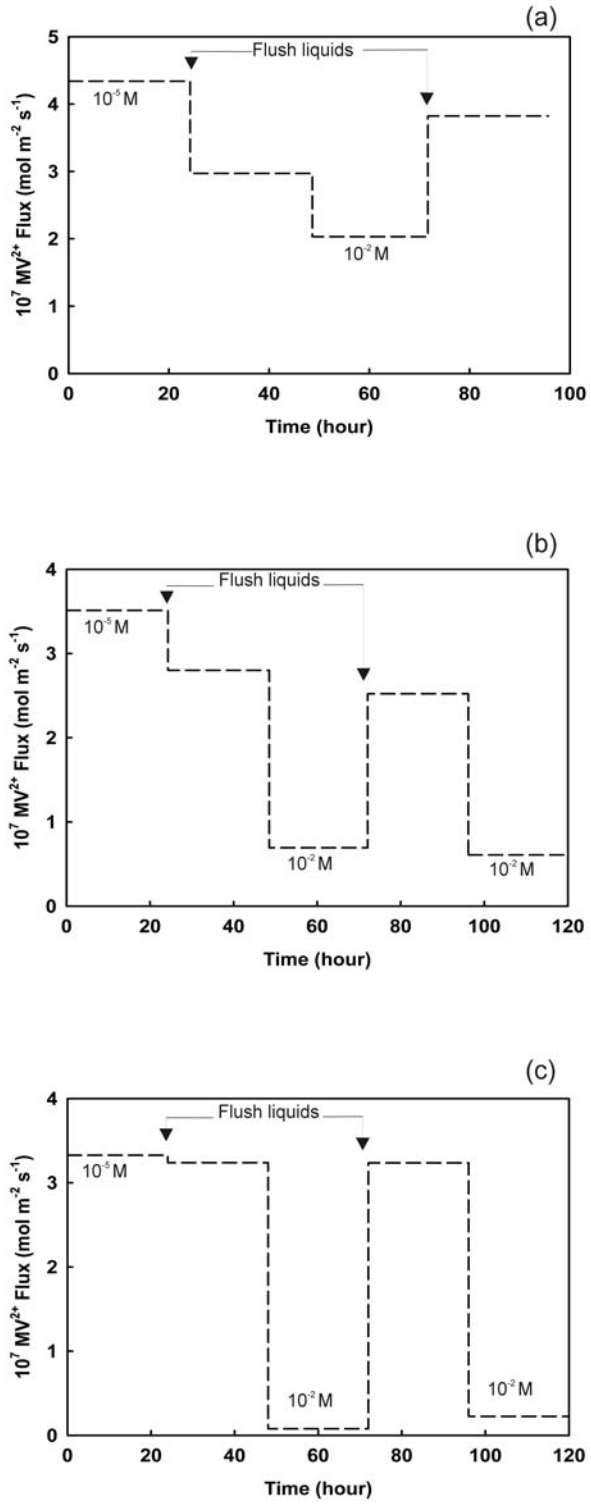

Figure 5.5: The influence of addition and removal of (a) C6TEA, (b) CTAB and (c) SDS surfactants on the transport rate of MV^{2+} through a γ/α-alumina membrane. The potential difference over the membrane ΔV = -2 V. [MV^{2+}] at feed side = $2 \cdot 10^{-4}$ M.

As can be seen in the figure, when a low concentration of C6TEA surfactant (~10^{-5} M) was present the transport rate of MV^{2+} ions at ΔV = -2 V was higher than after removal of all C6TEA by changing the liquids at the feed and permeate sides of the membrane. After 24 hours a high concentration (~10^{-2} M) of C6TEA was added to the system and the flux decreased even further. Finally, the system was again flushed to remove all surfactant, after which the flux changed to a value that was slightly higher than in the absence of surfactant the first time. However, the result indicates that it is indeed possible to close the pores by addition of C6TEA to the system, and to re-open them again upon removal of C6TEA. In Figure 5.5(b) and (c) similar behaviour is seen upon addition and removal of CTAB and SDS, respectively. It is noted that the blocking effect at high CTAB concentration in Figure 5.5(b) is more effective than for C6TEA. This is probably related to the longer hydrophobic tail of the CTA^+ ion. However, CTAB was less effective than C6TEA in increasing the flux at low surfactant concentrations. SDS seems to be even less effective in this regard; however it is the most effective species in blocking the MV^{2+} flux through the membrane at high surfactant concentrations. This may be due to the electrostatic interaction between the SDS and γ-alumina but the type and specific nature of the formed bilayer is possibly also an important factor in the blocking effect of the different surfactants. The attractive interaction between MV^{2+} and DS^- head groups in the bilayer may also lead to an electrostatic retardation of the flux and result in more effective blocking. In all cases presented in Figure 5.5 the blocking and de-blocking of the pores appears to be more or less reversible, demonstrating an *in situ* switchable membrane.

In order to determine if the same blocking behaviour could be seen in the case of anionic probe species the co-addition of CTAB with Fl^{2-} was investigated. In Figure 5.6 the effect of co-addition of low and high concentrations of CTAB on the flux of Fl^{2-} through a γ/α-alumina membrane is shown. In Chapter 2 it was already concluded that the γ/α-alumina membrane is a predominantly cation-permselective membrane. The flux of Fl^{2-} is therefore roughly two orders of magnitude smaller than the flux of the MV^{2+} under similar conditions (no surfactant). With the co-addition of a low concentration (~10^{-5} M) of CTAB to the feed side the flux of Fl^{2-} through the membrane increased, similar to what had been observed with MV^{2+}. With the removal of the CTAB from the system the flux decreased slightly but due to strong adsorption of Fl^{2-} on the membrane surface the initial flux was not completely restored. After a high concentration (~10^{-2} M) of CTAB was added to the system, a colour change was observed from green to reddish-brown. This indicates a strong interaction between Fl^{2-} and the CTA^+ ion, which is supported by the UV/Visual spectra due to the shift in adsorption maximum. It is unlikely that the same interaction occurred at low CTAB concentrations, because no changes were observed in the UV/Vis spectra of Fl^{2-}. The membrane switching effect observed in this case at high concentrations can be explained by a combination of two possible effects, namely the formation of some Fl-CTA complex, and/or steric hindrance by the CTAB bilayer inside the membrane.

Regarding MV^{2+}, the ability to influence the transport rate of ions by co-addition of surfactants is thought to be due to the adsorption of surfactants on the external and internal

membrane surface area, which alters the chemical nature of the pores of the membrane.[14] The possibility that the MV^{2+} flux was also influenced by a surfactant/probe interaction was investigated by UV/Visual spectroscopy on MV^{2+} in the presence of different concentrations of surfactant. No significant changes in the spectra were observed as a function of surfactant concentration, except at high (~10^{-2} M) concentration of SDS, where a shift in adsorption maximum was observed, indicating that there was interaction between the MV^{2+} and SDS molecules.

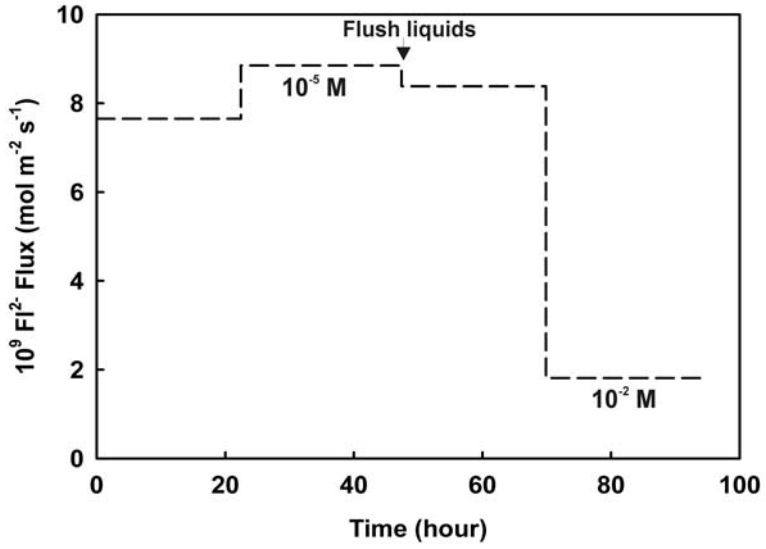

Figure 5.6: Influence of the presence and removal of CTAB surfactant on the transport of Fl^{2-} through a γ/α-alumina membrane over time. ΔV = +2V. [Fl^{2-}] at feed side = $2 \cdot 10^{-4}$ M.

The actual change of flux depended on the nature of the surfactant and the amount added to the system. Both flux enhancement and flux decrease were observed depending on surfactant concentration. At very low concentrations of C6TEA and CTAB (<<10^{-4} M), the MV^{2+} flux was substantially higher than when no surfactant was present, while no significant change of flux was observed upon addition of similar low concentrations of SDS. The formation of hemimicelles of CTAB and SDS on alumina, a region II-type adsorption phenomenon, occurs at different concentrations of $1 \cdot 10^{-5}$ M and $5\text{-}6 \cdot 10^{-5}$ M, respectively.[6,17] The formation of hemimicelles increases the hydrophobic patches on the alumina surface. These may thereby create a more favourable environment near the membrane surface for the MV^{2+} probe. However, they also neutralize the surface charge of the membrane surface. The Coulombic interactions between MV^{2+} ions and the membrane surface are therefore weaker than in the absence of surfactants. It is likely that strong Coulombic interactions between pore surface and the MV^{2+} probe ion will have a retarding effect on the MV^{2+} flux. Upon addition of a low surfactant concentration to the system a (partial) monolayer of surfactant molecules adsorbs onto the membrane surface, and this leads to effective neutralization of the membrane surface charges. Neutralization of this interaction by the adsorption of surfactant molecules can

therefore explain the experimentally observed enhancement of flux. For the experimental data it was seen that C6TEA was more effective in flux enhancement of the MV^{2+} probe than the CTAB and SDS. This may have to do with the size of the different surfactant molecules; C6TEA is a smaller molecule than the CTAB and SDS and therefore it may be able to adsorb in and around charged surface sites where the larger CTAB and SDS molecules are sterically hindered. This explanation may also hold for the Fl^{2-} flux increase seen at low CTAB concentrations.

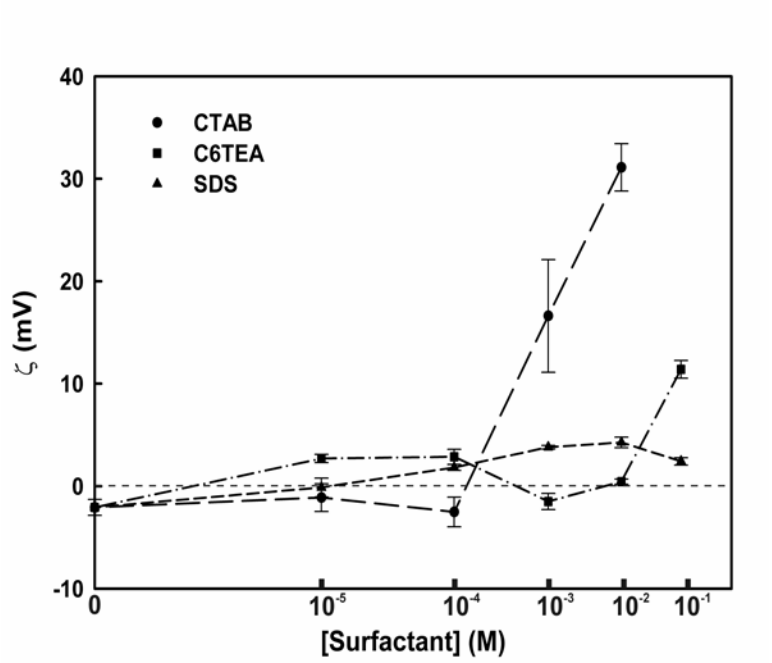

Figure 5.7: Zeta potential of γ-alumina powder as a function of different surfactant concentration in the presence of added phosphate buffer (pH 6) and under similar conditions as permeability measurements. Lines drawn serves as a guide to the eye.

According to the four-region model, when the concentration of surfactants increases the aggregates of surfactant molecules grow to form bilayers at concentrations at 10^{-2} M, which is the concentration range where small fluxes were observed in Figure 5.5 and 5.6. As the concentration of surfactant molecules increased the adsorption characteristics changed from region II-type to region IV-type at high concentration, as shown in Figure 5.1. The formation of bilayers changes the overall characteristics of the membrane pore and will increase steric hindrance of probe species transport, as the bilayer decreases the effective pore size and membrane porosity. This interpretation is supported by the electrophoretic mobility measurements, shown in Figure 5.7. This figure shows the zeta potential of γ-alumina powder as a function of added surfactant concentration. At low surfactant concentration the zeta potential increases, while at high concentration the formation of bi-layers can be seen for CTAB and C6TEA. The formation occurs at ~10^{-3} and ~10^{-1} M, respectively. When the concentration of surfactant molecules in the bulk solution is lowered the bilayer is reversibly destroyed. The bilayer properties are dependent on the surfactant/membrane interaction but also on the carbon chain length of the surfactant tail. In view of the zeta potential

measurements it is expected that CTAB and C6TEA form more complete bilayers in comparison with SDS. The MV^{2+} flux at high (~10^{-2} M) surfactant concentration decreases in the order C6TEA > CTAB > SDS, i.e., the effectiveness with which ion transport can be blocked appears to increase with increasing hydrocarbon chain length, but is in contradiction with the zeta potential of SDS at high concentration. However, the charge sign of the polar head groups of the surfactants is also a factor to consider in the blocking ability. From spectroscopic data it was observed that there is electrostatic interaction between the positive/negative surfactants head groups and the oppositely charged probes. Therefore, charge interaction between the SDS head groups and the ionic probe molecules can be expected, leading to stronger electrostatic retardation of the flux. This could possibly explain why SDS is more effective in pore blocking than CTAB and C6TEA while no bilayer seems to be formed according to data in Figure 5.7. This explanation also holds for the Fl^{2-} flux decrease in the presence of high CTAB concentrations.

5.4 Conclusions

This chapter described an *in situ* switchable ion selective membrane by co-addition and removal of three different surfactant molecules, C6TEA, CTAB and SDS. From the co-addition of different surfactant at different concentrations it was seen that the flux of probe molecules through a γ/α-alumina membrane could be manipulated. The presence of low concentrations of surfactants to the system enhanced the flux of the probe molecules through the membrane in the order SDS < CTAB < C6TEA. This is thought to occur by effective neutralization of the pore wall charges by the absorbed monolayer. With co-addition of high concentrations of surfactants the flux of probe molecules was retarded. This is though to be due to steric hindrance by the bilayers, and/or electrostatic interactions between the probe molecules and surfactants, with increasing efficiency C6TEA < CTAB < SDS. The switchability of the system was illustrated by the co-addition and removal of surfactant from the system. In all cases the blocking and de-blocking of pores appeared to be more or less reversible, demonstrating an *in situ* switchable membrane. The ability to physically open and close transport through the membrane can be envisioned for use as selective gates in biological, for DNA and protein, sampling routines as well as injectors for electrophoretic separations and on-demand therapeutic agents for application in microfluidic devices.

5.5 References

1. R. Schmuhl, J. Sekulić, S. Roy Chowdhury, C.J.M. van Rijn, K. Keizer, A. van den Berg, J.E. ten Elshof, D.H.A. Blank, *Adv. Mater.* **2004**, 16, 900
2. R. Schmuhl, W. Nijdam, J. Sekulić, S. Roy Chowdhury, C.J.M. van Rijn, A. van den Berg, J.E. ten Elshof, D.H.A. Blank, *Anal. Chem.* **2004**, accepted.
3. R. Schmuhl, K. Keizer, A. van den Berg, J.E. ten Elshof, D.H.A. Blank, *J. Colloid Interface Sci.* **2004**, 273, 331.
4. N.A. Kononenko, N.P. Berezina, N.V. Loza, *Colloid Surf. A*, **2004**, 239, 59.
5. S. Paria, K.C. Khilar, *Adv. Colloid Interface Sci*. **2004**, 110, 75.
6. A. Fan, P. Somasundaran, N.J. Turro, *Langmuir*, **1997**, 13, 506.
7. P. Somasundaran, D.W. Fuerstenau, *J. Phys. Chem*. **1966**, 70, 90.
8. R. Atkin, V.S.J. Graig, E.J. Wanless, S. Biggs, *Adv. Colloid Interface Sci*. **2003**, 103, 219.
9. G. Akay, R.J. Wakeman, *Trans IchemE*, **1993**, 71(A), 411.
10. N. Benes, A. Nijmeijer, H. Verweij, In *Membrane Science and Technology Series*, 6; Kanellopoulos, N.K.,Ed.; Elsevier: Amsterdam, 2000; pp 335-372.
11. G.Z. Cao, J. Meijerink, H.W. Brinkman, A.J. Burggraaf, *J. Membrane Sci.* **1993**, 83, 221.
12. W.B.S. de Lint, N.E. Benes, J. Lyklema, H.J.M. Bouwmeester, A.J. van der Linde and M. Wessling, *Langmuir* **2003**, 19, 5861.
13. T.-C. Kuo, L.A. Sloan, J.V. Sweedler, P.W. Bohn, *Langmuir* **2001**, 17, 6298.
14. A.A. Kavitskaya, N.A. Klimenko, A.V. Bildyukevich, A.A. Petrachkov, *Desalination*, **2003**, 158, 225.
15. A.F. Xie, S. Granick, *Nature Materials*, **2002**, 1, 129.
16. E. Sackmann, *Science*, **1996**, 271, 43.
17. P. Chandar, P. Somasundaran, N.J. Turro, *J. Colloid Interface Sci.* **1987**, 117, 31.

Chapter 6

Microfluidic Device Designs Utilizing Gateable Interconnects for Multilayer Architectures

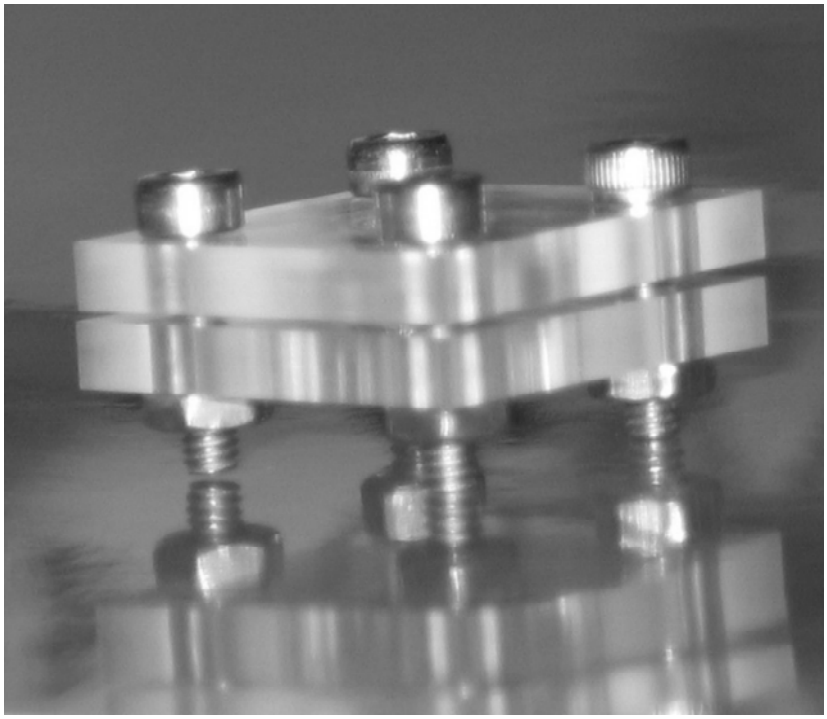

Picture of small scale experimental device, presented in Figure 6.2

Abstract: *With the increasing use of microfluidic devices in all areas of science, the demand for communication between microchannels is becoming more important. The application of microfluidic device technology is virtually endless and as the use of microfluidic devices increases, so does the demand on the architecture of these devices. One of the ways to achieve communication between different microchannels is with the use of ion selective gateable interconnects that were presented in previous chapters. The incorporation of these interconnects in microfluidic devices is a largely unexplored field of research. In this chapter a brief overview is given of the state of the art technology. Two potential designs to incorporate the microsieve-supported oxide thin films of Chapter 3 is presented. The advantages and possibilities of microfluidic gateable interconnects is also discussed.*

6.1 Introduction

In Chapter 4 the transport properties of ionic species across an interconnect under a potential difference driving force was investigated on bench scale to determine their performance as electrophoretic gates.[1] But as was already stated in Chapter 4, one of the potential uses of these switchable gates is in the field of micro total-analysis systems (μ-TAS) and in micrometer-scale laboratory chemical and biochemical manipulations. Miniaturization is of considerable interest because of the enhanced analysis and sensing sensitivity due to the small volumes, high surface-to-volume ratios and novel transport phenomena on micrometer-length scales.[2-5] Controlling the fluid flow is fundamental to the design of microfabricated analytical devises, especially for communication between micro-scale channels operating in vertically separated planes. Flexibility in transport protocols enhances the versatility of the device as well as making optimization easier for specific analyses. The implementation of sequential chemical manipulation and multidimensional analysis schemes requires that multiple fluidic tasks be integrated onto a single two-dimensional platform, placing extreme demands on design. For this reason three-dimensional microfluidic devices are being developed to achieve the complexity required for increasingly sophisticated schemes. The feasibility of applying the silicon-supported oxide interconnects of Chapter 3 in microfluidic type devices will be discussed.

6.2 Background

Microfluidics has been applied to single-molecule sensing[6], chemical separation[7,8], microfluidic interconnects[9,10] and fundamental studies of fluid transport at nanometer dimensions.[11,12] Bohn and Sweedler *et al.* demonstrated recently the advantages of nanoscale features by considering two crossed microfluidic channels fabricated from poly(dimethylsiloxane) (PDMS) in planes above and below a Polycarbonate nuclear track-etched (PCTE) nanoporous membrane. The fabrication of these PDMS channels was done by standard rapid prototyping protocols.[13] Placing a section of membrane on the bottom channel and then placing the top channel at a 90° angle to the bottom channel within the area of the membrane accomplished the assembly. A reservoir PDMS layer was sealed on top of the sandwiched device.[9] A schematic drawing representing the Bohn-Sweedler design can be seen in Figure 6.1. The channels were vacuum-filled with solution and platinum wires were mounted in the reservoirs. This provided electrical contact for bias application across channels and the PCTE membrane. A high voltage power supply relay system was used for switching electrical contact between electrodes and voltage source for different configurations of microfluidic manipulations.

The simplest implementation of this design is to let the PCTE membrane act as an externally gateable valve between channels. By manipulation of the electrical bias between the reservoirs the direction of flow between the crossed-channels could be controlled externally. Under a forward bias the probe species could be transferred from the source

channel to the receiving channel, via the membrane. The main transport mechanism of the species was via electroosmotic flow. This system can be used to concentrate dilute analytes or clean up analyte solutions.[14]

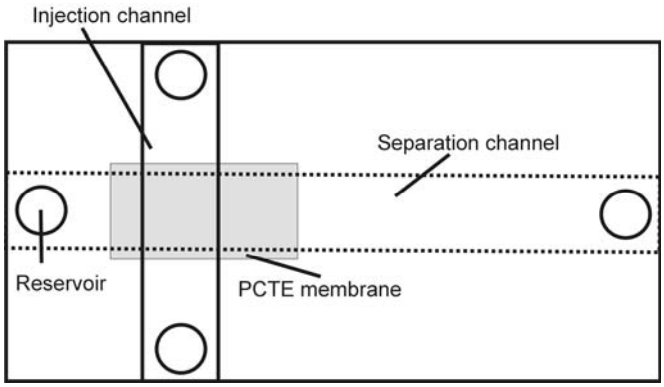

Figure 6.1: Schematic drawing representing the Bohn-Sweedler design of a three-dimensional gated-injection separation device, consisting of two PDMS channels and a PCTE membrane sandwich between the channels.[14]

The micro-injection system can also be used as nanocapillary-array.[10] Gated injections were used to control transport within a multilayer microfluidic device. In this device the injection system was coupled with a channel used for electrokinetic separations. The principle was demonstrated by Cannon *et al*. for injection of a sample from the injection channel into the separation channel, where electrophoretic separation of the mixture occurred.[10] In order to inject a sample plug a high positive bias voltage was applied between the injection channel and the separation channel. A plug of sample was then injected via the membrane into the separation channel. By applying a bias to the separation channel the plug was transported through the channel, ultimately resulting in separated analyte bands that could be detected down the channel.[10]

Recently, Kuo *et al*. showed that microfluidic devices can be a useful tool in kinetic studies of reactions, in which the amounts of reagents preclude bench-scale studies. Due to the short mixing time that can be achieved in microchannels because of the short diffusion paths it allows product formation in real-time for sequential reactions on the same target under identical experimental conditions.[15]

6.3 Device design

In this section the design of two devices that incorporate Si-based oxide interconnects will be discussed. The first design consists of two machined Perspex plates with integrated o-rings embedded in the plates, which form reservoirs on both sides of the membrane. The membrane is then sandwiched between these two plates and screwed together. This is shown in Figure 6.2, where top, bottom and side views of the device are shown.

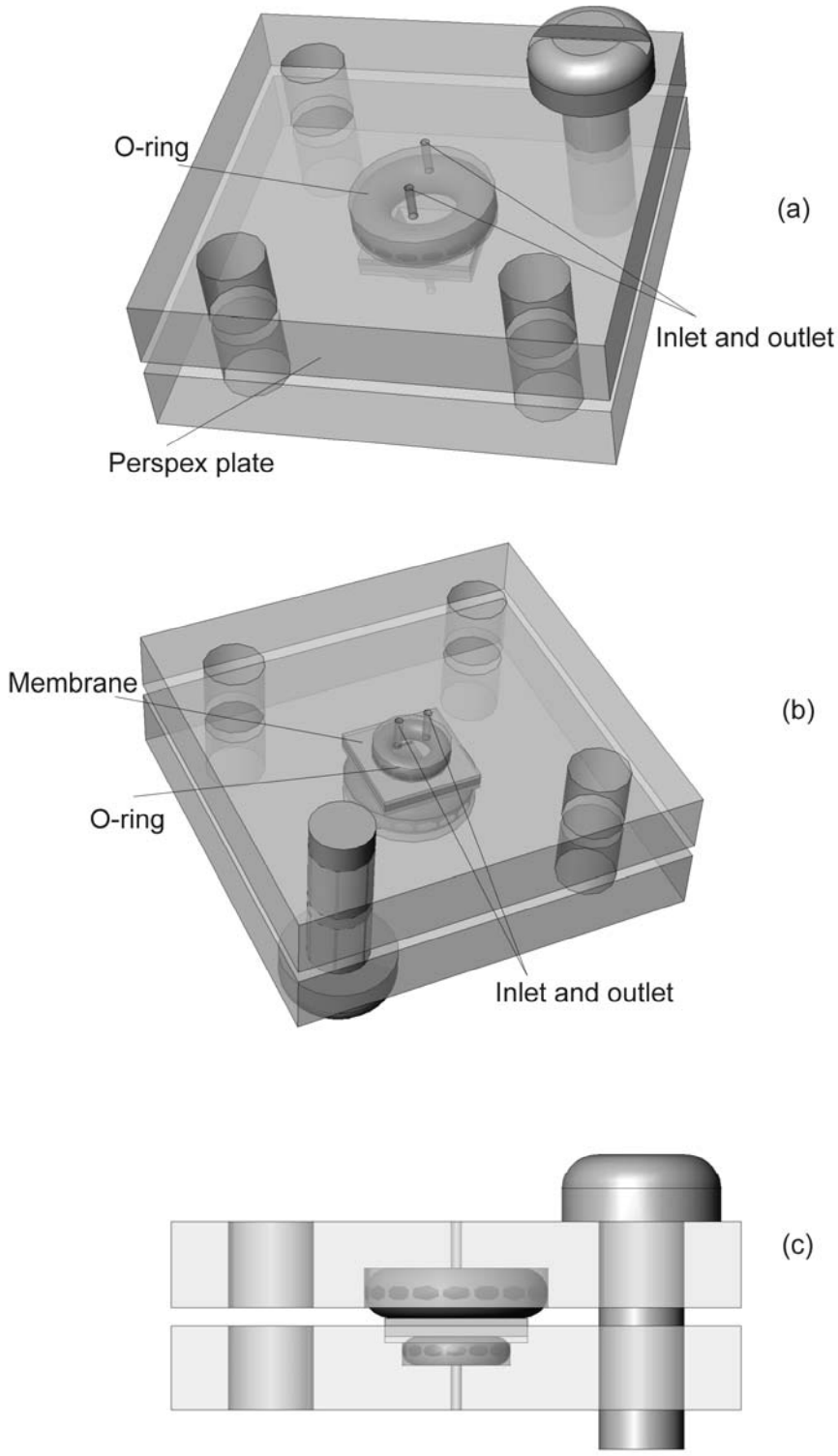

Figure 6.2: Representations of a proposed device for investigating the behavior of the switcheable gate on macro-scale. (a) Top, (b) bottom and (c) side view of the proposed device. Design made by Dr. Ir. Edwin Oosterbroek, Bios: The Lab-on-a-Chip group, University of Twente, The Netherlands

As can be seen in the figure the device contains inlet and outlet channels in both the top and bottom plates to which capillaries can be connected. What is not shown in the figure is an extra inlet so that platinum wires can be incorporated into the reservoirs on both sides. These act as electrodes for applying a potential difference across the membrane to manipulate transport, as discussed in Chapter 4.

The second proposed design is similar to the first design in the sense that it consists of two separate halves which sandwich the membrane between them, as shown in Figure 6.3(a). The two separate halves are made from glass. The electrodes can be deposited by a standard sputtering technique and can be seen in Figure 6.3(b). The sputtered platinum electrodes are connected to the external potentiostat via external wiring. The capillaries and wires can be glued into the device. The membrane can be sealed between the two glass halves by rubber foil or by Ordyl foil rings to ensure that there is no leakage between the glass and the membrane. Due to the fact that this design is made from glass and its fabrication involves standard processing techniques, the dimensions of the device can be reduced in order to arrive at truly microfluidic dimensions.

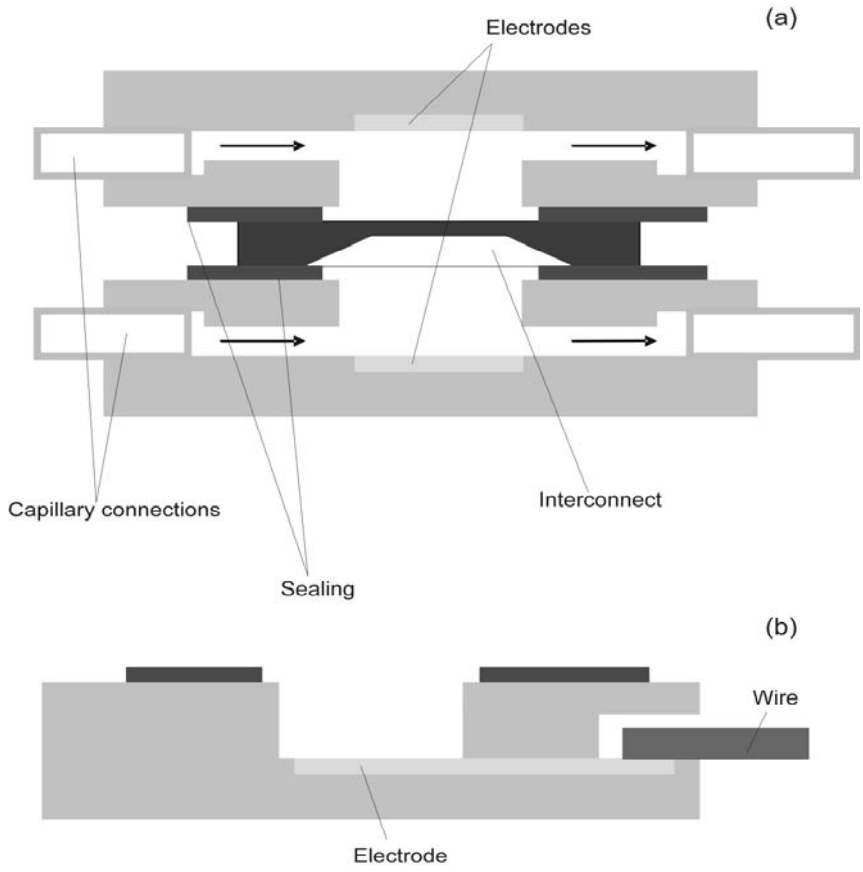

Figure 6.3: (a) Drawing of a proposed glass device for investigation of the behavior of the switcheable gate on micro-scale. (b) Cross-section of the proposed device showing the connection to the integrated electrodes. Design made by Ronnie van't Oever from Micronit Microfluidics B.V., http://www.micronit.com.

6.4 Conclusions

As microfluidic device technology becomes more important in various areas of science, the control of fluid flow and the manipulation of molecular or biological species in these devices also becomes more important. To carry out more complex manipulations, the fabrication of functional devices also becomes more complex. This has led to the development of switchable gated systems that can control fluid flow and manipulate the transport of species at will. The Si-based oxide interconnects described in Chapter 3 and 4 are one example of those. A principal advantage of gated interconnects is that microfluidic device design is no longer restricted to two dimensions. Gated interconnects open the possibility for designers of microfuidic devices to design more complex operational systems in three dimensions. The two device designs proposed here are meant as proof-of-principle devices. The ion injection technology discussed in this thesis can be useful to the field of analytical chemistry, but may also be useful in other fields of research. It has a potential use in kinetic studies of reactions due to the fast response time associated with microfluidic devices, but the use of these devices in the pharmaceutical industry as on-demand delivery systems of therapeutic agents remains largely unexplored.

Acknowledgments

We want to thank to following people of their time and work in designing the microfluidic devices presented in this chapter. For the design presented in Figure 6.2 we thank Dr. Ir. Edwin Oosterbroek at the Bios group, University of Twente, The Netherlands. For the glass design presented in Figure 6.3 we thank Ronnie van't Oever from Micronit Microfluidics B.V., P.O. Box 545, 7500 AM, Enschede, The Netherlands. http://www.micronit.com

6.5 References

1. R. Schmuhl, J. Sekulic, S. Roy Chowdhury, C.J.M. van Rijn, K. Keizer, A. van den Berg, J.E. ten Elshof, D.H.A. Blank, *Adv. Mater.* **2004**, 16, 900
2. R. Schmuhl, W. Nijdam, J. Sekulic, S. Roy Chowdhury, C.J.M. van Rijn, A. van den Berg, J.E. ten Elshof, D.H.A. Blank, *Anal. Chem.* **2004**,
3. R. Schmuhl, K. Keizer, A. van den Berg, J.E. ten Elshof, D.H.A. Blank, *J. Colloid Interface Sci.* **2004**, 273, 331.
4. T.-C. Kuo, L.A. Sloan, J.V. Sweedler, P.W. Bohn, *Langmuir* **2001**, 17, 6298.
5. D.C. Cannon Jr., B.R. Flachsbart, M.A. Shannon, J.V. Sweedler, P.W. Bohn, *Appl. Phys. Lett.* **2004**, 85(7), 1241.
6. J.J. Nakane, M. Akeson, A. Marziali, *J. Phys.: Condens. Matter*. **2003**, 15, R1365.
7. M. Nishizawa, V.P. Menon, C.R. Martin, *Science*, **1995**, 268, 700.
8. L.A. Wood, T.P. Roddy, T.L. Paxon, A.G. Ewing, *Anal. Chem*. **2001**, 73, 3687.
9. T.-C. Kuo, D.M. Cannon, Jr., Y. Chen, J.J. Tulock, M.A. Shannon, J.V. Sweedler, P.W. Bohn, *Anal. Chem.* **2003,** 75, 1861.
10. D.M. Cannon, Jr., T.-C. Kuo, P.W. Bohn, J.V. Sweedler, *Anal. Chem.* **2003,** 75, 2224.
11. A.T. Conlisk, J. McFerran, Z. Zheng, D. Hansford, *Anal Chem*. **2002**, 74, 2139.
12. R. Qiao, N.R. Aluru, *Nano Lett*. **2003**, 3, 1013.
13. J.C. McDonald, D.C. Duffy, J.R. Anderson, D.T. Chiu, H.K. Wu, O.J.A Schueller, G.M. Whitesides, *Electrophoresis*, **2000**, 21, 27.
14. T.-C. Kuo, D.M. Cannon, M.A. Shannon, P.W. Bohn, J.V. Sweedler, *Sensor Actuat A.* **2003,** 102, 223.
15. T.-C. Kuo, H.-K. Kim, D.M. Cannon, Jr., M.A. Shannon, J.V. Sweedler, P.W. Bohn, *Angew. Chem. Int. Ed.* **2004,** 43, 1862.

Chapter 7

Evaluation and Recommendations

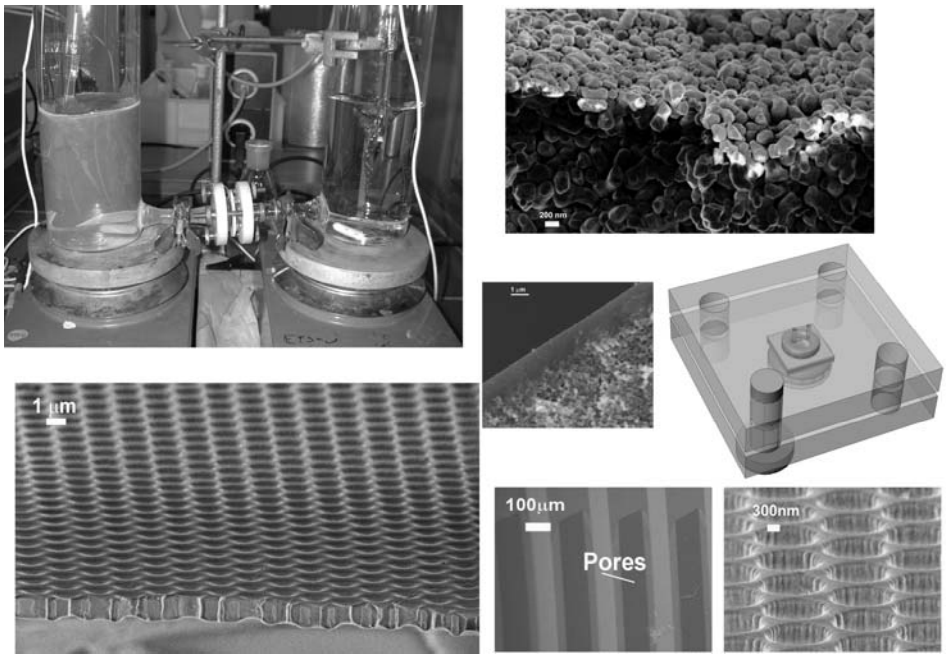

Abstract: *The goal of the thesis was to develop ion-selective interconnects for microfluidic device architectures. A number of model systems were developed using classical sol-gel methods, and the feasibility of using porous oxide thin films as selective interconnects with high tuneability was demonstrated. This chapter integrates the main results of the thesis and proposes some additional studies.*

7.1 Introduction

The use of an electric field for dosing of charged species via a mesoporous or microporous membrane formed the central theme of all chapters. By applying an external electric field over an interconnect it was possible to transport charged species from one liquid to the other by different transport mechanisms, i.e., ion migration, Fick diffusion and/or electro-osmotic flow. This chapter integrates the main results of the thesis and proposes some additional studies to fully integrate these oxide membranes as selective ion gates with high tuneability in microfluidic device design architectures.

7.2 Membrane properties

Till date, selective interconnects for microfluidic devices[1-6] are based on track-etched polymeric (NTEP) membranes and anodic aluminum oxide (AAO) thin films.[7] Sweedler, Bohn and co-workers[8] developed a gateable interconnect for analyte injection in microfluidic devices based on an NTEP membrane. Martin and co-workers showed how to influence the ion permselectivity of gold-plated NTEP membranes by imposing a bias potential on the membrane.[9] NTEP membranes are made by bombarding 6-20 μm thick nonporous sheets of polycarbonate or polyester with nuclear fission fragments which create straight damage tracks in the sheet, which are subsequently turned into pores by chemical etching. The main properties of the AAO and NTEP membranes are listed below in Table 7.1. Some properties of the membranes presented in this thesis are also listed.

Table 7.1: Physical structural and transport properties of membrane-interconnects.

		TiO_2	MCM-48	γ-Al_2O_3	α/γ-Al_2O_3	AAO	NTEP
Iso-electric point		4.2-4.8	2-3	8.5-9	8.5-9	8.8	none
Pore size (nm)		~0.9	2.8-3.4	5-7.5	5-7.5	10-20	10-15
Porosity (%)		34-41	~60	~55	~55	25-40	~1
Film thickness		~500 nm	~970 nm	~300 nm	300 nm	6-20 μm	~10 μm
Support material and thickness		Silicon 1 μm	Silicon 1 μm	Silicon 1 μm	α-Al_2O_3 2 mm	none	none
Permeability	A^{2-}	10^{-7}	10^{-8}	10^{-10}	$< 10^{-11}$	10^{-14}	10^{-9}
($cm^2\ s^{-1}$) [2,10,11]	C^{2+}	10^{-7}	10^{-6}	10^{-8}	10^{-9}	10^{-14}	10^{-9}

Commercially available NTEP membranes have porosities of ~1 % and pore diameters down to 10-15 nm.[8] AAO films are thicker, and contain straight cylindrical pores of 10 nm diameter or larger. They are prepared by anodization of aluminum metal foils in acidic solutions and have porosities of 25-40 %, much higher than in NTEP membranes. The oxide

interconnects were made of mesoporous γ-alumina or silica, or microporous titania.[8,12-16] These thin films can be made cheaply and easily. By proper choice of the oxide material the intrinsic properties of the membrane can be tuned. These oxide layers are less than 1 μm thick, have a total porosity of 35-60%, and pore diameters in the range of only 0.9-10 nm (see Table 7.1). Unlike NTEP and AAO membranes they do not have a straight channel pores, but have a disordered or mesostructured template-directed pore structure. The typical order of magnitude for anionic (A^{2-}) and cationic (C^{2-}) permeabilities for the different membranes is shown in Table 7.1. In most cases the membranes developed in this thesis yield higher fluxes and selectivities in comparison with AAO membranes and higher or similar fluxes and selectivities than NTEP membranes. The tuneability of all types of membranes is similar.

To give these layers sufficient mechanical stability they are deposited onto 0.5x0.5 cm Si-based Microsieves of 1 μm effective thickness, which contain areas with hexagonal arrays of circular perforations of 0.5 or 1.2 μm.[17] The overall porosity of the sieves is 30%. Because of the silicon support structure the oxide films can easily be integrated with existing silicon technology. The integration of thick alumina membranes as well as the NTEP membranes with silicon technology will be difficult and is unlikely. But the integration of NTEP membranes with PDMS, poly(dimethylsiloxane), technology is very likely, as was shown by Bohn.[4]

7.3 Evaluation and recommendation

In this section the most important results in this thesis are summarized, evaluated and discussed. A number of recommendations for further studies are also presented.

- The deposition of thin porous gold electrodes directly onto the γ/α alumina membrane surface (see Chapter 2) to create an injection system was done for the first time. It transformed a passive membrane into an active membrane of which the selectivity could be externally tuned. This concept could be further developed by making patterned porous gold electrodes on the membrane surface. Due to the fact that the transport of ions through the membrane is driven by Fick diffusion in combination with local ion accumulation at the external membrane surface, as was shown in Chapter 2, patterned electrodes may make it possible to locally create a sufficiently strong electric field to control the ion transport rate through these membranes laterally. Several injector electrodes can be operated independently from each other by proper choice of the bias potential applied to the electrodes.
- The transport of ionic probe molecules has been studied in Chapters 2 and 4. It was found that the transport mechanism can be influenced by the location of the electrodes relative to the membrane. By integration of the electrodes onto the membrane surface a bias potential is applied to the membrane surface to deplete or accumulate ions at the external membrane surface, and the resulting ion transport mechanism is Fick diffusion. But when the electrodes are isolated from the membrane surface, the main transport mechanism is ion migration as shown in Chapter 4. The essential difference between these two approaches,

the novel approach outlined in Chapter 2, and the conventional approach described in Chapter 4, is that in the latter case an ionic species is present in a more or less homogeneous electric field between the electrodes, and it is drawn toward the one with opposite charge. In the novel approach, the ion is either drawn towards the surface electrode when its charge is opposite, or repelled by it when its charge is of the same sign. Ions with opposite charge accumulate near the surface electrode, but once they have passed it, the electric field is directed backwards. So they obviously have to migrate by Fick diffusion through the membrane. Ionic species with the same charge as the surface electrode would be transported through the membrane by ion migration, but they cannot pass the surface porous electrode because of electrostatic repulsion. This mode of operation gives a high selectivity.

- Electro-osmotic flow (EOF) through the membrane can be induced by increasing the ionic strength of the system, thus decreasing the double layer thickness inside the pores, but it may also be possible to induce EOF by application of much larger potential differences over the membrane than were used in this thesis.
- The relatively large scale on which the experiments were performed, i.e., large liquid volumes of feed and permeate in the experiments, made it difficult to study the switching dynamics of the interconnects. The typical thickness of 2 mm of the α-alumina supports, which were used in Chapter 2 and Chapter 5, will have a marked influence on the response time of the interconnect, making it respond more sluggish than a thinner interconnect. Switching dynamics and speed are therefore an area of research for future studies.
- An alternative way to control the permeability of a gate is by the co-addition of surfactant molecules to the system, as was shown in Figure 5.1. Since 2 mm thick α-alumina supports and a bench-scale set-up were used, the switching speed of the blocking molecules was not investigated, since the response would be relatively sluggish. However, even when thinner interconnects are used, the rate of adsorption and desorption of surfactants will ultimately also determine its usability to manipulate flux in real time in small scale devices. As seen from the research presented in Chapter 5, different surfactants have a different influence on the permeability properties of the membranes. The presence of short carbon chain surfactants at low concentrations increases the transport rate, while long chain surfactants at high concentrations effectively block transport through the membrane. The chain length of the carbon chain may also influence the response time for surfactant adsorption and desorption; longer chains may be slower in this regard.
- A new type of Si-compatible thin mesoporous and microporous oxide membranes was developed for potential application as interconnect in microfluidic devices, and their use as selective and tuneable interconnect has been demonstrated. The next step will be to integrate the deposition of sol-gel derived oxide films into the fabrication methods of silicon devices, in order to make interconnects on silicon type lab-on-chip designs. A particularly interesting way to achieve integration is to pattern these oxide layers on silicon

wafers to a predefined area of the wafer, but a suitable processing technique will have to be developed to accomplish this.

- Integration of Si-supported oxide films into a smaller device type set-up is a potential way to establish communication between two microfluidic channels, and may be a useful component in a wide range of microfluidic device designs, because it may help expanding device architecture into the third dimension. Two designs have been presented in this thesis and this area of research is still largely unexplored.

7.4 References

1. Y. Fintschenko, A. van den Berg, *J. Chrom. A.* **1998**, *819*, 3.
2. A.M. Hollman, D. Bhattacharyya, *Langmuir* **2002**, *18*, 5946.
3. M. Nishizawa, V.P. Menon, C.R. Martin, *Science* **1995,** *268*, 700.
4. T.-C. Kuo, *et al*., *Anal. Chem.* **2003,** *75*, 1861.
5. S.B. Lee, C.R. Martin, *Anal. Chem.* **2001,** *73*, 768.
6. R.B.M. Schasfoort, S. Schlautmann, J. Hendrikse, A. van den Berg, *Science* **1999**, *286*, 942.
7. J.C. Hulteen, C.R. Martin, *J. Mater. Chem*. **1997**, *7*, 1075.
8. T.-C. Kuo, D.M. Cannon JR, M.A. Shannon, P.W. Bohn, J.V. Sweedler, *Sensor Actuat. A* **2003**, *102*, 223.
9. C.R. Martin, M. Nishizawa, K. Jirage, M. Kang, S.B. Lee, *Adv. Mater*. **2001**, *13*, 1351.
10. R. Schmuhl, J. Sekulic, S. Roy Chowdhury, C.J.M. van Rijn, K. Keizer, A. van den Berg, J.E. ten Elshof, D.H.A. Blank, *Adv. Mater.* **2004**, 16, 900.
11. P.J. Kemery, J.K. Steehler, P.W. Bohn, *Langmuir* **2001**, 14, 2884.
12. D.-H. Park, N. Nishiyama, Y. Egashira, K. Ueyama, *Ind. Eng. Chem. Res.* **2001,** *40*, 6105.
13. N. Nishiyama, D.H. Park, A. Koide, Y. Egashira, K. Ueyama, *J. Membrane Sci.* **2001,** *182*, 235.
14. Y.-S. Kim, S.-M. Yang, *Adv. Mater*. **2002,** *14*, 1078.
15. M. Klotz, A. Ayral, C. Guizard, L. Cot, *Sep. Purif. Tech.* **2001,** *25*, 71.
16. Roy Chowdhury, R. Schmuhl, K. Keizer, J.E. ten Elshof, D.H.A Blank,. *J. Membrane Sci.* **2003,** *225*, 177.
17. C.J.M. van Rijn, G. J. Veldhuis, S. Kuiper, *Nanotechnology* **1998,** *9*, 343.

Publication list

1. R. Schmuhl, J.E. ten Elshof, K. Keizer and A. van den Berg, "Tuneable ion-selective inorganic membranes", *Desalination.* **2002**, 146, 29-33.
2. R. Schmuhl, W.B.S. de Lint, K. Keizer, A. van den Berg and J.E. ten Elshof, "Electric field mediated ion transport through charged mesoporous membranes," Proc. Int. Symp. on *Membranes - Synthesis, Properties and Applications*, ed. V.N. Burganos, R.D. Noble, M. Asaeda, A. Ayral, and J.D. LeRoux, Mat. Res. Soc. Proc. 752, Materials Research Society, Pittsburg, USA, **2003**.
3. S. Roy Chowdhury, R. Schmuhl, K. Keizer, A. van den Berg, J.E. ten Elshof, and D.H.A. Blank, "Tailor-made nanostructured ion selective MCM-48 membranes", pp. in: *Mat. Res. Soc. Symp. Proc.*, Vol. 775. Edited by C.J. Brinker, M. Antonietti, Y. Lu, and C. Bai. Materials Research Society, 2003. Proc. Int. Symp. on Self-Assembled Nanostructured Materials, Pittsburg, **2003**.
4. S. Roy Chowdhury, R. Schmuhl, K. Keizer, J.E. ten Elshof and D.H.A. Blank, "Pore size and surface chemistry effects on the transport of hydrophobic and hydrophilic solvents through mesoporous γ-alumina and silica MCM-48," *J. Membrane Sci*. **2003**, 225, 177-186.
5. R. Schmuhl, K. Keizer, A. van den Berg, J.E. ten Elshof and D.H.A. Blank, "Controlling the transport of cations through permselective mesoporous alumina layers by manipulation of electric field and ionic strength", *J. Colloid Interf. Sci*. **2004**, 273, 331-338.
6. R. Schmuhl, J. Sekulić, S. Roy Chowdhury, C.J.M. van Rijn, K. Keizer, A. van den Berg, J.E. ten Elshof, and D.H.A. Blank, "Si-compatible ion selective mesoporous and microporous oxide interconnects with high tuneability", *Adv. Mater.* **2004**, 16, 900-904.
7. R. Schmuhl, S. Roy Chowdhury, J.E. ten Elshof, A. van den Berg and D.H.A. Blank, "Nanostructured ion-selective MCM-48 membranes", *J. Sol-Gel Sci. Tech.* **2004**, 31,249-252.
8. Riaan Schmuhl, Wietze Nijdam, Jelena Sekulić, Sankhanilay Roy Chowdhury, Cees J.M. van Rijn, Albert van den Berg, Johan E. ten Elshof and Dave H.A. Blank, "Si-supported Mesoporous and Microporous Oxide Interconnects as Electrophoretic Gates for Application in Microfluidic Devices", *Anal. Chem.* **2005**, 77, 178-184.

Acknowledgements

There are quite a few people that made life, work and writing of this thesis possible and mostly enjoyable, I would like to express my deepest thanks to all of them for making my dream a reality.

To Andre, for making PhD not only a great experience but also for having a lot of patience and for knowing when to give me a kick start.

My promoters Dave and Albert, thanks for all the support.

And then there are the friends that made life in the Netherlands an adventure. Especially Karen, Jelena, Boris, Frederic, Steve and Samuel, you guys are great!

To the people in the IMS group, thanks for making everyday at work truly an experience.

Dankie aan my Ma wat altyd in my glo, my familie en vriende in Suid Afrika.

About the author

Riaan Schmuhl was born on the 28th October 1973 in Rustenburg, South Africa. After matriculating from Bergsig High school in Rustenburg, he started his studies in 1992 at the North West University (formally known as Potchefstroom University for Higher Christian Education) in Potchefstroom, South Africa. He achieved his B.Sc. degree in Chemistry and Biochemistry in 1996, and continued with a B.Sc (honours) degree in Chemistry, and received it in 1997. In 1999 he obtained his M.Sc. degree in Atmospheric Chemistry, entitled: *Kinetic Study of the Oxidation Reaction of Metal-porphyrins with Peroxomonosulphate*, in the same department. From 1999 to 2000 he was working on his Ph.D. in the Membrane group of the School of Chemistry, but discontinued this study. From 2000 to 2001 he worked as a *Research fellow* in the Inorganic Materials Science group at the University of Twente. In February 2001 he started his Ph.D. work at the University of Twente in the Inorganic Materials Science Group, on the subject of Field-effect membranes, under the supervision of Dr. ir. J.E. ten Elshof.